ISTANBUL TECHNICAL UNIVERSITY ★ GRADUATE SCHOOL

INVESTIGATION OF MOTIONS ON FLOATING OFFSHORE PLATFORMS

M.Sc. THESIS

Abdullah Emin ULAŞ

Department of Shipbuilding and Ocean Engineering

Offshore Engineering Programme

MAY 2024

ISTANBUL TECHNICAL UNIVERSITY ★ GRADUATE SCHOOL

INVESTIGATION OF MOTIONS ON FLOATING OFFSHORE PLATFORMS

M.Sc. THESIS

Abdullah Emin ULAŞ
(508201236)

Department of Shipbuilding and Ocean Engineering

Offshore Engineering Programme

Thesis Advisor: Prof. Dr. Kadir SARIÖZ

MAY 2024

İSTANBUL TEKNİK ÜNİVERSİTESİ ★ LİSANSÜSTÜ EĞİTİM ENSTİTÜSÜ

YÜZER AÇIK DENİZ PLATFORMLARININ HAREKETLERİNİN İNCELENMESİ

YÜKSEK LİSANS TEZİ

Abdullah Emin ULAŞ
(508201236)

Gemi ve Deniz Teknolojisi Mühendisliği Anabilim Dalı

Açık Deniz Mühendisliği Programı

Tez Danışmanı: Prof. Dr. Kadir SARIÖZ

MAYIS 2024

Abdullah Emin ULAŞ, a M.Sc. student of ITU Graduate School student ID 508201236 successfully defended the thesis/dissertation entitled "INVESTIGATION OF MOTIONS ON FLOATING OFFSHORE PLATFORMS", which he prepared after fulfilling the requirements specified in the associated legislations, before the jury whose signatures are below.

Thesis Advisor :	**Prof. Dr. Kadir SARIÖZ** Istanbul Technical University	.....
Jury Members :	**Assoc. Prof. Dr. Bilge TUTAK** Istanbul Technical University	….....
Jury Members :	**Assoc. Prof. Dr. Ferdi ÇAKICI** Yıldız Technical University	….....

Date of Submission : 04 May 2024
Date of Defense : 29 May 2024

To my family and loved ones,

FOREWORD

I would like to express my gratitude to my valuable thesis advisor, Prof. Dr. Kadir SARIÖZ, who guided me throughout the entire study, gave me his valuable ideas, and understood me when I had difficulties.

I would also like to thank my dear friend Enver Kürşat GÜNER, with whom I constantly exchanged ideas while working on similar topics and supported me on issues that came to mind.

Additionally, I would like to thank Burak Tunç ÇEKİDEKÇİ, who took the time to help me when I asked my questions.

Finally, I would like to thank my entire family, loved ones and friends, especially my father, for their support during this busy and challenging process, for understanding when I could not spare time for them, for always encouraging me and being with me spiritually.

May 2024

Abdullah Emin ULAŞ
(Civil Engineer)

TABLE OF CONTENTS

Page

FOREWORD ..... **ix**
TABLE OF CONTENTS ..... **xi**
ABBREVIATIONS ..... **xiii**
SYMBOLS ..... **xv**
LIST OF TABLES ..... **xix**
LIST OF FIGURES ..... **xxi**
SUMMARY ..... **xxiii**
ÖZET ..... **xxvii**
1. INTRODUCTION **1**
2. FLOATING OFFSHORE WIND TURBINES **5**
2.1 General Information about Wind Turbines 5
2.1.1 Vertical axis wind turbine (VAWT) 6
2.1.2 Horizontal axis wind turbine (HAWT) 6
2.1.3 The internal structure of a wind turbine 8
2.1.3.1 Nacelle (Body) 8
2.1.3.2 Rotor blades 8
2.1.3.3 Rotor hub 8
2.1.3.4 Low-speed shaft 9
2.1.3.5 Gearbox 9
2.1.3.6 High speed with its mechanical brake 9
2.1.3.7 Electrical generator 9
2.1.3.8 Electronic control unit (Electronic controller) 10
2.1.3.9 Hydraulics system 10
2.1.3.10 Cooling unit 10
2.1.3.11 Tower 10
2.1.3.12 Yaw mechanism 10
2.1.3.13 Anemometer and wind wane 10
2.1.4 Working principle of wind turbines 11
2.1.5 Benefit-cost analysis of wind turbines 11
2.1.6 Capacity factor 13
2.2 Wind Turbines at Sea 13
2.2.1 Onshore wind turbines 14
2.2.2 Offshore wind turbines 17
3. MOTIONS OF FLOATING OFFSHORE STRUCTURES IN WAVES 19
3.1 Single Degree of Freedom Equation of Motion 20
3.1.1 Added mass (A) 21
3.1.2 Damping force (B) 21
3.1.3 Restoring force (C) 21
3.1.4 Wave excitation force 21
3.1.4.1 Froude-Krylov forces (F^{FK}) 22

3.1.4.2 Diffraction forces (F^D) 22
3.1.5 Linear wave theory 23
3.1.6 Heading and encounter frequency 25
3.1.7 Complex harmonic motion and solution of the equations of motion 27
3.1.8 Response amplitude operator (RAO) 29
3.2 Six Degree of Freedom Motions of a Floating Body 30
3.2.1 Assumptions and wave force in AQWA 33
3.3 Mathematical Representation of the Seaway 36
3.3.1 Linear superposition of regular waves 36
3.3.2 Relationship between body motion and wave spectrum 38
3.3.3 Wave and wind data 40
3.3.3.1 Wave measurements 40
3.3.3.2 Visual observations 40
3.3.3.3 Hindcasting 41
3.3.4 Short-term description of the sea by spectral analysis 43
3.3.4.1 Wave spectrum models 43
3.3.5 Characteristics of spectra 48
3.3.6 Directional spectrum 49
3.3.7 Long-term trends 50
4. ANALYTICAL AND NUMERICAL ANALYSIS OF A VERTICAL CIRCULAR CYLINDER 51
4.1 Vertical Circular Cylinder for Analytical and Numerical Solutions 51
4.2 Analytical Solution of Vertical Circular Cylinder 52
4.2.1 Added mass and damping coefficient 52
4.2.2 Wave exciting force (F_3) 54
4.2.3 Response amplitude operator (RAO) 57
4.2.3.1 Estimate the heaving amplitude 58
4.3 Numerical Solution of Vertical Circular Cylinder 59
4.3.1 Added mass and damping coefficient 60
4.3.2 Wave excitation forces 61
4.3.3 Response amplitude operator (RAO) 62
5. EXPERIMENTAL AND NUMERICAL ANALYSIS OF THE FLOATING OFFSHORE PLATFORM 65
5.1 Definition of the Experimental Study 65
5.1.1 Experiment setup 65
5.1.1.1 Tank design 65
5.1.1.2 Mooring design 67
5.1.1.3 Scaling methods and factors 67
5.1.1.4 Final model definition 68
5.1.2 Experiment conditions 70
5.2 Numerical Analysis 70
5.2.1 Comprising of Response Amplitude Operators (RAO) 71
5.2.1.1 Extreme deep sea conditions for Turkish seas 74
5.2.1.2 Pierson-Moskowitz sea states spectrum 75
5.2.1.3 Compearing of RAO and sea states 76
5.2.2 Motion Spectrums for no mooring line situation 77
5.2.3 Motion Spectrums for with mooring lines situation 79
6. CONCLUSIONS AND RECOMMENDATIONS 83
REFERENCES 87
CURRICULUM VITAE 91

ABBREVIATIONS

2D : Two Dimensional
3D : Three Dimensional
CG : Centre of Gravity
DOF : Degree of Freedom
FRA : Fixed Reference Axes
HAWT : Horizontal Axis Wind Turbine
ITTC : International Towing Tank Conference
JONSWAP : Joint North Sea Wave Project
KHL : Kelvin Hydrodynamics Laboratory
MEDCOAST : Mediterranean Coastal Foundation
METU : Middle East Technical University
NATO : North Atlantic Treaty Organization
NREL : National Renewable Energy Laboratory
RAO : Response Amplitude Operator
RMS : Root Mean Square
rpm : Revolutions Per Minute
R&D : Research and Development
SWL : Sea Water Level
VAWT : Vertical Axis Wind Turbine
WMO : World Meteorological Organization

SYMBOLS

$\boldsymbol{A}$	**:** Added mass
$\boldsymbol{B}$	**:** Damping force
$\boldsymbol{C}$	**:** Restoring force
$\boldsymbol{c}$	**:** Wave velocity
$\boldsymbol{D}$	**:** Rotor diameter
$\boldsymbol{D_c}$	**:** Vertical circular cylinder diameter
$\boldsymbol{E}$	**:** Energy
$\boldsymbol{d}$	**:** water depth
$\boldsymbol{f}$	**:** Wave frequency
$\boldsymbol{F^I}$	: Wave excitation force due to incident waves
$\boldsymbol{F^D}$	**:** Diffraction force
$\boldsymbol{F^{FK}}$	**:** Froude-Krylov force
$\boldsymbol{g}$	**:** Gravitational acceleration
$\boldsymbol{H}$	**:** Wave height
$\boldsymbol{H_s}$	**:** Significant wave height
$\boldsymbol{h_{hub}}$	**:** Altitude at which wind speed is sought
$\boldsymbol{h_{ref}}$	**:** Referenced height for wind speed
$\boldsymbol{k}$	**:** Wave number
$\boldsymbol{L}$	**:** Length
$\boldsymbol{M}$	**:** Body mass
$\boldsymbol{m_n}$	**:** n^{th} wave spectrum moment
$\boldsymbol{N_0}$	**:** Number of zero crossings in a long wave record
$\boldsymbol{N_1}$	**:** Number of crests in a long wave record
$\boldsymbol{P}$	**:** Power
$\boldsymbol{p}$	**:** Dynamic pressure
$\boldsymbol{R^2}$	: Calibration value
$\boldsymbol{R_p}$	**:** Recurrence period
$\boldsymbol{S_\zeta}$	**:** Wave energy spectrum
$\boldsymbol{T}$	**:** Wave period

T_1 : Average wave period

T_{-1} : Energy averaged period

T_c : Vertical circular cylinder draught

T_e : Encounter wave period

T_m : Mean wave period

T_{modal} : Modal wave period

T_p : Peak wave period

T_z : Average zero crossing period

t : Time

U : Wind speed

$U_{h_{hub}}$: Wind speed at searched altitude

$U_{h_{ref}}$: Wind speed at the reference height

u : Horizontal particle velocity

$\dot{u}$: Horizontal particle acceleration

V : Forward speed

w : Vertical particle velocity

$\dot{w}$: Vertical particle acceleration

x : Direction of propagation

z_0 : Roughness length

ε : Phase difference

ζ : Wave amplitude

ζ_s : Significant wave amplitude

ζ_{RMS} : RMS wave amplitude

ζ_w : Incident wave amplitude

η : Response displacement

$\dot{\eta}$: Response velocity

$\ddot{\eta}$: Response acceleration

λ : Wavelength

λ_0 : Deep-sea wavelength

μ : Direction angle

ρ : Water density

σ : Scale factor

ϕ, φ : Wave velocity potential

φ_1 : First-order incident wave potential with unit wave amplitude

φ_d : Corresponding diffraction wave potential

φ_r : Radiation wave potential

ω : Wave frequency (angular)

ω_e : Wave encounter frequency (angular)

ω_m : Wave modal frequency (angular)

LIST OF TABLES

Page

Table 2.1 : Wind power classification [8]. **6**
Table 2.2 : Roughness length (z_0) [9]. **7**
Table 3.1 : Regular wave's characteristic parameters. **24**
Table 3.2 : The velocity potential of a regular wave. **24**
Table 3.3 : The profile, dynamic pressure, particle velocities and accelerations in a regular, harmonic wave. **25**
Table 3.4 : Motions of a floating offshore structure in waves. **31**
Table 3.5 : World Meteorological Organization (WMO) standard sea state code. **40**
Table 3.6 : Annual Sea state occurrences in the open ocean North Atlantic. **42**
Table 3.7 : Annual Sea state occurrences in the open ocean North Pacific. **42**
Table 3.8 : Spectral wave statistical parameters. **49**
Table 5.1 : Established scaling factors in the experimental study [43, 47]. **68**
Table 5.2 : Model properties and parameters [43]. **69**
Table 5.3 : Wave parameters for the four sea states. **70**
Table 5.4 : Natural frequencies. **73**
Table 5.5 : Maximum H_s values of Turkish seas [48]. 74
Table 5.6 : Wave steepness of Turkish seas [49]. **75**
Table 5.7 : T_m and λ_0 values for Turkish seas' $H_{s,max}$ **75**

LIST OF FIGURES

Page

Figure 1.1 : Cumulative installations for wind power plants in Türkiye [1]. **2**
Figure 2.1 : Shape of HAWT and VAWT [3]. **5**
Figure 2.2 : Internal structure of a wind turbine [9]..... **8**
Figure 2.3: Principle of working wind turbines. **11**
Figure 2.4 : Relationship between rotor diameter and power output [14]. **12**
Figure 2.5 : Wind map of Türkiye [15]..... **13**
Figure 2.6 : Comparison of inland, onshore, and offshore applications. **14**
Figure 2.7 : Onshore wind turbine concepts [16]..... **14**
Figure 2.8 : Depths of the seas surrounding the British Isles [17]..... **15**
Figure 2.9 : North and Baltic Sea Depths [17]..... **16**
Figure 2.10 : Depths of Turkish seas [17]..... **16**
Figure 2.11 : Offshore wind turbine types [18]. **17**
Figure 2.12 : Depths of the openings of Dardanelle Strait and North Aegean Sea's Turkish side [17]..... **18**
Figure 2.13 : Depths of the openings of the Turkish Black Sea's west part [17]. **18**
Figure 2.14 : Depths of the openings of the Turkish Mediterranean Sea's west part [17]..... **18**
Figure 3.1 : Mass-spring-damper system..... **20**
Figure 3.2 : A regular wave geometry. **24**
Figure 3.3 : Heading convention [24]..... **26**
Figure 3.4 : Heave Response Amplitude Operator (RAO) for analytical solution.. **29**
Figure 3.5 : Motions of an offshore wind turbine platform in waves [25]. **30**
Figure 3.6 : Linear superposition of regular waves [24]..... **36**
Figure 3.7 : Relationship between body motion and wave spectrum [30]..... **39**
Figure 3.8 : Wave height and period statistics for Area 9 [31]..... **41**
Figure 3.9 : Pierson-Moskowitz energy spectrum for different significant wave heights [24]. **44**
Figure 3.10 : Typical Bretschneider-type spectral formulations for unit wave height [24]..... **46**
Figure 4.1 : Vertical circular cylinder selected for the primary geometry..... **52**
Figure 4.2 : The vertical circular cylinder model in AQWA..... **52**
Figure 4.3 : Added Mass ((A_3) for analytical solution..... **53**
Figure 4.4 : Damping coefficient (B_3) for analytical solution..... **53**
Figure 4.5 : Heave Froude-Krylov force (F_3^{FK}) from analytical solution..... **56**
Figure 4.6 : Heave diffraction force (F_3^D) from analytical solution..... **57**
Figure 4.7 : Heave total force (F_3) from analytical solution. **57**
Figure 4.8 : Heave Response Amplitude Operator (RAO) from analytical solution.**59**
Figure 4.9 : Added mass (A_3) from analytical and numerical solutions. **60**
Figure 4.10 : Damping coefficient (B_3) from analytical and numerical solutions.. **61**

Figure 4.11 : Heave Froude-Krylov force (F_3^{FK}) from analytical and numerical solutions. **61**
Figure 4.12 : Heave diffraction force (F_3^D) from analytical and numerical solutions. **62**
Figure 4.13 : Heave force (F_3) from analytical and numerical solutions. **62**
Figure 4.14 : Heave Response Amplitude Operator (RAO) from analytical and numerical solution. **63**
Figure 5.1 : Tank layout (a) Spar-only (b) Spar with realistic mooring lines [42]. .. **66**
Figure 5.2 : Spar-type offshore platform's tank scale model [42]. **69**
Figure 5.3 : The full-scale spar-type offshore platform model in AQWA..... **71**
Figure 5.4 : Heave RAO for the spar-type platform. **72**
Figure 5.5 : Surge/Sway RAO for spar platform**.** **72**
Figure 5.6: Pitch/Roll RAO for spar platform. **73**
Figure 5.7 : Pierson Moskowitz wave spectrums for sea states. **76**
Figure 5.8 : Heave RAO and sea states. **76**
Figure 5.9 : Surge/Sway RAO and sea states. **77**
Figure 5.10 : Pitch/Roll RAO and sea states. **77**
Figure 5.11 : Heave motion spectrum for sea state 8 (no mooring line). **78**
Figure 5.12 : Pitch/Roll motion spectrum for sea state 8 (no mooring line). **78**
Figure 5.13 : Heave motion spectrum for sea state 6 (with mooring lines). **79**
Figure 5.14 : Surge/Sway motion spectrum for sea state 6 (with mooring lines). **80**
Figure 5.15 : Pitch/Roll motion spectrum for sea state 6 (with mooring lines). **80**
Figure 5.16 : Heave motion spectrum for sea state 8 (with mooring lines). **81**

INVESTIGATION OF MOTIONS ON FLOATING OFFSHORE PLATFORMS

SUMMARY

Türkiye is a country that produces a significant portion of the energy it needs through imported fossil fuels. It should aim to diversify its energy production methods to reduce its dependence on foreign sources. Considering that the new methods targeted should be sustainable and have low adverse effects on the environment, it would be logical to turn to one of the renewable energy sources.

When evaluated specifically in Türkiye, wind energy is one of the most probable renewable energy sources in terms of its potential in geography. The country has seen this potential and has focused on producing wind energy, especially in recent years. In this context, a large amount of investment has been made in land-based wind energy. However, although it is much more efficient and promises potential, there has been no development in offshore wind energy. The main reason for this situation is that the seas surrounding Türkiye are profound. Deep seas do not allow the construction of conventional offshore platforms directly integrated into the seabed, theoretically and economically.

Currently deployed in offshore areas, offshore platforms host wind turbines or refinery facilities that process hydrocarbon resources. Many examples exist in the Baltic Sea and around the British Isles, especially off the coast of Western European countries. However, almost all platforms here are conventional platforms integrated into the ground. The shallowness of the seas in the mentioned areas enables these platforms to operate at a relatively low cost and with little effort.

In addition, semi-submerged floating platforms are designed to process hydrocarbon deposits that offer high economic income in offshore fields worldwide. However, these platforms have high construction costs and are immense structures compared to those examined in this study. Building such platforms without promising a severe economic potential is impractical or logical.

Developing technology in recent years has made it possible to design and manufacture smaller floating offshore platform systems for the deep sea. However, the R&D activities of such platforms are continuing.

Türkiye is a country that can benefit significantly from offshore wind energy due to its offshore potential. Studies on this subject are limited. A significant part of the studies did not focus on the design and implementation of the platforms. Generally, the economic potential of the country in this regard, possible application areas and the methods by which it can be applied are mentioned. This thesis study was prepared based on this deficiency. In addition, a methodology for creating the concept design of a floating offshore platform is also presented within the scope of the study. This methodology is not necessarily used only on floating offshore wind turbines. A

methodology used in this study can be followed for floating offshore platforms that serve different purposes.

Within the scope of this study, floating offshore wind turbines are first mentioned in outline. The working principle of the turbine system, platform types according to application areas and application conditions are briefly explained.

Afterwards, the theoretical and mathematical background of the movements of floating offshore structures was examined. First, a single degree of freedom (DOF) motion and its subcomponents are detailed. Based on this, motion with six degrees of freedom is explained. In addition, how the external effects that cause the movement are detected and the movement itself is also explained. External effects are also expressed mathematically. The mathematical background explained in the study details how analytical and numerical solutions are made and used in the solutions. In this study, a two-stage method was designed to examine the movements of a floating offshore platform.

In the first stage, a primary geometry that can be easily solved analytically and used in complex geometry was selected, and its analytical solution was made. Afterwards, the numerical solution of this simple geometry was made. Then, the aim was to verify the numerical solution by comparing this numerical solution with the analytical solution. The simple geometry chosen here is a floating vertical circular cylinder. AQWA, a submodule software within ANSYS Workbench, created the numerical solution. AQWA: It is a finite element-based software that works with meshing logic. The software works with the three-dimensional (3D) panel method. Theoretically, it is assumed that the fluid is ideal. Viscous effects are neglected.

In the second stage, the selected final complex geometry was solved by the validated numerical solution method. The numerical solution was compared with the experimental solutions applied in the laboratory environment on the same geometry, and because of this comparison, the realism of the numerical solution was discussed. The complex geometry whose results are examined is a mast-type floating offshore platform. The platform is designed to serve with a wind turbine on it. Especially when comparing sinking volumes, they resemble the primary geometry.

Satisfactory results were achieved in the first stage of the two-stage solution method. The analytical and numerical solutions' results were compatible with the verification study targeted for the numerical solution in the first stage. With this result, it can be said that the numerical method used is validated for this type of geometry.

In the second stage, satisfactory results were again obtained. The numerical solution verified by the experimental solution was applied to the final geometry. In the experiments, two separate basic scenarios with and without mooring lines were studied for different sea conditions. Studying two scenarios, with and without mooring lines, is valuable in evaluating the mooring effect.

For all parameters whose results were compared, the results were similar in the two basic scenarios. Increasing and decreasing trends were consistent in the intervals where the results were examined. The resulting levels are generally consistent for all parameters examined.

It has been observed that the responses in the results of the numerical solution are huge at points where the natural frequency is. The main reason for this situation is the extreme sensitivity of all examined parameters to frequency. In numerical solutions, natural frequency can be applied to the model with meagre error margins. This

situation captures the peak responses occurring at the natural frequency. In experimental solutions, frequency resolution is related to the capability of the experimental setup. Frequency resolution is limited compared to numerical solution. The limitation causes the peak responses at the natural frequency not to be captured. This situation was observed in all parameters and all scenarios examined.

Compatible results were obtained for both scenarios when the results with and without mooring lines were compared separately, showing that the solutions accurately reflect the mooring effect. It can be said that the solution methods applied for a mast-type floating offshore platform provide realistic and acceptable results. However, within the scope of this study, only wave-induced loads were investigated. In addition, it would be helpful to investigate the effects of wind and current-induced loads on the platform. However, considering that the significant loads for a floating structure are wave-induced, the results obtained in the study are valuable.

In addition to investigating the validity of the applied solutions, it was also investigated whether there was a danger of resonance during the economic life of the platform. For this purpose, natural frequencies were determined for the structure's motions.

Natural frequencies were determined using three different methods: analytical, numerical, and experimental. The values detected for all methods were compatible with each other. Based on this, it can be said that natural frequencies are reliable.

Afterwards, the most extreme sea conditions that the structure may encounter during its economic life were investigated. For this purpose, an attempt has been made to predict at which frequencies the most prominent wavelengths may occur in the Turkish seas. Additionally, Pierson-Moskowitz wave spectra were created for different sea states, and the frequencies at which the peak values of the spectra occurred were determined.

Finally, natural frequencies were compared with the frequency values for extreme sea conditions. It has been observed that the natural frequency values of the platform are much smaller than the frequencies expected in extreme sea conditions, showing no danger of resonance during the platform's economic life. This result is significant and optimistic regarding the applicability of a floating marine structure.

YÜZER AÇIK DENİZ PLATFORMLARININ HAREKETLERİNİN İNCELENMESİ

ÖZET

Türkiye ihtiyaç duyduğu enerjinin önemli bir kısmını ithal ettiği fosil yakıtlar vasıtası ile üreten bir ülkedir. Bu bağlamda hem atmosfere saldığı karbon salınımını sınırlaması; hem de dışa bağımlılığını azaltması açısından enerji üretim yöntemlerini çeşitlendirmeyi hedeflemelidir. Hedeflenen yeni yöntemlerin, sürdürülebilir ve çevreye olumsuz etkilerinin az olması gerektiği düşünüldüğünde yenilenebilir enerji kaynaklarından birine yönelmek mantıklı olacaktır.

Türkiye özelinde değerlendirildiğinde; en olası yenilebilir enerji kaynaklarından biri, bulunduğu coğrafyadaki potansiyeli açısından rüzgâr enerjisidir. Ülke bu potansiyeli görmüş ve özellikle son yıllarda rüzgâr enerjisi üretmek üzerine odaklanmıştır. Bu kapsamda karada konuşlanmış rüzgâr enerjisine büyük miktarda yatırım yapılmıştır. Ancak çok daha verimli ve potansiyel vadetmesine karşın açık deniz rüzgâr enerjisi alanında herhangi bir gelişme yaşanmamıştır. Bu durumun temel sebebi, Türkiye'yi çevreleyen denizlerin çok derin olmasıdır. Derin denizler doğrudan deniz tabanına entegre olan konvansiyonel açık deniz platformlarının inşasına teorik ve ekonomik açıdan imkân vermemektedir.

Şu anda açık deniz sahalarında konuşlanmış; üzerlerinde rüzgâr türbinleri veya hidrokarbon kaynakları işleyen rafineri tesisleri barındıran açık deniz platformları mevcuttur. Özellikle Batı Avrupa ülkelerinin açıklarında, Baltık Denizinde ve Britanya adalarının çevrelerinde pek çok örnek bulunmaktadır. Ancak buradaki platformların neredeyse tamamı yere entegre konvansiyonel platformlardır. Bahsi geçen sahalardaki denizlerin sığ olması, görece düşük maliyet ve eforla bu platformların faaliyet göstermesini sağlamaktadır.

Bunun yanında dünyanın çeşitli yerlerindeki açık deniz sahalarında, yüksek ekonomik gelir getirisi sunan hidrokarbon yataklarının işlenebilmesi için yarı batık tipte tasarlanmış yüzer platformlar mevcuttur. Ancak bu platformlar, yapım maliyeti çok yüksek ve bu çalışmada incelenenlere nazaran devasa yapılardır. Bu tarz platformların ciddi bir ekonomik potansiyel vadetmeden inşa edilmesi efektif ve mantıklı değildir.

Son yıllarda gelişen teknoloji, derin denizler için daha küçük boyutlarda yüzer açık deniz platform sistemlerinin tasarlanmasına ve imal edilebilmesine imkân sunmuştur. Ancak daha öncesinde bu imkanların olmaması sebebiyle dünya üzerinde örnekleri çok azdır. Bu sebepten ötürü bu tarz platformların AR-GE faaliyetleri henüz devam etmektedir. İdeal olan tasarım ve uygulama metotları henüz keşfedilmemiştir.

Türkiye, açık denizde bulundurduğu potansiyeli itibariyle açık deniz rüzgâr enerjisinden ziyadesiyle istifade edebilecek bir ülkedir. Bugüne kadar imkân dahilinde olmadığı için bu konu üzerine yapılan çalışmalar kısıtlıdır. Yapılan çalışmaların ciddi bir kısmı da platformların tasarımı ve hayata geçirilmesi üzerine odaklanmamıştır. Genellikle ülkenin bu konudaki ekonomik potansiyelinden, olası uygulama

sahalarından ve hangi yöntemlerle uygulanabileceğinden bahsedilmiştir. Bu tez çalışması bu eksikliğe binaen hazırlanmıştır.

Bunun yanında aynı zamanda çalışma kapsamında yüzer bir açık deniz platformunun konsept tasarımının nasıl oluşturacağına dair bir metodoloji de sunulmuştur. Bu metodolojinin sadece yüzer açık deniz rüzgâr türbinlerinin üzerinde kullanılması zorunlu değildir. Farklı amaçlara hitap eden yüzer açık deniz platformları için de bu çalışmadakine benzer bir metodoloji izlenebilir. Üç tarafı derin denizlerle çevrili bir ülke olan Türkiye'nin denizlerinden tam anlamıyla istifade edebilmesinin bir koşulu da açık deniz sahalarındaki faaliyetlerinin artmasından geçmektedir.

Yüzer açık deniz platformları, imal edilmesi ve ihtiyaç duyulan sahaya uygulaması oldukça zahmetli ve bir o kadar da maliyetli yapılardır. Yapıldıktan sonra da ekonomik ömrünü tamamlayacağı süre boyunca sürekli hizmet vermesi beklenen yapılardır. Gemiler gibi kendi tahrik sistemleri (hareket kabiliyetleri) olmadıkları ve devasa boyutlarda oldukları için uygulama sahasına yerleştirdikten sonra hareket etmeleri mümkün değildir. Bu sebeple yüzer açık deniz platformları için bakım onarım faaliyetleri gemilerdeki kadar uygulanması kolay bir prosedür değildir ve tasarım ömrünün sonuna kadar büyük çaplı bir bakım onarıma girmemeleri tercih edilir. Bütün bu bağlamda bir yüzer açık deniz platformu dizayn edilirken doğru tasarım konseptinin belirlenmiş olması hayati önem arz etmektedir.

Yüzer açık deniz platformları, kompleks geometrileri ve akışkan davranışının karmaşıklığı yüzünden, çoğu zaman konvansiyonel analitik yöntemler ile hareketlerinin incelemesi zor olan yapılardır. Bu nedenle sayısal yöntemlerden istifade edilerek platform hareketlerinin incelenmesi önemlidir. Ancak böylesi büyük yapılarda prototip üretmenin çok maliyetli olması nedeniyle yapılacak sayısal yöntemlerin deneysel çalışmalarla desteklenerek doğrulanması da ayrıca önemlidir.

Bu çalışma kapsamında ilk olarak yüzer açık deniz rüzgâr türbinlerinden ana hatlarıyla bahsedilmiştir. Türbin sisteminin çalışma prensibi, uygulama sahalarına göre platform çeşitleri, uygulama koşulları kısaca anlatılmıştır.

Sonrasında yüzer açık deniz yapılarının hareketlerinin teorik ve matematiksel arka planı incelenmiştir. Öncelikle tek serbestlik dereceli hareket ve bu hareketin alt bileşenleri detaylandırılmıştır. Buradan hareketle altı serbestlik dereceli hareket anlatılmıştır. Buna ek olarak hareketin kendisi ile beraber, harekete sebebiyet veren dış etkilerin de nasıl tespit edildiği de anlatılmıştır. Dış etkiler de yine matematiksel olarak ifade edilmiştir.

Çalışmada anlatılan matematiksel arka plan, analitik ve sayısal çözümlerin nasıl yapıldığını detaylandırmaktadır ve çözümlerde kullanılmıştır. Bu çalışmada yüzer bir açık deniz platformunun hareketlerinin incelenmesi için iki aşamalı bir yöntem kurgulanmıştır.

İlk aşamada analitik çözümü kolaylıkla yapılabilecek ve kompleks geometride kullanılan basit bir geometri seçilmiş ve analitik çözümü yapılmıştır. Sonrasında bahsi geçen bu basit geometrinin sayısal çözümü yapılmıştır. Ardından yapılan bu sayısal çözüm ile analitik çözüm kıyaslanarak sayısal çözümün doğrulanması amaçlanmıştır. Burada seçilen basit geometri yüzer dikey yuvarlak bir silindirdir. Sayısal çözüm için ise ANSYS Workbench içinde alt modül bir yazılım olan AQWA kullanılmıştır. AQWA; ağlama mantığıyla çalışan, sonlu elemanlar temelli bir yazılımdır. Yazılım üç boyutlu panel metodu ile çalışır. Teorik olarak akışkanın ideal olması ön kabulü vardır. Viskoz etkiler ihmal edilir.

İkinci aşamada doğrulanmış sayısal çözüm yöntemi ile seçilen nihai kompleks geometri çözülmüştür. Yapılan sayısal çözüm ile aynı geometri üzerine laboratuvar ortamında uygulanmış deneysel çözümler mukayese edilmiş ve bu mukayese neticesinde sayısal çözümün gerçekçiliği tartışılmıştır. Sonuçları irdelenen kompleks geometri, direk tipi yüzer bir açık deniz platformudur. Platform, üzerinde bir rüzgâr türbiniyle beraber hizmet verecek şekilde tasarlanmıştır. Özellikle batan hacimler kıyaslandığında basit geometri ile benzeşmektedir.

Yapılan iki aşamalı çözüm yönteminin ilk aşamasında tatmin edici sonuçlara ulaşılmıştır. İlk aşamada sayısal çözüm için hedeflenen doğrulama çalışmasında, analitik çözüm ile sayısal çözüm sonuçları oldukça uyumlu gelmiştir. Bu sonuç ile kullanılan sayısal yöntemin bu tarz bir geometri için doğrulandığı söylenebilir.

İkinci aşamada da yine tatmin edici sonuçlar elde edilmiştir. Nihai geometri üzerinde deneysel çözüm ile doğrulanmış sayısal çözüm uygulanmıştır. Deneylerde farklı deniz koşulları için bağlama hatları olan ve olmayan iki ayrı temel senaryo çalışılmıştır. Bağlama halatlarının olduğu ve olmadığı iki ayrı senaryonun çalışılması, halat etkisinin değerlendirilmesi açısından değerlidir.

Sonuçları kıyaslanan bütün parametreler için, iki temel senaryoda da sonuçlar benzeşmiştir. Sonuçların incelendiği aralıklarda artış ve azalış trendleri birbiriyle uyumlu gelmişlerdir. Sonuç mertebeleri de genel itibarıyla incelenen bütün parametreler için uyuşmaktadır.

Sayısal çözüme ait sonuçlardaki tepkilerin, doğal frekansın olduğu yerde noktasal olarak çok büyük çıktığı gözlenmiştir. Bu durumun temel sebebi incelenen bütün parametrelerin frekansa olan aşırı duyarlılığıdır. Sayısal çözümlerde doğal frekans çok düşük hata payları ile modele uygulanabilmektedir. Bu da doğal frekansta oluşan pik tepkilerin yakalanabilmesine olanak sağlamaktadır. Deneysel çözümlerde ise frekans çözünürlüğü deney düzeneğinin kabiliyeti ile alakalıdır. Frekans çözünürlüğü sayısal çözüme nazaran kısıtlıdır. Bu da doğal frekanstaki pik tepkilerin yakalanamamasına sebep olmaktadır. Bu durum incelenen bütün parametrelerde ve bütün senaryolarda gözlenmiştir.

Bağlama halatlarının olduğu ve olmadığı sonuçlar ayrı ayrı kıyaslandığında iki senaryo için de uyumlu sonuçlar alınmıştır. Bu da çözümlerin demirleme etkisini doğru yansıttığını göstermektedir.

Direk tipi yüzer bir açık deniz platformu için uygulanan çözüm yöntemlerinin için gerçekçi ve kabul edilebilir sonuçlar verdiği söylenebilir. Ancak bu çalışma kapsamında yalnızca dalga kaynaklı oluşacak yükler araştırılmıştır. Bunun yanında rüzgâr ve akıntı kaynaklı yüklerin de platforma oluşturacağı etkilerin araştırılması faydalı olacaktır. Ancak yüzer bir yapı için majör yüklerin dalga kaynaklı yükler olduğu düşünüldüğünde çalışmada elde edilen sonuçlar değerlidir.

Uygulanan çözümlerin geçerliliğinin araştırılmasının yanında platformun ekonomik ömrü boyunca rezonansa girme tehlikesi olup olmadığı da araştırılmıştır. Bunun için öncelikle yapının hareketleri için doğal frekanslar belirlenmiştir.

Doğal frekanslar analitik, nümerik ve deneysel olmak üzere üç farklı yöntemle tespit edilmiştir. Bütün yöntemler için tespit eden değerler birbiriyle uyumlu gelmiştir. Buradan hareketle doğal frekansların güvenilir olduğu söylenebilir.

Sonrasında yapının ekonomik ömrü boyunca karşılaşabileceği en ekstrem deniz koşulları araştırılmıştır. Bunun için Türkiye denizlerinde oluşabilecek en büyük dalga

boylarının hangi frekanslarda oluşacağı öngörülmeye çalışılmıştır. İlaveten farklı deniz durumları için Pierson-Moskowitz dalga spektrumları oluşturulmuş ve spektrumların pik değerlerinin hangi frekanslarda oluştuğu tespit edilmiştir.

Son olarak doğal frekanslar ile en ekstrem deniz koşulları için tespit edilen frekans değerleri kıyaslanmıştır. Platforma ait doğal frekans değerlerinin ekstrem deniz koşullarının beklendiği frekanslardan çok daha küçük olduğu görülmüştür. Bu durum platformun ekonomik ömrü boyunca rezonansa girme tehlikesinin olmadığını göstermektedir. Bu da yüzer bir deniz yapısının uygulanabilirliği açısından oldukça önemli ve olumludur.

1. INTRODUCTION

The increasing population and developing technology in the world also cause an increase in energy demand. Countries have turned to different methods from past to present to supply this demand. Fossil fuels were used extensively to meet the increasing demand in the 19th and 20th centuries. Intensive use of fossil fuels has caused an increase in carbon emissions and a greenhouse gas effect. Following this, the global warming process accelerated. In particular, the visible effects of the warming process from the end of the 20th century to the present have increased. This significant change has directed countries toward alternative energy production methods that produce lower carbon emissions.

Today, population growth, industrialization, technological breakthroughs in the world, the increasing demand for energy, and global warming have directed the agenda of societies to determine how energy supply will be. Today, we no longer focus only on the amount produced when producing energy. In addition, the environmental effects of the energy production method are also considered. Besides all these, producing energy from finite sources poses a danger in future projections. Renewable energy sources also come to the fore in this sense.

Türkiye is a developing country with a population that is regularly increasing. For this reason, the amount of energy needed is increasing daily. Considering its resources, the country produces a significant part of the energy it needs through imported fossil fuels. Considering global climate change and foreign dependency, Türkiye should diversify its energy production portfolio.

One of the most probable renewable energy sources is wind energy in terms of its potential in its geography. The country has seen this potential and has produced wind energy inland, especially in recent years. As seen in Figure 1.1, the cumulative installed capacity for wind power plants in Türkiye is increasing regularly [1].

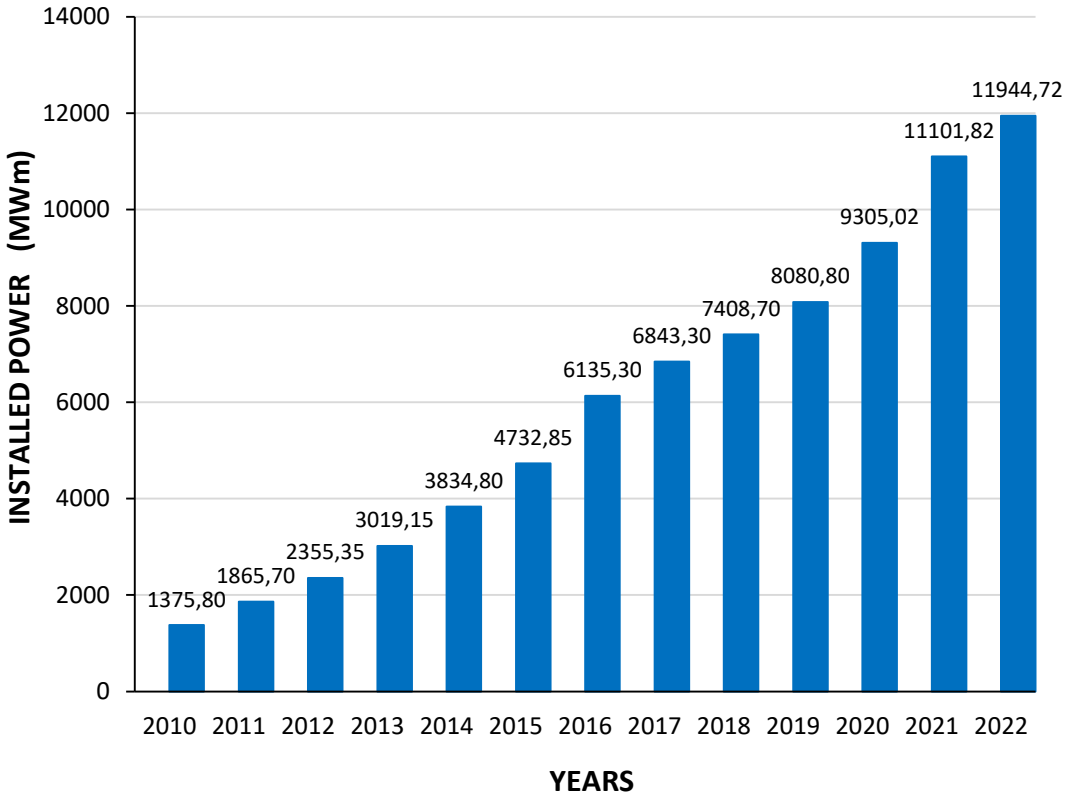

Figure 1.1 : Cumulative installations for wind power plants in Türkiye [1].

However, although it is much more efficient and has potential, there has been no development in offshore wind energy. The main reason for this situation is that the seas surrounding Türkiye are deep. Deep seas do not allow the construction of conventional offshore platforms directly integrated into the seabed, theoretically and economically.

Semi-submerged floating platforms are available to process hydrocarbon deposits that provide high economic income in offshore fields in various parts of the world. However, these platforms have very high construction costs and are massive structures compared to those examined in this study. Building such platforms without promising a severe economic potential is impractical and logical.

Developing technology in recent years has enabled the designing and manufacturing smaller floating offshore platform systems for deep seas. However, few examples exist worldwide since these opportunities were not available before. For this reason, the R&D activities of such platforms are continuing. Ideal design and application methods have not yet been discovered.

Türkiye is a country that can benefit significantly from offshore wind energy due to its potential. Studies on this subject are limited because building these platforms has not been possible to date. A significant part of the studies did not focus on the design of the platforms. Generally, the economic potential of the country in this regard, as well as possible application areas and methods, are mentioned. This thesis study was prepared based on this deficiency.

In addition, a methodology for creating the concept design of a floating offshore platform is also presented within the scope of the study. This methodology is not necessarily used only on floating offshore wind turbines. A methodology used in this study can be followed for floating offshore platforms that serve different purposes. As a country surrounded by deep seas on three sides, one of the conditions for Türkiye to fully benefit from its seas is to increase its activities in offshore areas.

Floating offshore platforms are laborious and costly to manufacture and apply to the required site. These structures are expected to provide continuous service after they are built throughout their economic life. Since they do not have a propulsion system (mobility) like a ship and are gigantic, moving them after placing them in the application area is impossible. For this reason, maintenance and repair activities for floating offshore platforms are not as easy to implement as a ship, and it is preferred not to undergo large-scale maintenance and repair until the end of the design life. In this context, the correct design concept must be determined when designing a floating offshore platform.

Floating offshore platforms are buildings whose motions are often complex and challenging to examine with conventional analytical methods due to their complex geometries. For this reason, it is essential to solving the platform motions using numerical methods. However, since producing prototypes for such large structures is very costly, verifying the numerical methods with experimental studies is also essential.

In this study, a two-stage method was designed to examine the motions of a floating offshore platform. First, a simple geometry that can be solved analytically and is frequently used in complex geometries was selected, and its analytical solution was made. Afterwards, the numerical solution of this simple geometry was made. Then, the numerical solution was validated by comparing this numerical solution with the analytic solution. The selected final complex geometry was solved in the second stage

with the validated numerical solution method. The numerical solution was compared with the experimental solutions applied in the laboratory environment on the same geometry, and because of this comparison, the realism of the numerical solution was discussed.

Within the scope of the study, floating offshore wind turbines are first mentioned in the outline in Section 2. Wind turbine operating principles, which types of offshore platforms can be applied to which areas, and what kind of potential wind turbines promise in which areas are mentioned.

Section 3 first focused on the movements of floating offshore platforms in waves. Single degree of freedom (DOF) motion and its subcomponents are detailed. Then, based on this, the background of the six degrees of freedom motion for analytical and numerical solutions is explained. Afterwards, in Section 3, the wind and wave climate in the world's seas are explained and how the related wave conditions are determined. Short-term and long-term wave climate trends are mentioned. The methods mentioned here were used in Section 5, the later part of the thesis, where the expected platform movements are examined.

In Section 4, the first of the two-stage method is detailed. A vertical circular cylinder was chosen as the simple geometry. First, this geometry was solved analytically. Then, this geometry was modelled in ANSYS AQWA, the software used to make and solve the problem numerically. AQWA is a submodule software accessed from within ANSYS Workbench. The software uses the 3D panel method. It is a software that works with mesh logic and provides solutions using the finite element method. The program was validated by making and comparing analytical and numerical solutions, and whether it was suitable for such a numerical solution was investigated.

In Section 5, the second of the two-stage method is detailed. A spar-type floating offshore platform, previously tested and studied, was chosen as the complex geometry. This platform is modelled into AQWA and solved numerically. Then, the convergence of the obtained solutions and the experimental results was investigated. The study's results have been tested to determine whether they present a realistic approach. In addition, it was investigated whether the platform could be applied to Turkish seas regarding wave climate with the obtained parameters.

2. FLOATING OFFSHORE WIND TURBINES

2.1 General Information about Wind Turbines

Wind turbines aim to produce electric energy by using the wind current. A wind turbine generally consists of a tower, generator, speed converters (gearbox), electrical-electronic elements, and rotor. Wind's kinetic energy is converted into mechanical energy in the rotor, and the rotational movement of the rotor shaft is accelerated and transferred to the generator in the body. The electrical energy obtained from the generator is stored in batteries or delivered directly to the buyers [2].

Although existing wind turbines vary in size and type, the first thing to consider is the axis of rotation. Wind turbines are divided into two classes according to their axis of rotation: "Horizontal Axis Wind Turbines" (HAWT) and "Vertical Axis Wind Turbines" (VAWT). The mentioned turbine types are given in Figure 2.1.

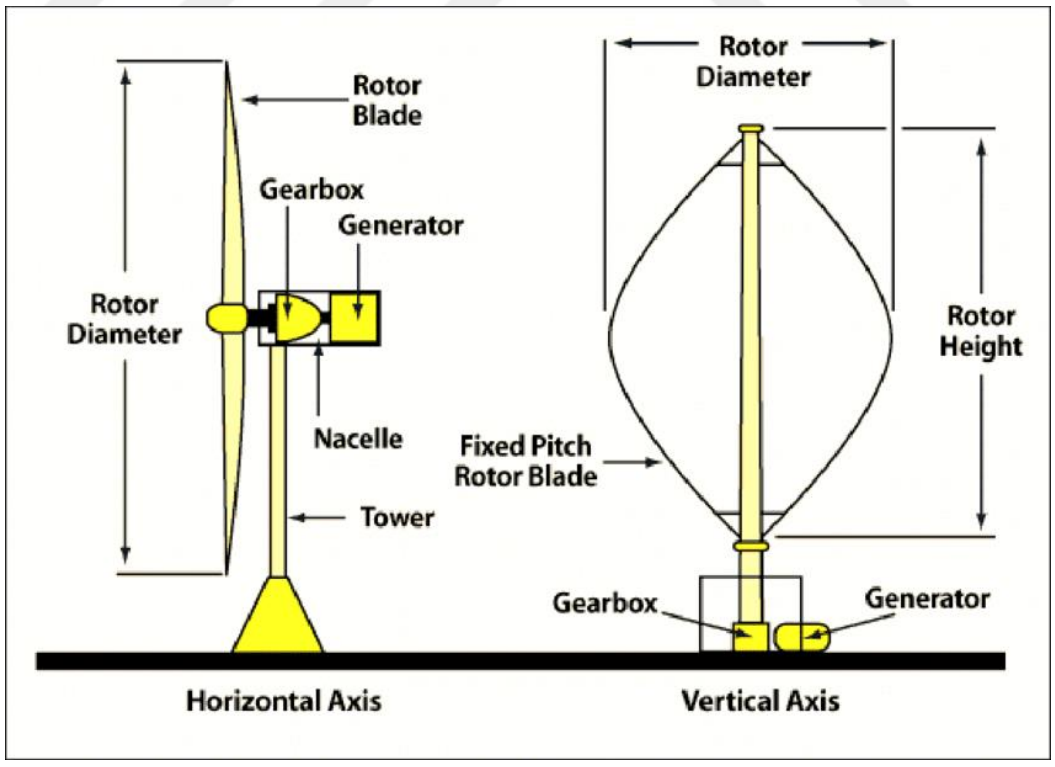

Figure 2.1 : Shape of HAWT and VAWT [3].

2.1.1 Vertical axis wind turbine (VAWT)

Vertical Axis Wind Turbines (VAWT) are designed with their vertical axis perpendicular to the ground. They are always adjusted to the direction of the wind, and their horizontal axis does not need to be adjusted to the wind. Usually, it requires an electric motor for the first move. The turbine is fixed from its axis with auxiliary wires. The device's efficiency is low since it receives less wind in places close to sea level. Although having all the necessary equipment at ground level is advantageous, it has many adverse effects on environments such as marine and agricultural lands. For example, when the VAWT system is installed in the sea, critical parts are likely to be damaged by the adverse effects of the sea in adverse weather conditions because the essential elements of the turbine are close to the water level. In addition, the wind potential increases as it goes up from the water level [4, 5]. For these reasons, the application of VAWTs at sea has been limited. Another disadvantage is that the technical equipment may be damaged in the storm conditions.

2.1.2 Horizontal axis wind turbine (HAWT)

Another critical design is the HAWT, called the “Horizontal Axis Wind Turbine”. The axis of rotation is designed to parallel the ground. With the help of an electric motor, the rotor direction can be adjusted according to the wind direction. HAWT systems must be at least 30 meters above sea level to operate efficiently [4, 6]. The latest offshore wind turbines installed in the China Sea are 250 meters above sea level [7]. This height varies according to the wind profiles. The desired wind speed should be selected to determine the hub height value. Wind power classification is given in Table 2.1. While choosing the wind speed, the wind potential and class in the study area should be considered.

Table 2.1 : Wind power classification [8].

Wind Power Class	Resource Potential	Wind Power Density at 50 m (W/m^2)	Wind Speed at 50 m (m/s)
1	Poor	0 - 200	0.0 - 4.4
2	Marginal	200 - 300	4.4 - 5.0
3	Fair	300 - 400	5.0 - 5.5
4	Good	400 - 500	5.5 - 5.9
5	Excellent	500 - 600	5.9 - 6.3
6	Outstanding	600 - 800	6.3 - 7.0
7	Superb	> 800	> 7.0

The hub height can be calculated according to the desired wind speeds. Equation 2.1 is used to calculate hub height.

$$U_{h_{hub}} = U_{h_{ref}} * \left[\frac{ln\left(\frac{h_{hub}}{z_0}\right)}{ln\left(\frac{h_{ref}}{z_0}\right)}\right] \quad (2.1)$$

In equation 2.1, the desired height and wind speed are taken as references. The wind speed at the height (in our case, the hub height) is calculated.

In the formula

h_{ref} : Referenced height;

$U_{h_{ref}}$: Wind speed at the reference height;

h_{hub} : Altitude at which wind speed is sought;

$U_{h_{hub}}$: Wind speed at searched altitude;

z_0 : Roughness length.

Roughness length values are shared in Table 2.2.

Table 2.2 : Roughness length (z_0) [9].

Roughness Class	Roughness Length (m)	Landscape Type
0	0.0002	Water surface
0.5	0.0024	Completely open terrain with a smooth surface, e.g., concrete runways in airports, mowed grass, etc.
1	0.03	Open agricultural area without fences and hedgerows and very scattered buildings. Only softly rounded hills
1.5	0.055	Agricultural land with some houses and eight-metre-tall sheltering hedgerows at approximately 1,250 metres
2	0.1	Agricultural land with some houses and eight-metre-tall sheltering hedgerows with approximately 500 metres
2.5	0.2	Agricultural land with many places, shrubs and plants, or eight-metre-tall sheltering hedgerows with a length of approx. 250 metres
3	0.4	Villages, small towns, agricultural land with many or tall sheltering hedgerows, forests, and very rough and uneven terrain
3.5	0.8	Larger cities with tall buildings
4	1.6	Massive cities with tall buildings and skyscrapers

As seen in Table 2.2, the roughness length (z_0) value at the water surface is minimal. For this reason, the efficiency loss due to roughness is very low on the water surface, so the HAWT systems are more suitable for offshore applications.

2.1.3 The internal structure of a wind turbine

Figure 2.2 shows the internal structure of a wind turbine.

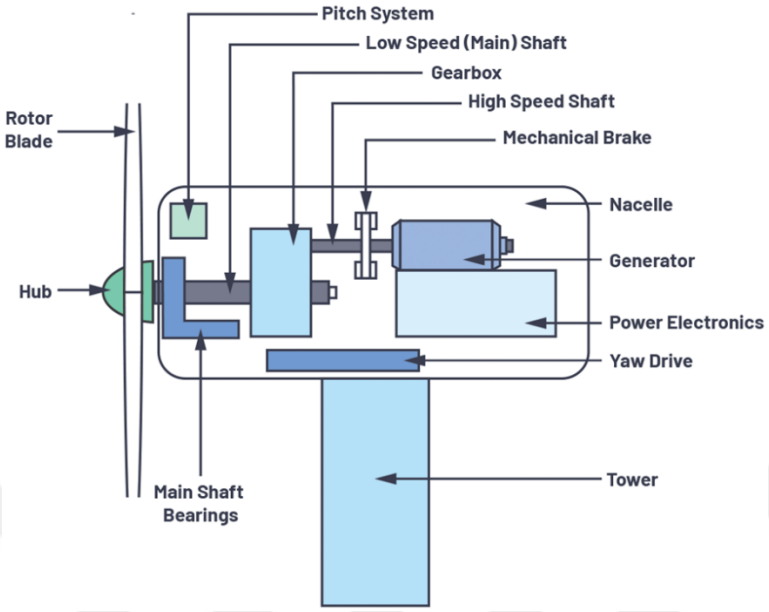

Figure 2.2 : Internal structure of a wind turbine [10].

2.1.3.1 Nacelle (Body)

Nacelle includes vital parts of the wind turbine, including the gearbox and electricity generator. Service personnel can enter the machine from the turbine tower to the wind turbine rotor, the rotor blades, and the hub.

2.1.3.2 Rotor blades

Rotor blades catch the wind with their aerodynamic structure and transfer the power of the wind to the rotor hub. Rotor blades are designed like aeroplane wings because of the similar working principle. The rotor blade length varies in a modern wind turbine. Recently, examples of rotor blade lengths exceeding 100 meters are frequently encountered. Finally, there is a Vestas brand V236 model turbine with a rotor diameter of 236 meters. The rotor blade length of this turbine is 115.5 meters. It is the wind turbine with the most extended rotor blade length as of the date of the study [11].

2.1.3.3 Rotor hub

The rotor hub is the part that connects the rotors, and it connects to the low-speed shaft of the wind turbine. In the turbine's drive-train, turbine blades fit into the hub connected to the turbine's main shaft for inland-type wind turbines. An offshore wind

turbine has a direct-drive hub system. Turbine blades fit into the hub connected to the turbine's generator [6].

2.1.3.4 Low-speed shaft

The low-speed shaft of the wind turbine connects the rotor hub to the gearbox. In a typical 600 kW wind turbine, the gear rotates relatively slowly, at 19 – 30 revolutions per minute (rpm). In models above 2000 kW, which provide more outstanding energy production, the number of revolutions per minute falls to 8-20. This shaft contains pipes for the hydraulic system to operate the aerodynamic brakes [4, 6].

2.1.3.5 Gearbox

The gearbox has a low-speed shaft on one side, allowing the high-speed shaft on the other to rotate up to 50 times faster than the low-speed shaft. It transfers the low-speed shaft rotating at 8-20 rpm to the high-speed shaft at 1000-1800 rpm. The drive-train comprises the rotor, main bearing, main shaft, gearbox, and generator. The drive-train converts the low-speed, high-torque rotation of the turbine's rotor (blades and hub assembly) into electrical energy [4, 6].

2.1.3.6 High speed with its mechanical brake

The high-speed mechanical drives the electricity generator. It has an emergency mechanical brake, used when the aerodynamic brakes fail or the turbine is in service [4, 6].

2.1.3.7 Electrical generator

The generator is synchronous or asynchronous. The value of electrical power for wind turbines varies. Wind velocity, roughness length, and hub height are the main factors determining electrical power. Some turbines are primarily between 0.5 MW and 5.0 MW for the inland type. These values remain low, especially when considered offshore. Models that produce electricity at this level in offshore models are entry-level. 5.0 – 10.00 MW models are frequently used [4, 5, 12]. Examples that produce up to 15 MW of energy are available [11]. However, there are wind turbine applications that fall below or above these ranges.

2.1.3.8 Electronic control unit (Electronic controller)

The electronic control unit contains a computer that constantly monitors the status of the wind turbine and controls the tilt mechanism. In case of a malfunction (for example, overheating the gearbox or generator), it automatically stops the wind turbine and warns the turbine operator's computer via the telephone modem line.

2.1.3.9 Hydraulics system

The hydraulics system is the part that contains the wind turbine's aerodynamic brakes.

2.1.3.10 Cooling unit

The cooling unit includes a unit used to cool the generator. Moreover, it contains a unit to cool the gearbox's oil.

2.1.3.11 Tower

The tower of the wind turbine carries the nacelle and rotors. Usually, the higher tower is an advantage. Because as the hub of the turbine rises above the ground, the speed potential of the wind increases. A typical 600 kW wind turbine has a 40-60 meters tower [4]. However, for offshore models, tower height often varies with the site [12]. Finally, there is a Vestas brand V236 model turbine with a tower height of 280 meters. The V236 currently has the tallest tower height in the world. The towers can be circular or lattice. Circular towers contain an interior staircase to reach the turbine's top, providing a safer working environment for the service personnel to look after the turbines. The main advantage of lattice towers is that they are cheaper than lattice ones.

2.1.3.12 Yaw mechanism

The yaw mechanism turns the rotor and nacelle against the wind. Electric motors are used for this maneuverer mechanism and are operated by the electronic control unit, which detects the wind direction using the wind wane. Typically, the turbine only tilts a few degrees when the wind changes direction.

2.1.3.13 Anemometer and wind wane

An anemometer (wind gauge) and wind wane are used to measure the speed and direction of the wind. The electronic signals from the anemometer are used by the electronic control unit of the wind turbine to operate the wind turbine when the wind

speed approaches about 5.0 m/s [4, 6]. The computer automatically stops the turbine when the wind speed exceeds 25.0 m/s to protect it and its surroundings [4, 6]. These value ranges also apply to offshore wind turbine models. [12, 13]. The minute hand is used by the electronic control unit of the wind turbine to turn the Wind turbine against the wind to turn it against the wind.

2.1.4 Working principle of wind turbines

The primary purpose of wind turbines is to produce electric energy. First, the rotor blades collect the incoming wind and convert it into rotational motion. In the second stage, the shaft transmits the rotational motion to the generator. Meanwhile, the gearbox increases the speed between the rotor and the shaft, allowing faster movement to be transferred to the generator. So, the efficiency is improved. Then, the generator generates electrical energy from the rotational motion. After this stage, electricity is directed to the transmission line with the help of electronic equipment. The electricity that reaches the electrical grid last is distributed for use [4, 6]. The working principle diagram of wind turbines is shared in Figure 2.3.

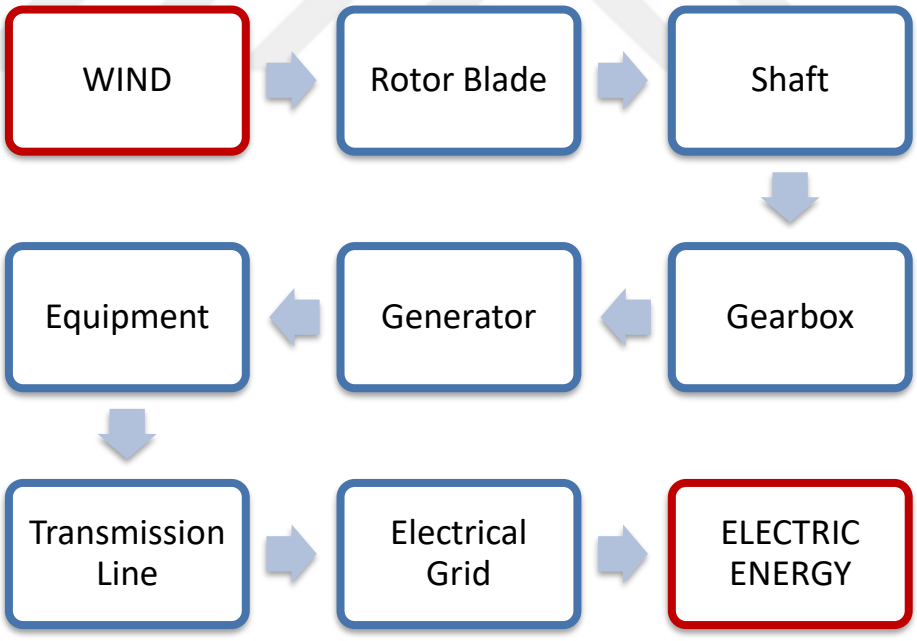

Figure 2.3: Principle of working wind turbines.

2.1.5 Benefit-cost analysis of wind turbines

Two considerations should be considered when making a cost-benefit analysis for wind turbines. These issues are the amount of energy produced and the installation-operation costs, and these parameters may vary according to the application areas.

Wind speed and rotor diameter are needed to calculate the energy produced by a wind turbine. Theoretically, the rotor diameter should increase to increase the energy produced, which means that the wind turbine's height also increases. This way, more wind is obtained, and a faster rotational movement is provided.

Generally, wind turbines operate at total capacity when the wind speed arrives at 15 m/sec. The system automatically stops when the wind speed arrives at 25 m/sec [14]. Because of the danger and damage the system can create at high speeds, and many systems are stopped when the turbine accelerates too much. As can be understood from here, the increase in the blowing wind intensity does not mean that the energy production capacity will increase. Regular and moderate winds are more favourable in energy efficiency than discontinuous wind profiles, and such wind profiles are more likely to be achieved offshore and on shorelines. The graph of the relationship between rotor diameter and power output is shared in Figure 2.4 [15].

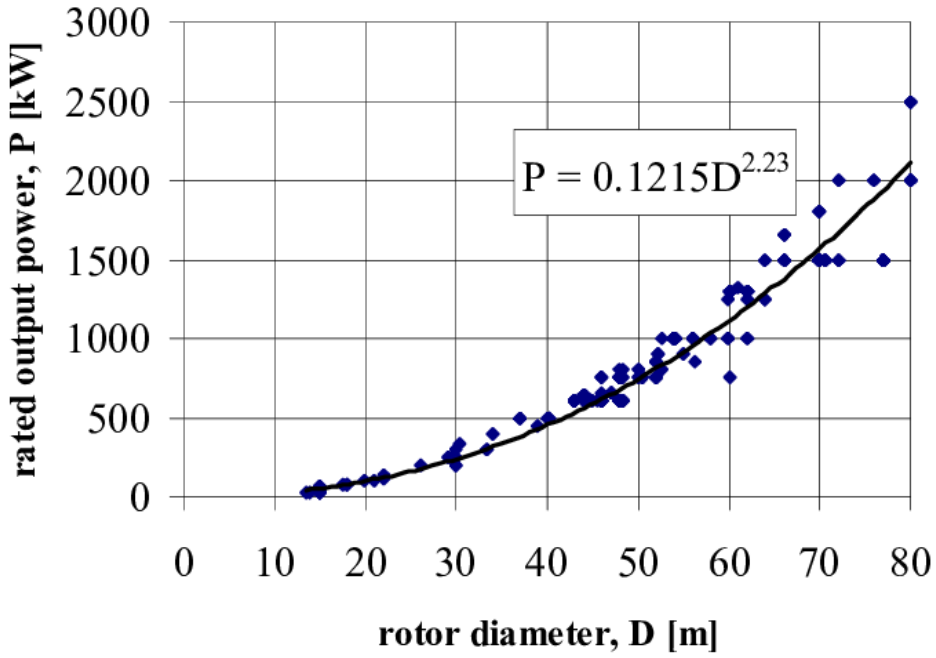

Figure 2.4 : Relationship between rotor diameter and power output [15].

$$P = 0.1215 * D^{2.23} \tag{2.2}$$

An empirical relationship (equation 2.2) was established between energy production and rotor diameter in a study based on examples [15]. As seen in Figure 2.4, increasing the rotor diameter is very efficient for energy production. Large windy areas are required for a large rotor radius, and obtaining them only onshore or offshore is possible.

2.1.6 Capacity factor

The capacity factor is one of the critical factors determining wind turbine production, and it is a coefficient representing how long energy can be produced during a year. While making these calculations, many parameters, such as annual wind profiles and planned-unplanned maintenance-repair shifts, are considered. In particular, the continuous and intense offshore wind profiles enable offshore wind turbines to have much higher capacity factor coefficients. The wind atlas of Türkiye is shown in Figure 2.5.

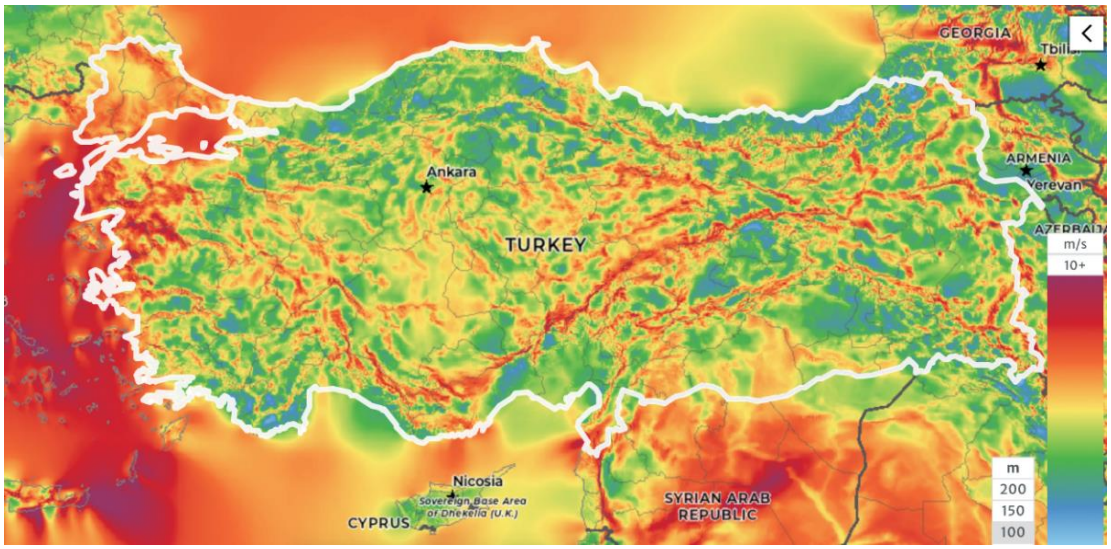

Figure 2.5 : Wind map of Türkiye [16].

As seen in Figure 2.5, there is a much higher wind potential on the seas than on the land. Especially considering the roughness calculation, the sea surface will be much more favourable than the land. As the wave goes from the coast to offshore, the roughness coefficient will decrease further as the wave decreases, which means that the energy produced by the wind turbine will increase.

2.2 Wind Turbines at Sea

Wind turbines can be installed inland, onshore, or offshore. All three alternatives have advantages and disadvantages. Regarding a primary trend, the construction cost and implementation difficulty increase from land to offshore. However, energy production efficiency increases from land to offshore while the risk of environmental damage decreases. When long-term and significant investments are considered, it becomes

advantageous to prefer offshore applications. Wind turbine comparisons according to their location are shared in Figure 2.6.

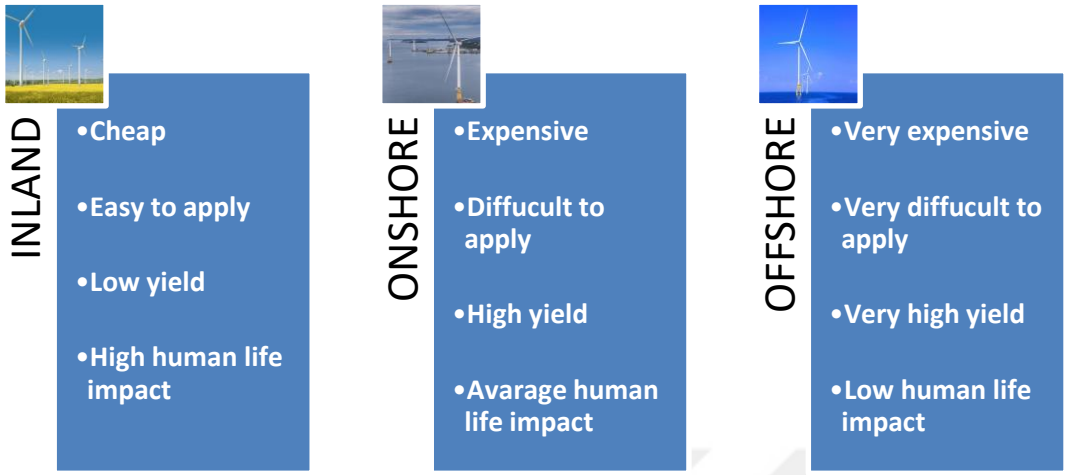

Figure 2.6 : Comparison of inland, onshore, and offshore applications.

2.2.1 Onshore wind turbines

Onshore or coastal wind turbines can be referred to as turbines that use offshore wind in the coastal region. Such turbines can be placed on land or in the sea area. We can call onshore wind turbines the wind turbines placed in the sea and the coastal region. These turbines are located on what is called the continental shelf. It has various applications according to depth, sea, and ground conditions, and shallow and medium-depth waters are the application areas. Onshore wind turbine concepts are shared in Figure 2.7 [17]. As the figure shows, onshore platform types become more complex and challenging to implement as you move from shallow to deeper waters.

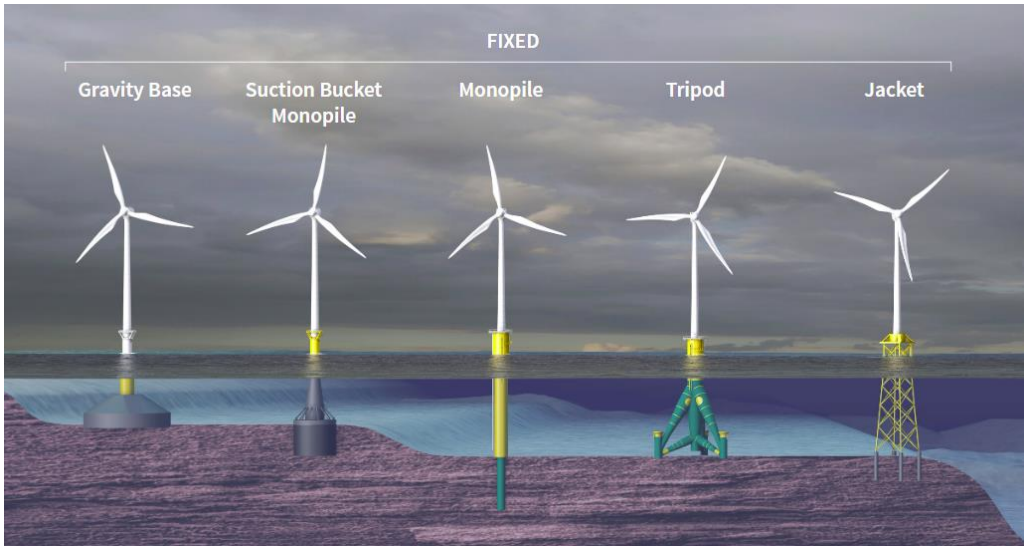

Figure 2.7 : Onshore wind turbine concepts [17].

For complex solutions, the initial setup costs of the platform also increase. However, it is still possible to produce solutions with direct access to the seafloor, as the onshore platforms are in the continental shelf region. These solutions are more accessible than floating systems, so they can be made cheaper.

Onshore wind turbines should not be near the shore because human activities exist in the coastal region. Ports, maritime transport lines, and commercial and tourism activities are concentrated on the coastlines. At the same time, the seaside is a socialising area for people. Installing wind turbines on abruptly deepening coastal profiles creates wind turbine farms close to the shore, negatively affecting daily life. Onshore wind turbines should be as far from the shore as possible to avoid adversely affecting these activities. There is a depth restriction since it cannot be used after a certain depth for onshore wind turbines. However, it is the ideal solution for shallow seas. The northwest coast of the European continent is like a gigantic continental shelf. The British Isles and surrounding areas, the Dutch coast, the northern coast of France, the Baltic Sea and the North Sea contain vast shallow seas [18]. This situation can be confirmed by the bathymetry maps in Figure 2.8 and Figure 2.9.

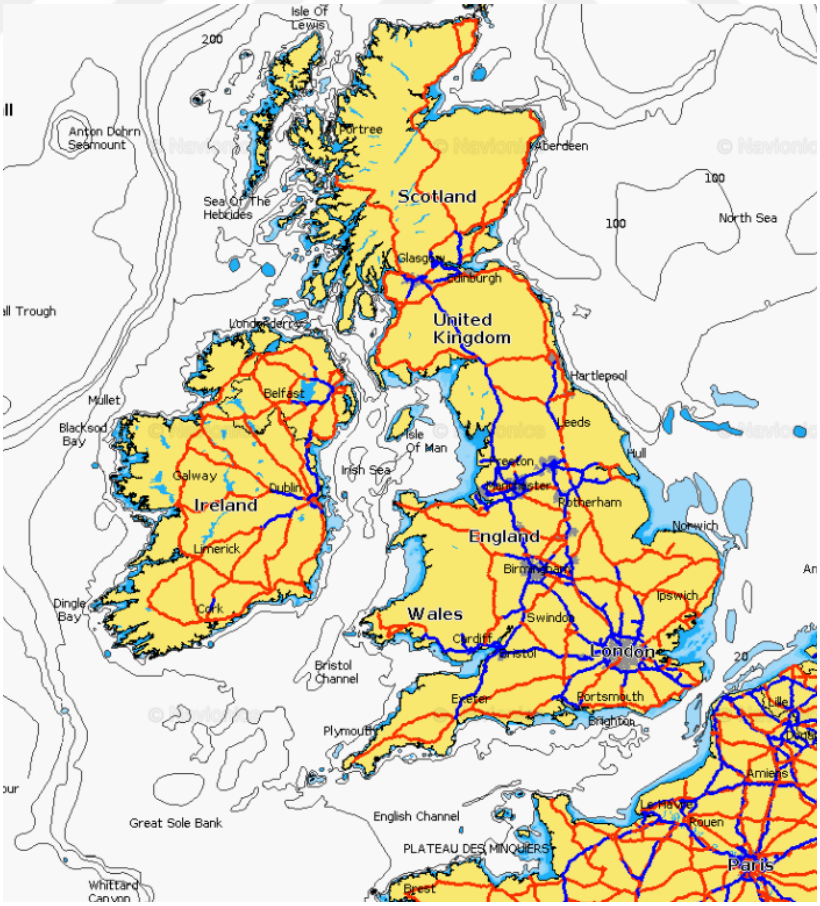

Figure 2.8 : Depths of the seas surrounding the British Isles [18].

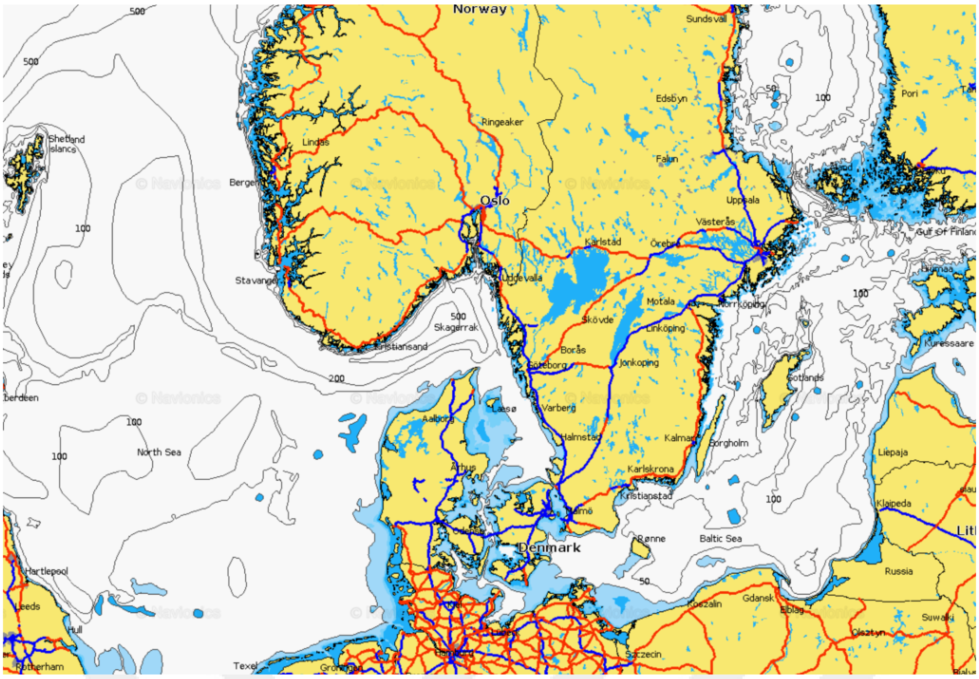

Figure 2.9 : North and Baltic Sea Depths [18].

Türkiye consists of two peninsulas called Eastern Thrace and Anatolia, which are geographically surrounded by seas. Thanks to its expansive shorelines, it has a severe potential for onshore and offshore wind turbines. However, Türkiye's seas suddenly got deeper. For this reason, onshore turbines can only be installed close to the shoreline, and this should not be preferred as it will adversely affect human activities. Therefore, Turkish seas are generally unsuitable for onshore wind turbines [5, 18]. It can be confirmed from the bathymetry map in Figure 2.10 that the Turkish seas are deep.

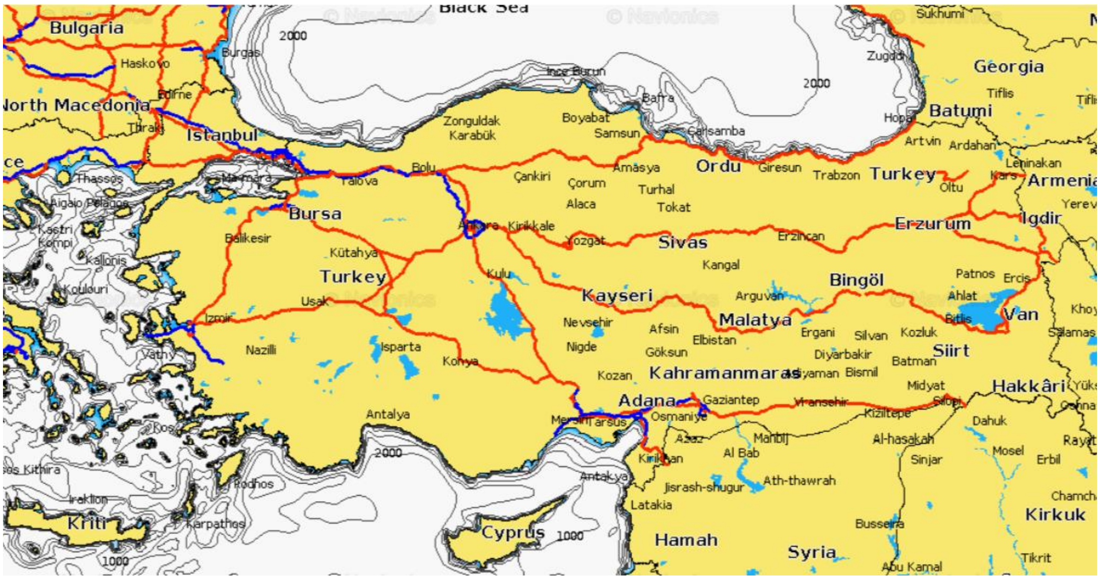

Figure 2.10 : Depths of Turkish seas [18].

2.2.2 Offshore wind turbines

Offshore-type or floating offshore wind turbines are used for offshore conditions away from the coast and the continental shelf. They are the preferred solutions, especially for situations where the seas are deep. Applications of this type of turbine are provided with complex solutions and high costs. However, the turbines have high efficiency, and since they are far from the coast, they have minimal adverse effects on aquatic life and human life.

Thanks to their high efficiency, offshore wind turbines can provide a high energy gain after the depreciation period. The farther from the shore, the more severe the wind regimes become. Besides, the roughness length (z_0) decreases and approaches zero, which is the ideal working environment for a wind turbine, and these conditions provide high efficiency for the wind turbine. Floating offshore wind turbine types are shared in Figure 2.11 [19].

Figure 2.11 : Offshore wind turbine types [19].

Deep seas surround Türkiye, making offshore wind turbine options more convenient. The openings of the Dardanelles, the Northern Aegean, and the Western Black Seas contain high-profile wind fields. However, floating offshore wind turbine types must be used due to the high depths, and Onshore-type (sitting on the seabed) platforms cannot be used. The bathymetry maps shared in Figure 2.12, Figure 2.13 and Figure 2.14 can confirm sea depths in the mentioned areas.

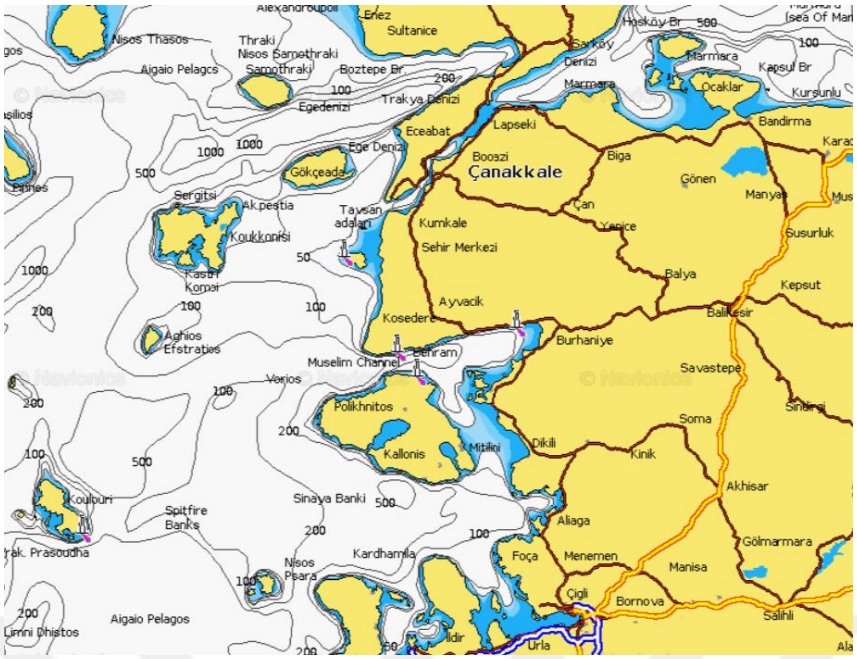

Figure 2.12 : Depths of the openings of Dardanelle Strait and North Aegean Sea's Turkish side [18].

Figure 2.13 : Depths of the openings of the Turkish Black Sea's west part [18].

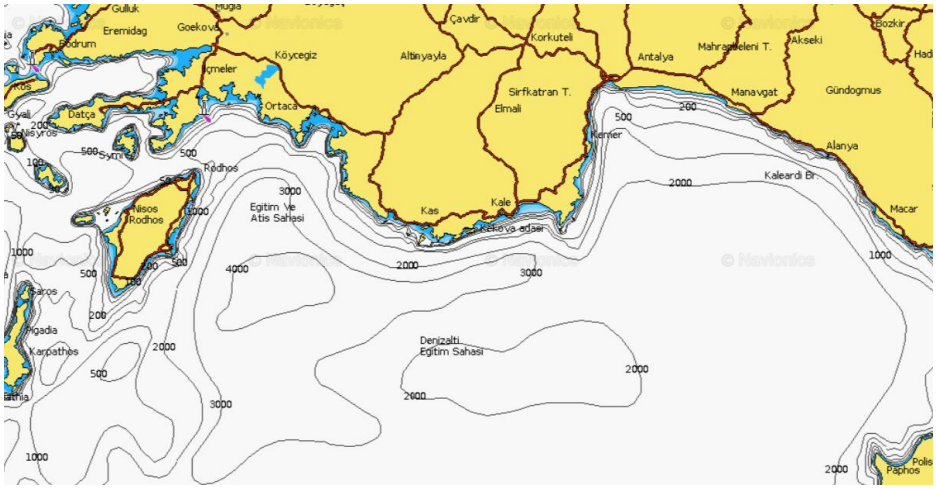

Figure 2.14 : Depths of the openings of the Turkish Mediterranean Sea's west part [18].

3. MOTIONS OF FLOATING OFFSHORE STRUCTURES IN WAVES

Prediction of responses of a floating offshore structure in a random seaway involves dynamics (the determination of the forces imposed by the seaway on the structure) and kinetics (the determination of the motions resulting from the forces imposed by the seaway).

It has been found that the irregular motions of a floating structure in a seaway can be described as the linear superposition of the responses of the floating structure to all the wave components of such a seaway. This superposition principle requires knowledge of the sea components and the floating offshore structure's responses to them. Hence, the vitally crucial linear theory of motions in simple regular waves is developed.

Section 3.1 derives a single degree of freedom equation of motion for a floating structure in regular waves. The crucial step in calculating the motions of the floating structure in regular waves is to predict the wave forces acting on the structure. These forces consist of dynamic pressure and diffraction components. The linear wave theory assumptions could easily predict the dynamic pressure or Froude-Krylov wave force. Alternative formulations are suggested for the diffraction force component. Section 3.1 explains the development of harmonic motion for a floating body, linear wave theory, and the principle of linear superposition in water waves. What the Response Amplitude Operator produced depending on frequency is mentioned.

Section 3.2 presents the equations of motion for the general case of six degrees of freedom in regular waves and the hydrodynamic forces evaluated based on potential theory. Strip theory is then described as a convenient way to perform the calculations under the assumption of a slender body. Again, Section 3.2 mentions the assumptions of AQWA, the software in which the numerical solution is made, and how it calculates the wave force for the zero forward speed situation.

Section 3.3 presents the application of the spectral response analysis technique to predict the seakeeping responses in a random seaway defined by a wave spectrum formulation.

3.1 Single Degree of Freedom Equation of Motion

The single-degree motion of a floating body in waves can be considered a spring-mass system moving under linear excitation forces and moments. The motion characteristics of such a system depend on the wave frequency. The linear behaviour of such a system in only one axis is a motion with one degree of freedom.

As a typical example of a single degree of motion, we can consider the heave motion of a floating body in regular waves as represented by a mass-spring-damper system, as shown in Figure 3.1.

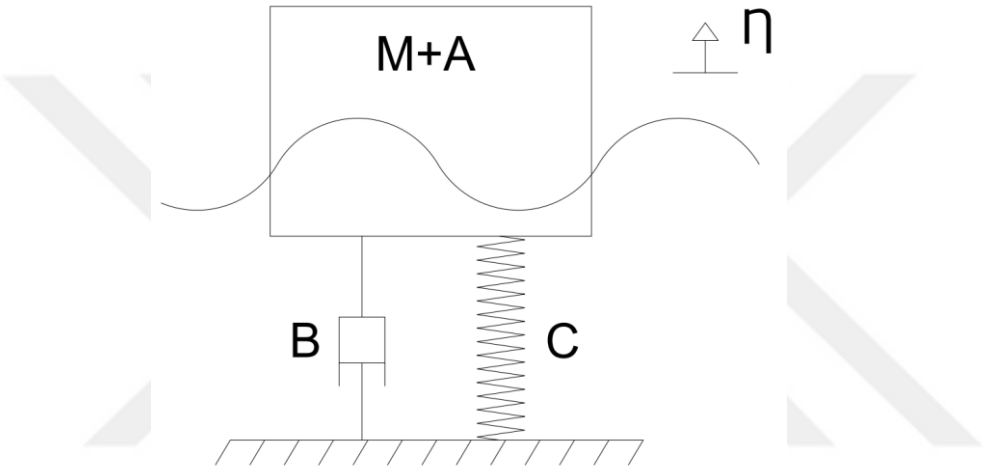

Figure 3.1 : Mass-spring-damper system.

According to Newton's second law, the equation of motion for the mass-spring-damper system can be expressed as follows:

$$(M + A)\ddot{\eta}(t) + B\dot{\eta}(t) + C\eta(t) = F(t) \tag{3.1}$$

where

M : body mass

A : added mass

B : damping force

C : restoring force

η : response displacement

$\dot{\eta}$: response velocity

$\ddot{\eta}$: response acceleration

3.1.1 Added mass (A)

Added mass is the hydrodynamic constant resulting from the movement of a floating body in water. The added mass of the body is proportional to the acceleration ($\ddot{\eta}$) of the motion of a floating body in the water caused by the acceleration of the water particles around the body. This force does not draw energy from the body and acts like a standing wave system around the body.

3.1.2 Damping force (B)

A floating body's motion in the water creates waves that begin to propagate over the body. Since these waves draw energy from the freely oscillating body, the motion of the body is damped over time. This hydrodynamic damping of the body is proportional to the velocity of motion ($\dot{\eta}$), and expressed by the damping coefficient (B**).** In a genuine viscous fluid, friction-induced damping occurs, but this non-linear damping contribution is often ignored. However, in some cases, such as the roll motion, the viscous effects may be significant and should be considered.

3.1.3 Restoring force (C)

Restoring is the force that occurs to balance the effect of external disturbing forces that a floating object is exposed to and ensure that the object returns to its equilibrium position. This force brings the object to its equilibrium position in the water.

Restoring force is based on Archimedes' principle. Archimedes' principle states that a floating body is repelled by the liquid in which it floats to replace the weight lost in the liquid. This thrust force depends on the density of the liquid in which the object floats and the volume of the object in the liquid. When an object sinks or floats into the liquid, the liquid exerts an upward force, which keeps the object in balance while floating. If another force acts against the direction of the force in this equilibrium, the restoring force helps the object to return to its equilibrium position.

3.1.4 Wave excitation force

Wave Excitation Forces refer to the forces of wave movements on the water that can cause the movement of a floating offshore structure. The movements of the floating structure on the water are due to the pressure and friction forces created by the wave movements. Wave Excitation Forces consist of two parts: Dynamic pressure force due

to incident waves or the Froude-Krylov force and the diffraction force. The sum of these two forces is expressed as total wave excitation forces:

$$F = F^{FK} + F^{D} \tag{3.2}$$

3.1.4.1 Froude-Krylov forces (F^{FK})

The Froude–Krylov force is introduced by the unsteady pressure field generated by undisturbed waves. William Froude [20, 21] and Aleksey Nikolaevich Krylov [22] independently suggested that wave forces acting on a floating body can be estimated by assuming the body is sufficiently small to not affect the pressure field due to an incident wave. The Froude-Krylov hypothesis essentially implies that:

- At any point on the submerged hull surface, the pressure acting is the same as the pressure occurring at the same point in the wave system in the absence of the floating body.
- The wave geometry and dynamic state are not affected by the ship's presence, and the diffraction effects are neglected.

3.1.4.2 Diffraction forces (F^{D})

Diffraction is a phenomenon that occurs because of wave propagation and bending when a wave encounters an object. When the wave propagating on water encounters a floating object, this object may cause diffraction.

For example, when a wave on the water's surface encounters an obstacle, such as any floating object, the wave energy begins to bend around this obstacle. The part of the wave that passes in front of it propagates in a different direction behind the obstacle, which is a fundamental diffraction property.

Diffraction affects how a wave propagates and generally depends on the relationship between the wavelength and the object's size. If the wavelength is much larger than the object's size, diffraction is not observed, and the wave passes through the obstacle without affecting it. However, diffraction is observed if the wavelength is close to or smaller than the object's size and the wave is distorted around the obstacle.

As a result of the distortion in the wave, changes occur in the dynamic wave pressure on the object. These changes in wave pressure are a phenomenon in which water particles on the wave surface rise and fall as the wave propagates, and this undulating

motion exerts a force on the floating object. Therefore, water waves move a floating object up and down, providing an effect of wave pressure. This effect is called diffraction force.

The force calculated here is the diffraction correction of the Froude-Krylov forces. Because it causes diffraction in the waveform of the floating object, this diffraction correction can also be called the diffraction force. This force is smaller than the Froude-Krylov force [23].

3.1.5 Linear wave theory

Linear wave theory explains water waves with the following basic assumptions:

- **Incompressibility:** This assumption states that the density of water does not change during the movement of waves. The number of water particles does not change, and the density remains constant throughout the wavelengths formed by the water waves.
- **Non-viscosity:** It is assumed that the fluid does not behave viscously; that is, it does not show any resistance to flow.
- **Surface tension:** This assumption states that tension at the water surface is an essential factor during wave formation. The tension on the water's surface is a force that acts on the formation and behaviour of waves.
- **Neglect of the Coriolis effect:** As the Earth rotates around itself, it also rotates the air mass above it, thus distorting the movement of the objects on it [24]. The effect of this deflection on sea waves is neglected.
- **Wave geometry:** The wave motion is assumed to be two-dimensional and has minimal amplitude.
- **Uniform and stability:** It is assumed that the fluid (water) that creates the wave behaves uniformly and constantly everywhere (same density and same surface tension).

According to the linear wave theory, a water wave is based on the relationships between the wavelength (λ), the period of the wave (T), and the velocity of the wave (c). These relationships are as follows:

$$T = \frac{\lambda}{c} \tag{3.3}$$

λ : wavelength

c : wave velocity

Linear wave theory starts with a regular wave with a sinusoidal form both in space and time. Sinusoidal inputs result in a sinusoidal response. A regular wave geometry is shown schematically in Figure 3.2.

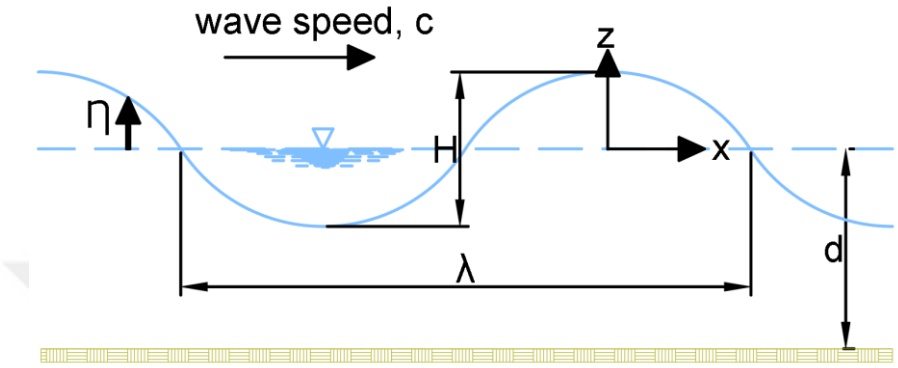

Figure 3.2 : A regular wave geometry.

The essential characteristics of a single-frequency, deep-water gravity wave can be summarised in Table 3.1.

Table 3.1 : Regular wave's characteristic parameters.

Wave Parameters	Formula
Length	$\lambda = gT^2/2\pi$
Period	$T = \sqrt{2\pi\lambda/g}$
Number	$k = 2\pi/\lambda = \omega^2/g$
Height	$H = 2\zeta$
Velocity or celerity	$c = \lambda/T = gT/2\pi$

The velocity potential of a regular wave can be derived by using the linearised free surface conditions in Table 3.2 (Note that the waves are propagating in the direction of the positive x-axis).

Table 3.2 : The velocity potential of a regular wave.

Category	Condition	Wave Velocity Potential
Deep-water	$\frac{d}{\lambda} \geq \frac{1}{2}$	$\phi = \frac{g\zeta}{\omega} e^{ikx} e^{kz} e^{i\omega t}$
Intermediate water	$\frac{1}{20} < \frac{d}{\lambda} < \frac{1}{2}$	$\phi = \frac{g\zeta}{\omega} e^{ikx} \frac{cosh[k(z+d)]}{cosh(kd)} e^{kz} e^{i\omega t}$
Shallow water	$\frac{d}{\lambda} \leq \frac{1}{20}$	$\phi = \frac{g\zeta}{\omega} e^{ikx} \frac{cosh[k(z+d)]}{cosh(kd)} e^{kz} e^{i\omega t}$

x : direction of propagation

z : vertical coordinate, positive upward, origin at still water level

d : water depth

t : time

ζ : wave amplitude

Profile, dynamic pressure, particle velocities, and accelerations in a regular, harmonic wave are summarised in Table 3.3.

Table 3.3 : The profile, dynamic pressure, particle velocities and accelerations in a regular, harmonic wave.

Wave property		Shallow water $\frac{d}{\lambda} \leq \frac{1}{20}$	Intermediate water $\frac{1}{20} < \frac{d}{\lambda} < \frac{1}{2}$	Deep-water $\frac{d}{\lambda} \geq \frac{1}{2}$
Dispersion relation		$\omega^2 = gk^2d$	$\omega^2 = gk\tanh(kd)$	$\omega^2 = gk$
Wavelength	λ	$T\sqrt{gd}$	$\frac{gT^2}{2\pi}\tanh\left(\frac{2\pi d}{\lambda}\right)$	$\frac{gT^2}{2\pi}$
Wave profile	η	$\zeta\sin(\omega t - kx)$	$\zeta\sin(\omega t - kx)$	$\zeta\sin(\omega t - kx)$
Dynamic pressure	p	$\rho g\zeta e^{ikx}e^{i\omega t}$	$\rho g\zeta e^{ikx}\frac{cosh[k(z+d)]}{cosh(kd)}e^{i\omega t}$	$\rho g\zeta e^{ikx}e^{kz}e^{i\omega t}$
Horizontal particle velocity	u	$\frac{\omega}{kd}\zeta e^{ikx}e^{i\omega t}$	$\omega\zeta e^{ikx}\frac{cosh[k(z+d)]}{sinh(kd)}e^{i\omega t}$	$\omega\zeta e^{ikx}e^{kz}e^{i\omega t}$
Vertical particle velocity	w	$\omega\zeta e^{ikx}\frac{z+d}{d}e^{i\omega t}$	$\omega\zeta e^{ikx}\frac{sinh[k(z+d)]}{sinh(kd)}e^{i\omega t}$	$\omega\zeta e^{ikx}e^{kz}e^{i\omega t}$
Horizontal particle acceleration	$\dot{u}$	$\frac{\omega^2}{kd}\zeta e^{ikx}e^{i\omega t}$	$\omega^2\zeta e^{ikx}\frac{cosh[k(z+d)]}{sinh(kd)}e^{i\omega t}$	$\omega^2\zeta e^{ikx}e^{kz}e^{i\omega t}$
Vertical particle acceleration	$\dot{w}$	$-\omega^2\zeta e^{ikx}\frac{z+d}{d}e^{i\omega t}$	$-\omega^2\zeta e^{ikx}\frac{sinh[k(z+d)]}{sinh(kd)}e^{i\omega t}$	$-\omega^2\zeta e^{ikx}e^{kz}e^{i\omega t}$

3.1.6 Heading and encounter frequency

The vessel's heading is defined concerning the direction of propagation of the waves. The convention chosen is shown in Figure 3.3. The ship's speed is constant for each concentric circle, and 180 degrees represent the head seas.

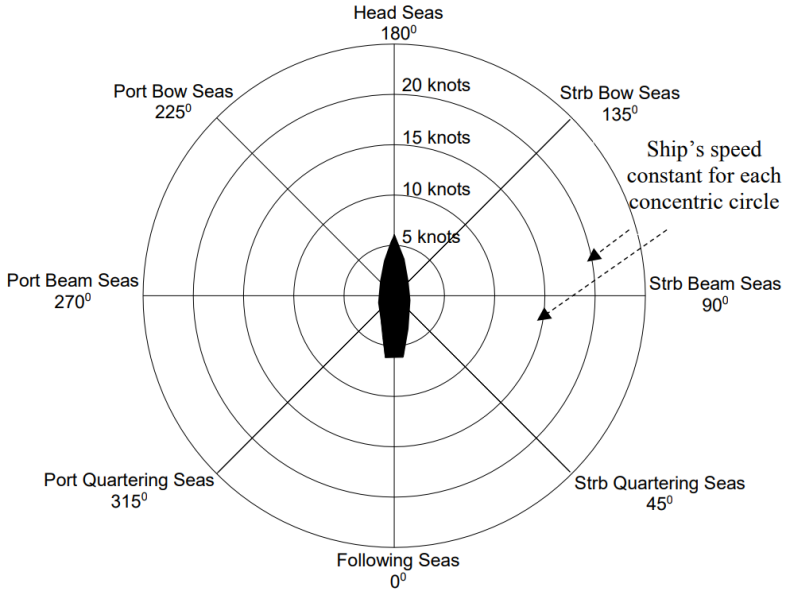

Figure 3.3 : Heading convention [25].

The motions of a vessel are critically dependent on the frequency with which a moving ship would encounter the waves. The component velocity of the vessel in the direction of wave propagation is $Vcos\mu$, and the waves will overtake the ship with a relative velocity.

$$c - Vcos\mu \tag{3.4}$$

Since the wave crests are λ meters apart, a crest will meet the ship once every T_e seconds, where the encounter period is given by

$$T_e = \frac{\lambda}{c\ -\ Vcos\mu} \tag{3.5}$$

The corresponding encounter frequency is defined as

$$\omega_e = \frac{2\pi}{T_e} = \frac{2\pi}{\lambda}(c - Vcos\mu) \tag{3.6}$$

Since $k\ = \frac{2\pi}{\lambda}$ and $c\ = \frac{\lambda\omega}{2\pi}$ in deep water, this reduces to the fundamental relationship

$$\omega_e = \omega - kVcos\mu = \omega - \frac{\omega^2 V}{g}cos\mu \tag{3.7}$$

In the seas forward of the beam ($90^0 < \mu < 270^0$), $cos\mu$ is always negative, and the encounter frequency is always more significant than the wave frequency. In beam seas $cos\mu\ = 0$, the encounter frequency is then equal to the wave frequency regardless of the speed of the vessel.

In seas abaft of the beam ($0^0 < \mu < 90^0$) and ($270^0 < \mu < 360^0$), $cos\mu$ is always positive, and the encounter frequency now has a maximum value

$$\omega_{e_{max}} = \frac{g}{4Vcos\mu} \tag{3.8}$$

Which occurs when the wave frequency is

$$\omega \ = 2\omega_{e_{max}} = \frac{g}{2Vcos\mu} \tag{3.9}$$

The encounter frequency is zero when

$$\omega \ = \frac{g}{2Vcos\mu} = 4\omega_{e_{max}} \tag{3.10}$$

Since $\omega = \frac{g}{c}$ in deep water, this corresponds to the condition when the component velocity is equal to the wave celerity

$$Vcos\mu = c \tag{3.11}$$

The encounter frequency is negative for higher values of ω. These high-frequency waves advance only slowly, and the negative encounter frequency means that the ship is overtaking the waves.

However, the floating offshore platform examined in this study has no forward speed. For this reason, the components of the formula here that depend on V, that is, forward speed, will be zero. The result of that situation is $\omega_e = \omega$.

3.1.7 Complex harmonic motion and solution of the equations of motion

For a wave with a fixed wavelength and a fixed height to maintain this form for a regular period means that a wave has a simple harmonic motion. The harmonic responses of the platform, η_k, will be proportional to the amplitude of the exciting forces and persist at the same frequency but with a phase difference.

Unlike simple harmonic motion, the amplitude is not a constant value in complex harmonic motion. It fades or intensifies depending on external influences. The motion of the mass-spring-damper system mentioned in Section 3.1 is a damped harmonic motion. In this form, it is a complex harmonic motion.

It is not possible to see a simple harmonic motion that continues forever in the form of an ideal system in nature. Energy is exported from the system by absorbing motion

energy, such as friction force, or energy is imported into the system by receiving an external force. For this reason, complex harmonic motions are preferred for systems that imitate nature. The same is true for the sea. In nature, sea waves intensify or fade over time.

The general form of the displacement equation for such a complex harmonic motion can be written as follows.

$$\eta_k(t) = \bar{\eta}_k cos(\omega_e t + \varepsilon_k) = \bar{\eta}_k e^{i\omega_e t} \tag{3.12}$$

Here η_k is the complex response amplitude, $\bar{\eta}_k$ is the magnitude or absolute value of the response amplitude and ε_k is the phase difference of the response. The initial motion and initial speed determine these parameters.

When the time-dependent first derivative of this complex harmonic motion displacement equation is taken, the velocity equation of the same motion is obtained.

$$\dot{\eta}_k(t) = i\omega_e \bar{\eta}_k e^{i\omega_e t} \tag{3.13}$$

When the resulting velocity equation is differentiated concerning time, the acceleration equation of the same movement is obtained.

$$\ddot{\eta}_k(t) = -\omega_e^2 \bar{\eta}_k e^{i\omega_e t} \tag{3.14}$$

When displacement, velocity and acceleration are substituted in the mass-spring-damper system equation in equation 3.1, the equation is formed as follows:

$$(M_k + A_k) - \omega_e^2 \bar{\eta}_k e^{i\omega_e t} + B_k i\omega_e \bar{\eta}_k e^{i\omega_e t} + C_k \bar{\eta}_k e^{i\omega_e t} = F e^{i\omega_e t} \tag{3.15}$$

The complex harmonic motion amplitude can be represented as follows:

$$\eta_k = \bar{\eta}_k e^{i\omega_e t} = \bar{\eta}_{kr} + i\bar{\eta}_{ki} \tag{3.16}$$

The solution of this equation yields the real and imaginary parts of the response as follows:

$$\eta_{kr} = \frac{[-\omega_e^2(M_k + A_k) + C_k](F_{kr}^I + F_{kr}^D) + [\omega_e B_k](F_{ki}^I + F_{ki}^D)}{[-\omega_e^2(M_k + A_k) + C_k]^2 + [\omega_e B_k]^2} \tag{3.17}$$

$$\eta_{ki} = \frac{-[\omega_e B_k](F_{kr}^I + F_{kr}^D) + [-\omega_e^2(M_k + A_k) + C_k](F_{ki}^I + F_{ki}^D)}{[-\omega_e^2(M_k + A_k) + C_k]^2 + [\omega_e B_k]^2} \tag{3.18}$$

3.1.8 Response amplitude operator (RAO)

RAO (Response Amplitude Operator) is a parameter used to compare the amplitude and phase of the motion of a floating body under the influence of wave with wave motion. RAO is essential for the design and performance analysis of marine vehicles and structures. This parameter can predict how the floating body will move under wave action. RAO plays a vital role in determining factors such as a marine structure's stability, capabilities, and safety. RAO also affects the resistance and performance of the sea structure to wave action.

It is the ratio of the displacement of the movement and the amplitude. This ratio generally gives meaningful results when examined in the frequency domain.

$$RAO(\omega) = \frac{\eta_k(t)}{\bar{\eta}_k} \tag{3.19}$$

To examine the RAO graph, in this study, the RAO graph of the vertical circular cylinder, which was used as simple geometry in Section 4 and obtained by the analytical method, was used (Figure 3.4). The calculations for obtaining this graph are shared in detail in Section 4.

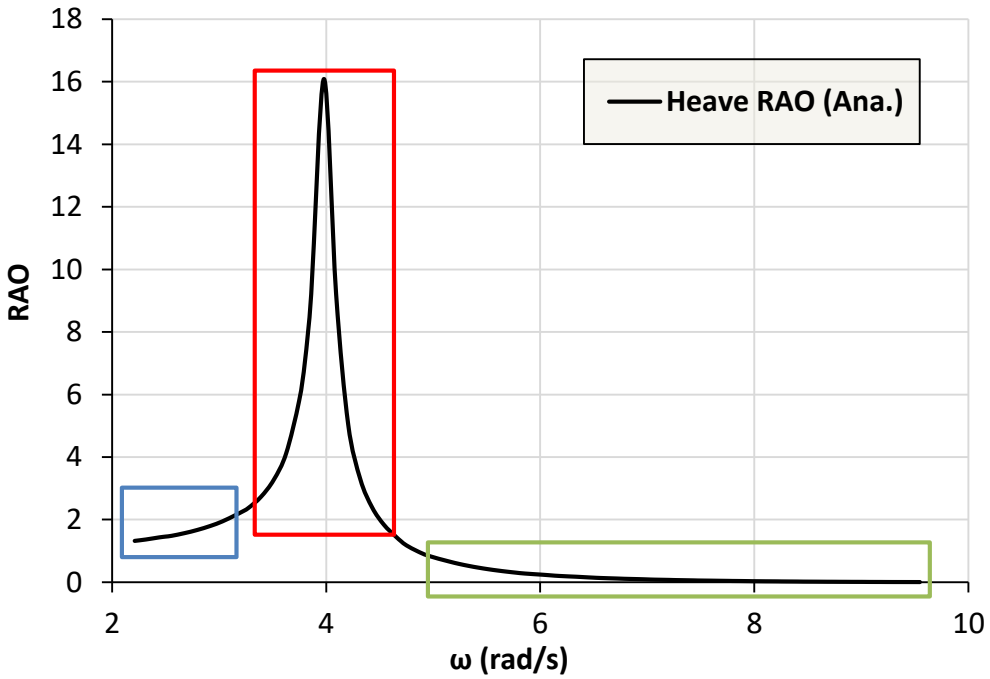

Figure 3.4 : Heave Response Amplitude Operator (RAO) for analytical solution.

As shown in Figure 3.4, the heave motion of the vertical circular cylinder shows different characteristics in three different regions. If we examine these regions:

Blue Region: In this low-frequency region, $\omega_e^2 \ll \frac{C_k}{(M_k + A_k)}$ the spring constant dominates the vertical movements of the structure "C_k". In this region, the length of the incoming wave is quite large compared to the structure's diameter, and the structure moves with the incoming wave as if it were whole; in other words, it follows the wave. In this region, the response amplitude operator appears as 1.0.

Red Region: This region is also called the natural frequency region and is $\omega_e^2 \approx \frac{C_k}{(M_k + A_k)}$ in this region. In this region, the vertical movements of the structure are controlled by the damping term. If the damping is small, the structure resonates in this region.

Green Region: This region is where $\omega_e^2 \gg \frac{C_k}{(M_k + A_k)}$ the relationship exists and represents the region where the effect of waves on structure movements disappears. The high wave frequency in this region means that many wave crests and troughs act simultaneously along the structure's diameter.

3.2 Six Degree of Freedom Motions of a Floating Body

A floating offshore structure in a random seaway has 6 degrees of freedom about the x-y-z axis system, three rotary and three translators. These motions are shown in Table 3.4 and Figure 3.5.

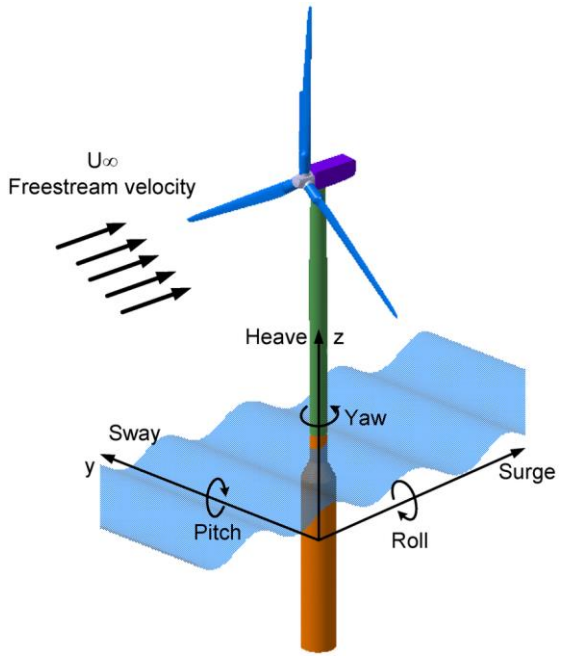

Figure 3.5 : Motions of an offshore wind turbine platform in waves [26].

Table 3.4 : Motions of a floating offshore structure in waves.

Degree of Freedom	Motion	Axis
1	Surge	X
2	Sway	Y
3	Heave	Z
4	Roll	RX
5	Pitch	RY
6	Yaw	RZ

The six degrees of equations of motion for a freely floating body can be formed based on Newton's second law as follows:

$$\sum_{k=1}^{6}\left[\left(M_{jk}+A_{jk}\right)\ddot{\eta}_k+B_{jk}\dot{\eta}_k+C_{jk}\eta_k\right]=F_j e^{i\omega_e t}\;;\quad j=1,2,\ldots.6 \tag{3.20}$$

M_{jk} : mass or inertia matrix

A_{jk} : added mass matrix

B_{jk} : damping force matrix

C_{jk} : restoring force matrix

F^I : wave excitation force due to the incident waves

In linear theory, the harmonic responses of the platform, η_k, will be proportional to the amplitude of the exciting forces and persist at the same frequency but with a phase difference. Consequently, the displacement, velocity, and acceleration in the kth direction can be expressed in the form

$$\eta_k(t)=\bar{\eta}_k cos(\omega_e t+\varepsilon_k)=\bar{\eta}_k e^{i\omega_e t} \tag{3.21}$$

$$\dot{\eta}_k(t)=i\omega_e\bar{\eta}_k e^{i\omega_e t} \tag{3.22}$$

$$\ddot{\eta}_k(t)=-\omega_e^2\bar{\eta}_k e^{i\omega_e t} \tag{3.23}$$

Here η_k is the complex response amplitude, $\bar{\eta}_k$ is the magnitude or absolute value of the response amplitude and ε_k is the phase difference of the response.

The solution of the above equations yields the real and imaginary parts of the response amplitude; η_{kr} and η_{ki}. Then, the amplitude and phase lag of the kth response is

$$\bar{\eta}_k = \sqrt{\eta_{kr}^2 + \eta_{ki}^2} \tag{3.24}$$

$$\varepsilon_k = tan^{-1}\left(\frac{\eta_{ki}}{\eta_{kr}}\right) \tag{3.25}$$

Then, the six-degree-of-freedom harmonic motions in regular waves for a freely floating body can be written as follows:

$$\sum_{k=1}^{6}\left[-\omega_e^2\left(M_{jk} + A_{jk}\right) + i\omega_e B_{jk} + C_{jk}\right]\eta_k = F_j^I + F_j^D \;\; ; \quad j = 1,2,\ldots.6 \tag{3.26}$$

If it is assumed that the ship has port-starboard symmetry (symmetric about the x, z plane), with corresponding mass symmetry so that the centre of gravity is located at $(0, 0,\ z_G)$, then the generalised mass matrix can be written in the form

$$M_{jk} = \begin{bmatrix} M & 0 & 0 & 0 & Mz_G & 0 \\ 0 & M & 0 & -Mz_G & 0 & 0 \\ 0 & 0 & M & 0 & 0 & 0 \\ 0 & -Mz_G & 0 & M_{44} & 0 & -M_{46} \\ Mz_G & 0 & 0 & 0 & M_{55} & 0 \\ 0 & 0 & 0 & -M_{46} & 0 & M_{66} \end{bmatrix} \tag{3.27}$$

where M is the mass of the ship, M_{jk} is the mass moment of inertia in the j[th] mode due to motion in the k[th] mode. The product of inertia M_{46} , representing the roll-yaw product, will vanish if the ship has fore-and-aft mass symmetry or is sufficiently small otherwise. Zero products of inertia mean that the coordinate axes are also principal axes. The other non-diagonal elements of equation 3.27 all vanish if the coordinate system's origin coincides with the ship's centre of gravity.

In principle, there are 36 distinct hydrodynamic inertia and wave damping coefficients, but geometric symmetry makes for a consequential reduction in number. For hulls with port-starboard symmetry, the non-zero hydrodynamic coefficients have an even-even or an odd-odd combination of i, j indices, indicating that the longitudinal motions are not coupled with the lateral ones [25]. The resulting added mass matrix has the form

$$A_{jk} = \begin{bmatrix} A_{11} & 0 & A_{13} & 0 & A_{15} & 0 \\ 0 & A_{22} & 0 & A_{24} & 0 & A_{26} \\ A_{31} & 0 & A_{33} & 0 & A_{35} & 0 \\ 0 & A_{42} & 0 & A_{44} & 0 & A_{46} \\ A_{51} & 0 & A_{53} & 0 & A_{55} & 0 \\ 0 & A_{62} & 0 & A_{64} & 0 & A_{66} \end{bmatrix} \tag{3.28}$$

with $[B_{jk}]$ having a similar form.

3.2.1 Assumptions and wave force in AQWA

The main theoretical assumptions and limitations of linear potential theory employed in AQWA are listed below [27]:

- The body or bodies have zero or very small forward speed.
- The fluid is inviscid and incompressible, and the fluid flow is irrotational.
- The incident regular wave train is of small amplitude compared to its length (slight slope).
- The motions are to the first order and must be of small amplitude. All body motions are harmonic. The linearised drag damping on the Morison elements or any additional user-defined viscous damping can be optionally included in the equation of motion.

This section deals with the hydrodynamic fluid loading of a diffracting body in regular harmonic waves. The theory may be used to calculate the wave excitation on a fixed body or the wave exciting forces and radiation forces on a floating body.

Since the first-order potential theory of diffraction and radiation waves is used here for radiation and diffraction analysis, the linear superposition theorem may be used to formulate the velocity potential within the fluid domain.

The fluid flow field surrounding a floating body by a velocity potential is defined by

$$\phi(\vec{X}, t) = \zeta_w \varphi(\vec{X}) e^{-i\omega_e t} \tag{3.29}$$

Where ζ_w is the incident wave amplitude, and ω is the wave frequency.

In equation 3.29, the isolated space-dependent term $\varphi(\vec{X})$ may be separated into contributions from the radiation waves due to six basic modes of body motion: the incident wave and the diffracted or scattered wave. The potential functions are complex, but the resultant physical quantities, such as fluid pressure and body motions in time domain analysis, will be obtained only by considering the real part.

Adopting the conventional notation of the six rigid body motions in seakeeping theory, as demonstrated in Figure 3.5, three translational and three rotational motions of the body's centre of gravity are excited by an incident regular wave with unit amplitude:

$$x_j = u_j, (j = 1,3) x_j = \theta_{j-3}, (j = 4,6) \tag{3.30}$$

The potential due to incident, diffraction, and radiation waves may therefore be written as:

$$\varphi(\vec{X})e^{-i\omega_e t} = [(\varphi_1 + \varphi_d)\sum_{6}^{j=!} \varphi_{rj}x_j]e^{-i\omega_e t} \tag{3.30}$$

where φ_1 is the first-order incident wave potential with unit wave amplitude, φ_d is the corresponding diffraction wave potential φ_{rj} is the radiation wave potential due to the j[th] motion with unit motion amplitude.

In finite-depth water, the linear incident wave potential φ_1 at a point $\vec{X} = (X, Y, Z)$ in equation 3.31 that as a particular case of unit amplitude $\zeta_w = 1$.

When the wave velocity potentials are known, the first-order hydrodynamic pressure distribution may be calculated by using the linearised Bernoulli's equation,

$$p^{(1)} = -\rho\frac{\partial\phi(\vec{X}, t)}{\partial t} = i\omega\rho\varphi(\vec{X})e^{-i\omega_e t} \tag{3.32}$$

From the pressure distribution, the various fluid forces may be calculated by integrating the pressure over the wetted surface of the body. To have a general form for the forces and moments acting on the body, we extend the notation of the unit average vector of the hull surface into six components corresponding to the six basic rigid body motions, such as

$$(n_1, n_2, n_3) = \vec{n} and (n_4, n_5, n_6) = \vec{r}x\vec{n} \tag{3.33}$$

here $\vec{r} = \vec{X} - \overrightarrow{X_g}$ is the position vector of a point on the hull surface concerning the centre of gravity in the fixed reference axes (FRA). Employing this notation, the first-order hydrodynamic force and moment components can be expressed in a generalised form:

$$F_j e^{-i\omega_e t} = \omega\rho\int_{S_0} p^{(1)}n_j dS = [-i\omega\rho\int_{S_0} \varphi(\vec{X})n_j dS]e^{-i\omega_e t} \tag{3.34}$$

where is the mean wetted surface of the body.

From equation 3.31, the total first-order hydrodynamic force can be written as

$$F_j = \left[(F_{Ij} + F_{dj}) + \sum_{k=1}^{6} F_{rjk}x_k\right] where j = 1,6 \tag{3.35}$$

of which the j[th] Froude-Krylov force due to incident wave is

$$F_{Ij} = -i\omega\rho \int_{S_0} \varphi_I(\vec{X}) n_j dS \tag{3.36}$$

the j[th] diffracting force due to the diffraction wave is

$$F_{dj} = -i\omega\rho \int_{S_0} \varphi_d(\vec{X}) n_j dS \tag{3.37}$$

the j[th] radiation force due to the radiation wave induced by the k[th] unit amplitude body rigid motion is

$$F_{rjk} = -i\omega\rho \int_{S_0} \varphi_{rk}(\vec{X}) n_j dS \tag{3.38}$$

Fluid forces can be further described in terms of reactive and active components. The active force, or the wave exciting force, comprises the Froude-Krylov and diffraction forces. The reactive force is the radiation force due to the waves induced by body motions.

The radiation wave potential, φ_{rk}, may be expressed in real and imaginary parts and substituted into equation 3.38 to produce the added mass and wave-damping coefficients

$$F_{rjk} = -i\omega\rho \int_{S_0} \{Re[\varphi_{rk}(\vec{X})] + iIm[\varphi_{rk}(\vec{X})]\} n_j dS \tag{3.39a}$$

$$F_{rjk} = \omega\rho \int_{S_0} Im[\varphi_{rk}(\vec{X})] n_j dS - i\omega\rho \int_{S_0} Re[\varphi_{rk}(\vec{X})] n_j dS \tag{3.39b}$$

$$= \omega^2 \rho A_{jk} + i\omega\rho B_{jk} \tag{3.39c}$$

where the added mass and damping are

$$A_{jk} = \frac{\rho}{\omega} \int_{S_0} Im[\varphi_{rk}(\vec{X})] n_j dS \tag{3.40}$$

$$B_{jk} = -\rho \int_{S_0} Re\left[\varphi_{rk}\left(\vec{X}\right)\right] n_j dS \tag{3.41}$$

If a problem requires wave loading on a fixed body, then only the active wave forces are of interest. The active and reactive fluid forces must be considered when the body is floating. It is also worth noting that all fluid forces calculated above are a function of the wetted body surface geometry only and are independent of the structural mass characteristics of the body [27].

3.3 Mathematical Representation of the Seaway

3.3.1 Linear superposition of regular waves

In its simplest form, the linear model assumes a normal or Gaussian stochastic process that (over periods long enough for analysis but not so long that significant weather changes occur) is stationary in time and space, i.e., the statistical properties remain unchanged.

The model assumes that at any location and instant, the sea's surface results from the linear superposition of many progressive regular harmonic wave trains of random amplitude, wave frequency and phase [25]. The principle of linear superposition of regular waves is shared in Figure 3.6.

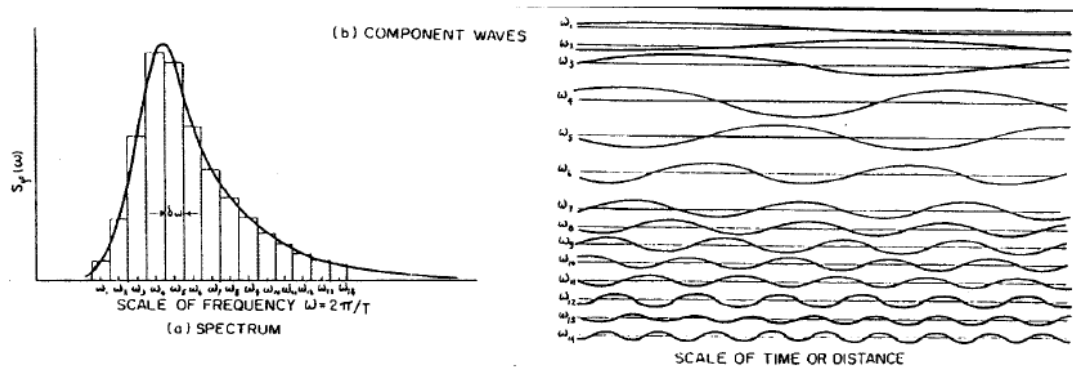

Figure 3.6 : Linear superposition of regular waves [25].

This assumption was first remarked by Froude (1905) that "*irregular wave systems are only a compound of several regular wave systems (individually of comparatively small amplitudes) of various periods ... and the effect of such a compound wave series would be more or less a compound of the effects proper to the individual units*

composing of it" [28]. These assumptions are the basis of the linear spectral analysis technique introduced by St. Denis and Pierson (1953), which makes it possible to predict the response of a ship in a seaway when the wave spectrum and the response to regular waves are known [25, 29].

Using the linear superposition principle, the superposition of regular sinusoidal waves of the form can represent the irregular sea surface

$$\zeta(t) = \zeta_a \cos(kx - \omega t) \tag{3.42}$$

where $\zeta(t)$ is the wave elevation at time t, ζ_a is the wave amplitude, k is the wave number of the wave propagating in the coordinate direction x, and ω is the wave frequency. When the wave is studied at a fixed point, $x = 0$, say, then

$$\zeta(t) = \zeta_a \cos(-\omega t) = \zeta_a \cos(\omega t) \tag{3.43}$$

describes the harmonic nature of the passing wave. Using the linear superposition principle, a long-crested irregular sea surface can be formulated as

$$\zeta(t) = \sum_{n=1}^{\infty} \zeta_{an} \cos(k_n x - \omega_n t + \varepsilon_n) \tag{3.44}$$

where ζ_{an}, k_n, ω_n, and ε_n are the amplitude, wave number, circular frequency, and phase of the nth component wave. At the selected fixed point, $x = 0$, the harmonic nature of the wave system is described by

$$\zeta(t) = \sum_{n=1}^{\infty} \zeta_{an} \cos(\omega_n t + \varepsilon_n) \tag{3.45}$$

It can be shown that for a regular sinusoidal wave, the energy per unit surface area is given by the expression,

$$E = \frac{1}{2} \rho g \zeta_a^2 \tag{3.46}$$

If the irregular sea is defined as a discrete number, N, of regular sinusoidal waves of varying wavelength and minimal amplitude, the total energy in the sea will be

$$E = \frac{1}{2} \rho g \sum_{n=1}^{N} \zeta_{an}^2 \tag{3.47}$$

Defining the wave spectral density function or the wave energy spectrum $S_\zeta(\omega)$ as the distribution of energy is a function of wave frequency, one can provide arguments that lead to the

$$S_\zeta(\omega_n) = \frac{\frac{1}{2}\sum_{\omega_n - \frac{\delta\omega}{2}}^{\omega_n + \frac{\delta\omega}{2}} \zeta_{an}^2}{\delta\omega} \tag{3.48}$$

That is $S_\zeta(\omega_n)\delta\omega$ represents the total energy of all component waves in a frequency band $\delta\omega$ centred on the component wave frequency ω_n. The total energy of the wave system of all component energies thus amounts to

$$E = \rho g \int_0^\infty S_\zeta(\omega) d\omega \tag{3.49}$$

The sea spectrum has the advantage of characterising the condition of a given seaway without regard to its behaviour at an exact location in space or an instant in time. This situation eliminates much of the difficulty in dealing with the inherent randomness of the process. However, the form of $S_\zeta(\omega)$ will change with the sea area and the seasons.

3.3.2 Relationship between body motion and wave spectrum

In a marine environment with irregular waves, the energy distributions of these waves correspond to the wave frequencies that form the wave spectrum. These irregular waves affect a structure with linear characteristics and create its movements. Model experiments or numerical calculations obtain the linear characteristics of the structure. The final motion characteristics of the floating structure are obtained from the interaction of irregular waves and the structure system. These motion characteristics also show an irregular character, like waves. Frequency-based characteristics of a floating structure are obtained by frequency domain analysis. A floating barge generally shows a linear characteristic. This situation means a constant ratio between the structure motion amplitude and the wave amplitude for each frequency. Doubling the wave amplitude means doubling the movement amplitude of the structure.

As a result of linear theory, the ultimate movements of the structure in irregular waves can be found by adding together the results obtained from regular waves of different amplitudes, frequencies, and directions. For a given area and structure, if the wave spectrum is known and the frequency characteristics of the structure have been

calculated, the final motion spectrum can be generated. Figure 3.7 shows the mentioned principle [30, 31].

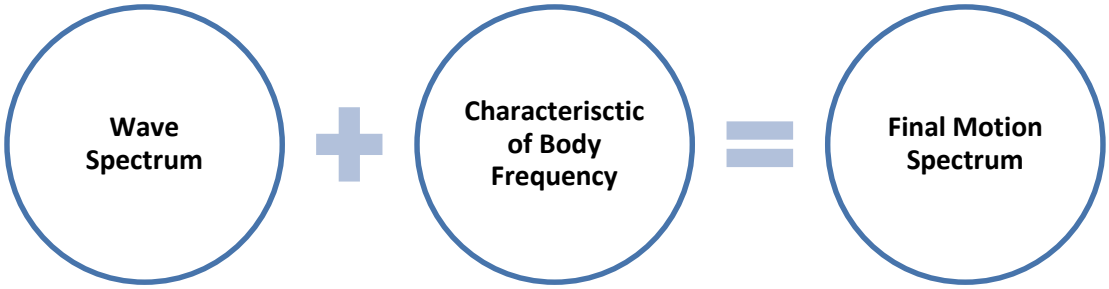

Figure 3.7 : Relationship between body motion and wave spectrum [31].

No matter how successful an offshore structure's design, its mission's performance will be affected by the natural environment. The understanding of motions at sea and the ability to predict the behaviour of any floating offshore structure in the design stage begins with studying the nature of ocean waves that constitute the environment.

The sea waves continually change height, length, and direction of travel. Such changes manifest randomness, the description of which also varies with time. However, the sea may maintain a characteristic appearance over a reasonably wide area and often for a half-hour or more because record analyses indicate it is very nearly statistically steady or stationary. The sea condition will differ at other times or places, yet there will again be a characteristic appearance with different but steady statistical parameters. The interval over which the random sea state may be considered (statistically) to remain reasonably constant ranges from a few minutes to a few weeks, depending on the locality of observation and meteorological circumstances. Statistical models can only adequately describe this randomness of the seaway [25].

The random character of the seaway, in turn, reflects itself in the platform motions it stimulates, so that prediction of the ship motions is also statistical. Hence, for most problems concerning the behaviour of floating offshore structures at sea, attention can be focused on describing mathematically the surface waves as a random process under short-term statistically stationary conditions. Determination of the responses in a generic seaway is considered in short-term prediction. The corresponding prediction of an offshore structure's extreme behaviour requires determining the long-term trends in maximum values of the different responses in the seaways it is expected to encounter during its operating life [25].

Analysis of the motions of an offshore structure in a seaway can be approached in two directions: in the time domain or the frequency domain. Steady processes are conveniently solved in the frequency domain. The associated level of analysis is also considerably less burdensome by such a choice.

3.3.3 Wave and wind data

The early quantification of the sea environment was due to the keen observation of ship operators. As a common maritime practice, the roughness of the ocean surface is quantified by strata called sea state number, which is characterised by the significant wave height and modal period pair. Available ocean wave data for ship design and operation fall into several categories.

3.3.3.1 Wave measurements

Wave measurements collected from weather ships, fixed platforms, buoys, et cetera allow the shape of spectra to be estimated, although directional properties are rarely deducible. However, measuring wave data over a long period (years) is an expensive and complicated process, and relatively few attempts at systematic data collection have been made. In 1970, the World Meteorological Organization (WMO) agreed to the standard sea state code presented in Table 3.5.

Table 3.5 : World Meteorological Organization (WMO) standard sea state code.

	Significant Wave Height (m)		Wind Speed (knots)		Beaufort Force
Sea State	Range	Mean	Range	Mean	BF
0-1(Calm)	0.00 - 0.10	0.05	0-6	3	0-1-2
2 (Smooth)	0.10 - 0.50	0.30	7-10	8.5	3
3 (Slight)	0.50 - 1.25	0.88	11-16	13.5	4
4 (Moderate)	1.25 - 2.50	1.88	17-21	19	5
5(Rough)	2.50 - 4.00	3.25	22-27	24.5	6
6 (Very Rough)	4.00 - 6.00	5.00	28-47	37.5	7-8-9

3.3.3.2 Visual observations

The publication of a comprehensive atlas based on over 55 million visual observations from ships on passage between 1854 and 1984 by Hogben and Lumb (1967) provided general data on global ocean occurrences of wave height, period, and direction parameters [32].

The data was collected by voluntarily observing ships, which reported the direction from which the dominant waves came, the period and the height of both sea and swell. The data can be readily turned into frequencies of occurrence for wave height and period for an arbitrary offshore route. These data are usually presented in the form of a scatter diagram. This matrix describes the probability of a sea state occurring at a specified significant wave height and characteristic period in a given sea area, in a specific direction, and at a given time of year [25].

Wave statistics based on visual observations must always be considered less reliable than direct measurements of wave conditions. A severe criticism of visually observed data is that ships' captains generally try to avoid bad weather, which will likely introduce a fair-weather bias into the results. So, the published tables will likely underestimate the probability of extremely severe weather conditions simply because ships' captains will try to avoid the storms. Figure 3.8 shows a typical winter data set from Area 9 [25].

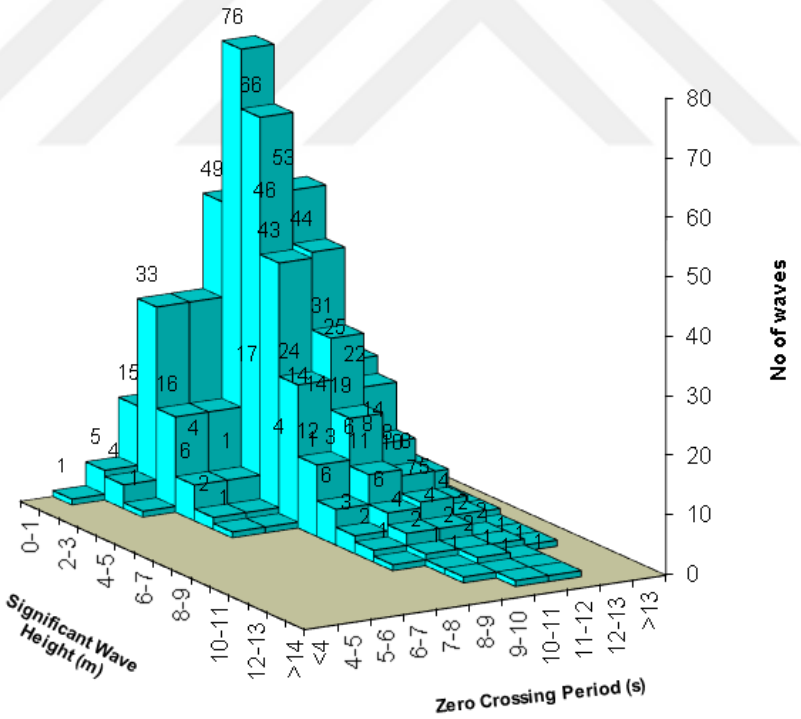

Figure 3.8 : Wave height and period statistics for Area 9 [32].

3.3.3.3 Hindcasting

This technique is based on measured wind data obtained over a long period for a sea area to hindcast the waves resulting from measured winds. Bales, Lee and Voelker (1981) published a wave atlas for the North Atlantic, North, Mediterranean, Black, and

Baltic seas [33]. Using long-term wave and wind climate statistics, these data can generate parametric models relating wave height to wind speed and wave period [25]. Annual sea state occurrences are shared in Table 3.6 and Table 3.7.

Table 3.6 : Annual Sea state occurrences in the open ocean North Atlantic.

Sea State Number	Significant Wave Height (m)		Sustained Wind Speed (knots)		Percentage Probability of Sea State	Modal Wave Period (s)	
	Range	Mean	Range	Mean		Range	Probable
0-1	0-0.10	0.05	0-6	3	0	-	-
2	0.1-0.5	0.3	7-10	8.5	7.2	3.3-12.8	7.5
3	0.5-1.25	0.88	11-16	13.5	22.4	5-14.8	7.5
4	1.25-2.5	1.88	17-21	19	28.7	6.1-15.2	8.8
5	2.5-4	3.25	22-27	24.5	15.5	8.3-15.5	9.7
6	4-6	5	28-47	37.5	18.7	9.8-16.2	12.4
7	6-9	7.5	48-55	51.5	6.1	11.8-18.5	15
8	9-14	11.5	56-63	59.5	1.2	14.2-18.6	16.4
>8	>14	>14	>63	>63	<0.05	18-23.7	20

Table 3.7 : Annual Sea state occurrences in the open ocean North Pacific.

Sea State Number	Significant Wave Height (m)		Sustained Wind Speed (knots)		Percentage Probability of Sea State	Modal Wave Period (s)	
	Range	Mean	Range	Mean		Range	Probable
0-1	0-0.1	0.05	0-6	3	0	-	-
2	0.1-0.5	0.3	7-10	8.5	4.1	3-15	7.5
3	0.5-1.25	0.88	11-16	13.5	16.9	5.2-15.5	7.5
4	1.25-2.5	1.88	17-21	19	27.8	5.9-15.5	8.8
5	2.5-4	3.25	22-27	24.5	23.5	7.2-16.5	9.7
6	4-6	5	28-47	37.5	16.3	9.3-16.5	13.8
7	6-9	7.5	48-55	51.5	9.1	10.0-17.2	13.8
8	9-14	11.5	56-63	59.5	2.2	13.0-18.4	18.0
>8	>14	>14	>63	>63	0.1	20	20

In addition to wave height probabilities, it is necessary to characterise the wave energy distribution within various wave height bands or groups. The characterisation is accomplished by using a wave spectral family, sample spectra selected to represent the range of wave conditions known to occur within a particular area. The spectral family estimates the expected mean and variance of the vessel response amplitude throughout a range of sea severity. The availability of measured wave spectra in sufficient quantity is minimal. In many cases, it is necessary to use mathematical spectral formulations [25].

3.3.4 Short-term description of the sea by spectral analysis

The availability of wave data, such as the height and period values and their frequency of occurrence for specific locations, is inadequate for predicting offshore structure's responses to irregular seas. A definition of the sea surface must be available, along with the primary transfer function of the ship. The latter is expressed as the response per unit wave amplitude as a function of wave frequency. A statistical model cannot yet describe the full range of seaways observable in nature, from light to mountainous, straight-propagating to radially-spreading, ocean-running to surf beat. Indeed, only the linear wave theory is valid over a specific seaway area and an interval within which no significant change occurs [25]. This theory is touched on in Section 3.1.5.

3.3.4.1 Wave spectrum models

Ideally, measured spectra for the specific area of interest are preferred. However, the limited availability of such precise wave data has led to the use of mathematical descriptions for the actual spectra.

The usual input parameters required to generate the theoretical spectrum include wave height and period, though other additional parameters, such as fetch or the spectral width parameter, may help generate a more realistic spectral shape. Probably the best-known spectral formulation is that of Pierson and Moskowitz (1964) for fully developed seas [34], that is

$$S_\zeta(\omega) = \frac{A}{\omega^5} exp\left(-\frac{B}{\omega^4}\right) \tag{3.50}$$

with the significant wave height, $H_S\ (H_{1/3})$, used to specify the parameters A and B through the relationships

$$A = 0.0081g^2 \qquad B = 0.032\frac{g^2}{H_S^2} \tag{3.51}$$

where g is the gravitational acceleration.

The variation of the Pierson-Moskowitz spectrum with significant wave height and wave frequency is shown in Figure 3.9.

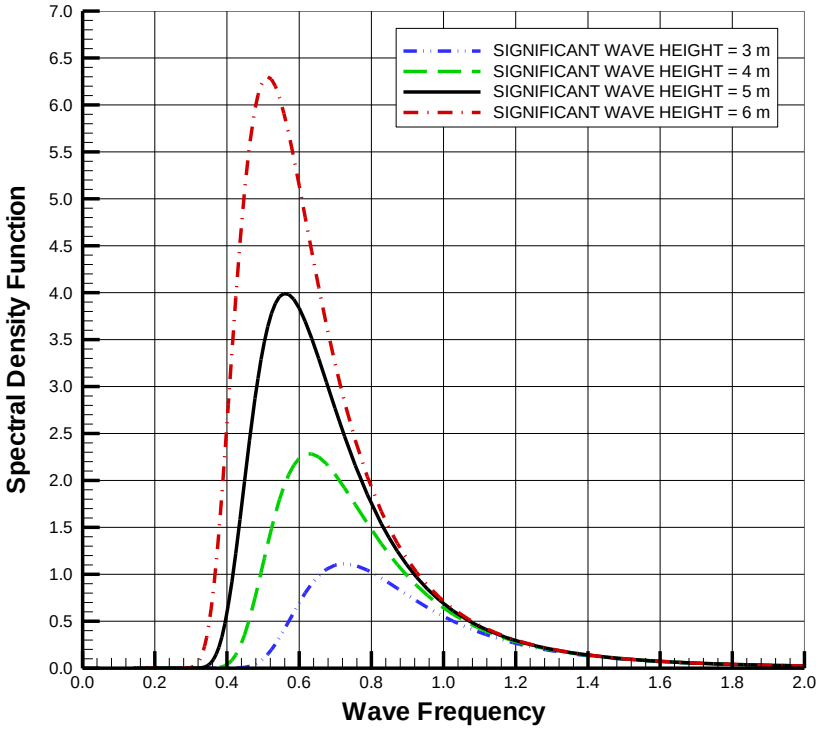

Figure 3.9 : Pierson-Moskowitz energy spectrum for different significant wave heights [25].

Thus, in this case, the spectrum's shape is controlled by a single parameter, the significant wave height. The modal frequency, ω_m, becomes a fixed value for a given significant wave height. That is,

$$\frac{dS_\zeta}{d\omega} = 0 \quad \Rightarrow \quad \frac{d}{d\omega}\left[\frac{A}{\omega^5} exp\left(-\frac{B}{\omega^4}\right)\right] = 0 \tag{3.52a}$$

$$-\frac{5A\omega^4}{\omega^{10}} exp\left(-\frac{B}{\omega^4}\right) + \frac{A}{\omega^5}\frac{4B\omega^3}{\omega^8} exp\left(-\frac{B}{\omega^4}\right) = 0 \tag{3.52b}$$

$$-\frac{5A}{\omega^6} + \frac{A}{\omega^5}\frac{4B}{\omega^5} = 0 \quad \Rightarrow \quad -\frac{5}{\omega} + \frac{4B}{\omega^5} = 0 \tag{3.52c}$$

$$\omega_m = (0.8B)^{1/4} = 0.4\sqrt{\frac{g}{H_S}} \tag{3.52d}$$

The maximum value of the Pierson-Moskowitz spectrum is

$$S_{\zeta max}(\omega_m) = \frac{A}{(0.8B)^{\frac{5}{4}}} exp\left(-\frac{B}{0.8B}\right) \tag{3.53a}$$

$$S_{\zeta max}(\omega_m) = \frac{0.2865A}{(0.8B)^{1.25}} = \frac{0.2865 \times 0.0081g^2}{\left(0.8 \times 0.032\frac{g^2}{H_S^2}\right)^{1.25}} = \frac{0.223H_S^{2.5}}{3.0865} = 0.072H_S^{2.5} \tag{3.53b}$$

Bretschneider (1957) proposed the first readily usable two-parameter sea spectrum representing seaways in all stages of development [35]. Under the assumption of narrow-mindedness, the Bretschneider spectrum can be written as

$$S_\zeta(\omega) = 0.3125\frac{\omega_m^4 H_S^2}{\omega^5} exp\left[-1.25\left(\frac{\omega_m}{\omega}\right)^4\right] \tag{3.54}$$

This can also be expressed in the standard form

$$S_\zeta(\omega) = \frac{A}{\omega^5} exp\left(-\frac{B}{\omega^4}\right) \tag{3.55}$$

where

$$A = \frac{487.3H_S^2}{T_m^4} = \frac{172.75H_S^2}{T_1^4} = \frac{123.8H_S^2}{T_Z^4} \tag{3.55a}$$

$$B = \frac{1948}{T_m^4} = \frac{691}{T_1^4} = \frac{495}{T_Z^4} \tag{3.55b}$$

The modal frequency, ω_m, at which the wave spectrum is maximum can be found as follows:

$$\frac{dS_\zeta}{d\omega} = 0 \quad \Rightarrow \quad \omega_m = (0.8B)^{\frac{1}{4}} \tag{3.56}$$

The maximum value of the Bretschneider spectrum is

$$S_{\zeta max}(\omega_m) = \frac{A}{(0.8B)^{\frac{5}{4}}} exp\left(-\frac{B}{0.8B}\right) \tag{3.57}$$

$$S_{\zeta max}(\omega_m) = \frac{487.3H_S^2}{T_m^4}\left(\frac{T_m^4}{0.8\times 1948}\right)^{5/4} exp(-1.25) = 0.01426H_S^2T_m \tag{3.57a}$$

$$S_{\zeta max}(\omega_m) = \frac{172.75H_S^2}{T_1^4}\left(\frac{T_1^4}{0.8\times 691}\right)^{5/4} exp(-1.25) = 0.01846H_S^2T_1 \tag{3.57b}$$

$$S_{\zeta max}(\omega_m) = \frac{123.8H_S^2}{T_Z^4}\left(\frac{T_Z^4}{0.8\times 495}\right)^{5/4} exp(-1.25) = 0.02008H_S^2T_Z \tag{3.57c}$$

The 15th International Towing Tank Conference [ITTC (1978)] recommended the use of the Bretschneider spectrum (for average conditions, not fully developed seas) in the form [36]

$$S_\zeta(\omega) = \frac{A}{\omega^5} exp\left(-\frac{B}{\omega^4}\right) \tag{3.58}$$

with $A = \frac{172.75H_S^2}{T_1^4}$ and $B = \frac{691}{T_1^4}$ when, more specifically, appropriate spectral forms are not known. Here T_1 is the average wave period defined by

$$T_1 = 2\pi \frac{m_0}{m_1} \tag{3.59}$$

with m_0 and m_1 corresponding to the zeroth and first moments of the wave spectra. In general, the n[th] moment of the spectrum is defined as follows:

$$m_n = \int_0^\infty \omega^n S_\zeta(\omega) d\omega \tag{3.60}$$

In Figure 3.10, spectral density functions are presented for unit-significant wave height and a range of spectral modal (peak) period as a function of wave frequency, based on the Bretschneider formulation.

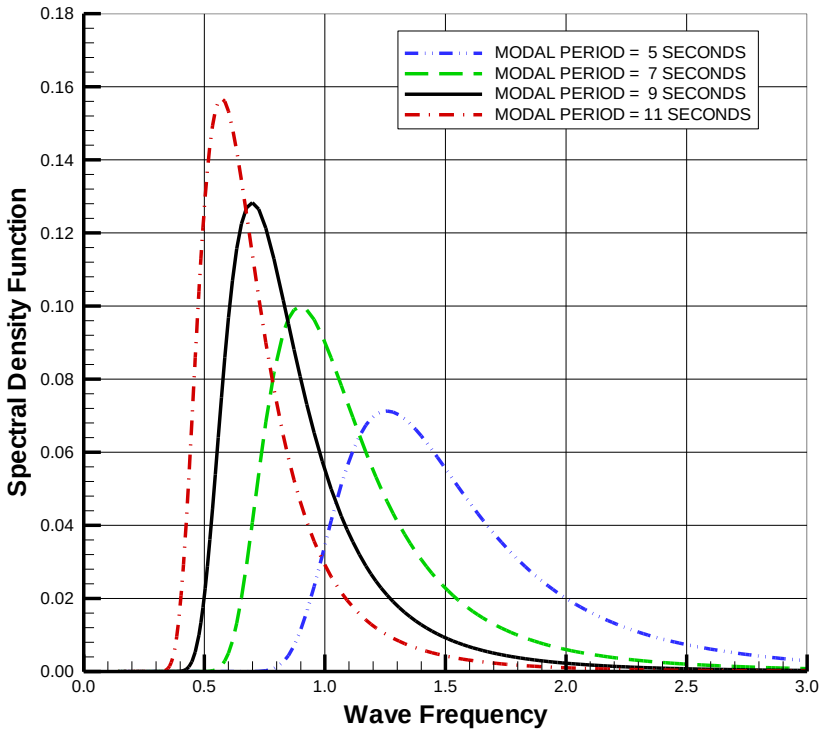

Figure 3.10 : Typical Bretschneider-type spectral formulations for unit wave height [25].

An extensive wave measurement program known as the Joint North Sea Wave Project (JONSWAP), reported by Hasselman (1973) and Ewing (1975), was carried out in 1968 and 1969 along a line extending over 100 miles into the North Sea from the island of Sylt [37, 38]. Various functional forms were tested to represent the measured data, and the following formulation was suggested for fetch-limited wind-generated seas

$$S_\zeta(\omega) = \alpha \frac{g^2}{\omega^5} exp\left[-1.25\left(\frac{\omega_m}{\omega}\right)^4\right] \gamma^{exp\left[-\frac{(\omega-\omega_m)^2}{2\sigma^2\omega_m^2}\right]} \tag{3.61}$$

where γ and σ describe the spectrum's shape, with γ defined as the ratio of the maximum of the energy spectrum to the maximum of the corresponding Pierson-Moskowitz wave spectrum. No definite trend with fetch was found for the parameters γ and σ, and as a first approximation

$$\gamma = 3.3 \tag{3.61a}$$

$$\sigma = 0.07 \quad for \quad \omega \leq \omega_m \tag{3.61b}$$

$$\sigma = 0.09 \quad for \quad \omega > \omega_m \tag{3.61c}$$

were taken to define a mean spectrum. α coefficient was specified as

$$\alpha = 0.076(\bar{x})^{-0.22} \qquad \bar{x} = \frac{gx}{U^2} \tag{3.61d}$$

Here the parameter $\bar{x}$ is the fetch in nautical miles, and U is the wind speed in knots.

The 17th International Towing Tank Conference [ITTC (1984)] recommended that fetch limited sea spectra be described in the form [39]

$$S_\zeta(\omega) = 155 \frac{H_S^2}{T_1^4 \omega^5} exp\left[-\frac{944}{T_1^4 \omega^4}\right] 3.3^\gamma \tag{3.62}$$

where

$$\gamma = exp\left[-\left(\frac{0.191\omega T_1 - 1}{\sqrt{2\sigma}}\right)^2\right] \tag{3.62a}$$

and

$$\sigma = 0.07 \quad for \quad \omega \leq \frac{5.24}{T_1} \tag{3.62b}$$

$$\sigma = 0.09 \quad for \quad \omega > \frac{5.24}{T_1} \tag{3.62c}$$

This formulation can be used with other characteristic periods by use of the following relationships

$$T_1 = 0.924T_{-1} = 0.834T_m = 1.073T_Z \tag{3.62d}$$

where the time-related parameters T_1, T_{-1}, T_m and T_Z correspond to the average wave period, energy averaged period, modal period and average zero up-crossing period.

$$A = \frac{487.3H_S^2}{T_m^4} = \frac{172.75H_S^2}{T_1^4} = \frac{123.8H_S^2}{T_Z^4} \qquad (3.62e)$$

$$B = \frac{1948}{T_m^4} = \frac{691}{T_1^4} = \frac{495}{T_Z^4} \qquad (3.62f)$$

3.3.5 Characteristics of spectra

The size and shape of a spectrum can be defined through its moments defined by

$$m_n = \int_0^\infty \omega^n S_\zeta(\omega) d\omega; n = 0,1,2, \ldots. \qquad (3.63)$$

The moment of order zero m_0 is the area under the spectrum, that is

$$m_0 = \int_0^\infty S_\zeta(\omega) d\omega \qquad (3.63a)$$

Since m_0 is equal to the mean square wave elevation about the undisturbed calm water level, the root mean square (RMS) wave elevation is $\sqrt{m_0}$. The second and fourth moments of the spectrum are simply

$$m_2 = \int_0^\infty \omega^2 S_\zeta(\omega) d\omega \qquad (3.63b)$$

with

$$m_4 = \int_0^\infty \omega^4 S_\zeta(\omega) d\omega \qquad (3.63c)$$

Moreover, it can be shown that these moments measure the mean square velocity and mean square acceleration, respectively, at the measurement point.

For Pierson-Moskowitz wave spectrum

$$m_0 = \int_0^\infty S_\zeta(\omega) d\omega = \int_0^\infty \left[\frac{A}{\omega^5} exp\left(-\frac{B}{\omega^4}\right)\right] d\omega = \frac{A}{4B} \qquad (3.64)$$

$$m_0 = \frac{A}{4B} = \frac{0.0081g^2}{4 \times 0.032 \frac{g^2}{H_S^2}} = \frac{H_S^2}{15.8} \qquad (3.65)$$

The statistical properties of an irregular seaway may be assumed to remain constant over several hours (referred to as short-term), and the spectrum defines many of these properties. Among them are various wave statistics, or averages, which may be computed from measured wave data records or estimated visually. For narrow-banded

spectra, these statistics are functionally related to the spectral moments. Spectral wave statistical parameters are shared in Table 3.8.

Table 3.8 : Spectral wave statistical parameters.

Parameter	Formula
Energy averaged period	$T_{-1} = 2\pi(m_{-1}/m_0)$
Average wave period	$T_1 = 2\pi(m_0/m_1)$
Average zero crossing period	$T_Z = 2\pi\sqrt{m_0/m_2}$
Modal wave period	$T_{modal} = 2\pi/\omega_m$
RMS wave amplitude	$\zeta_{RMS} = \sqrt{m_0}$
Significant wave amplitude	$\zeta_S = 2\zeta_w = 2\sqrt{m_0}$
Average wave amplitude	$\bar{\zeta} = 1.25\sqrt{m_0}$

The spectral width parameter, which varies between 0 and 1, is defined as

$$\varepsilon = \sqrt{1 - \frac{m_2^2}{m_0 m_4}} \tag{3.66}$$

Values near zero correspond to a narrow-banded spectrum, implying that the total energy is concentrated in a narrow band of wave frequencies. Values near unity indicate a wide-banded spectrum corresponding to an irregular waveform with components at all frequencies over a broad band of wave frequencies. Alternatively, ε can be estimated from the relationship

$$\varepsilon = \sqrt{1 - \left(\frac{N_0}{N_1}\right)^2} \tag{3.67}$$

where N_0 is the number of zero crossings and N_1 is the number of crests in a long wave record. It is apparent that for near-sinusoidal waves such as low swell, each zero crossing will almost always correspond to one crest and $\frac{N_0}{N_1}$ will approach unity. Conversely, for an irregular sea, each crossing may be followed by many crests, and so $\frac{N_0}{N_1}$ will have a value nearer to zero.

3.3.6 Directional spectrum

For a complete description of an irregular sea, it is necessary to have a directional spectrum. This fuller description indicates the energy distribution with frequency and direction, with the direction angle μ measured relative to the dominant wind direction. The energy per unit surface area contributed by the frequency band $d\omega$ (centred on the

frequency ω) for an angular spread $d\mu$ (centred on the angle μ) is given by $S(\omega,\mu)d\omega d\mu$.

In most applications, it is convenient to assume that the distribution of energy by frequency is independent of direction so that we may write

$$S_\zeta(\omega,\mu) = S_\zeta(\omega)M(\mu) \tag{3.68}$$

where $S_\zeta(\omega)$ is the point spectrum, and $M(\mu)$ is called the spreading function. A commonly used form of the spreading function is

$$M(\mu) = A_n cos^n \mu \qquad \left(-\frac{\pi}{2} \le \mu \le \frac{\pi}{2}\right) \tag{3.68a}$$

where

$$A_2 = \frac{2}{\pi}\,, \quad A_4 = \frac{8}{3\pi} \tag{3.68b}$$

3.3.7 Long-term trends

Long-term responses arise when a period is considered, such as a voyage, a year's service, or a ship's lifetime, exceeding the few hours a sea state remains constant. The main applications of long-term statistics in ship design and operations are:

- Prediction of extreme bending moments and wave-induced loads: In this case, the extreme value is the most significant value the ship may experience in its lifetime [25].
- Estimating long-term motion probabilities and ship operability is particularly important for naval, service, and passenger vessels [25].
- Estimation of average speed during a voyage. In predicting the average speed, two factors should be considered: the natural speed reduction due to the added resistance and loss in propulsive efficiency in waves and the voluntary speed reduction by the ship's captain to ease severe motions. This estimation requires probability distribution of the ship's service speed depending on loading conditions and probability distribution of the ship's required course, depending on location and season [25].

4. ANALYTICAL AND NUMERICAL ANALYSIS OF A VERTICAL CIRCULAR CYLINDER

Before the offshore wind turbine platform analysis, a simple vertical circular cylinder was studied numerically and analytically. In this way, the aim was to verify the numerical analyses. After the validation step of the study, a numerical analysis of the offshore wind turbine platform was performed, and the analysis of the platform was discussed in the next section.

Heave (vertical) motion was studied in comparison to the analysis. First, the hydromechanical coefficients added mass and damping coefficient were compared. Then, Froude-Krylov Forces (F_3^{FK}), Diffraction Forces (F_3^D), and the Total Wave Excitation Forces (F_3), obtained from the coefficients and object geometry here, were compared. Finally, the Response Amplitude Operator (RAO) values obtained using all parameters were compared.

4.1 Vertical Circular Cylinder for Analytical and Numerical Solutions

While choosing the vertical circular cylinder, care was taken to ensure it was vertically axisymmetric. In this way, it is aimed to facilitate the analytical calculation of the forces and other parameters to be obtained. At the same time, the spar-type offshore platform uses complex geometry in vertical axisymmetric structures.

Below is a representative image of the vertical circular cylinder used as the primary geometry in Figure 4.1. The model used for the numerical solution is shown in Figure 4.2. The vertical circular cylinder's draught is $T_c = 0.45\ (m)$ and diameter is $D_c = 0.60\ (m)$.

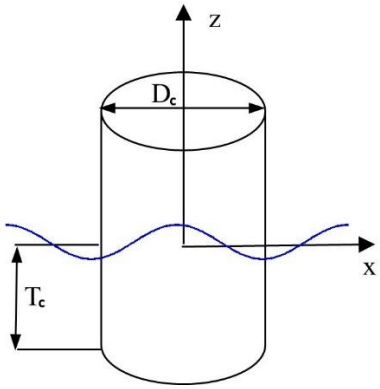

Figure 4.1 : Vertical circular cylinder selected for the primary geometry.

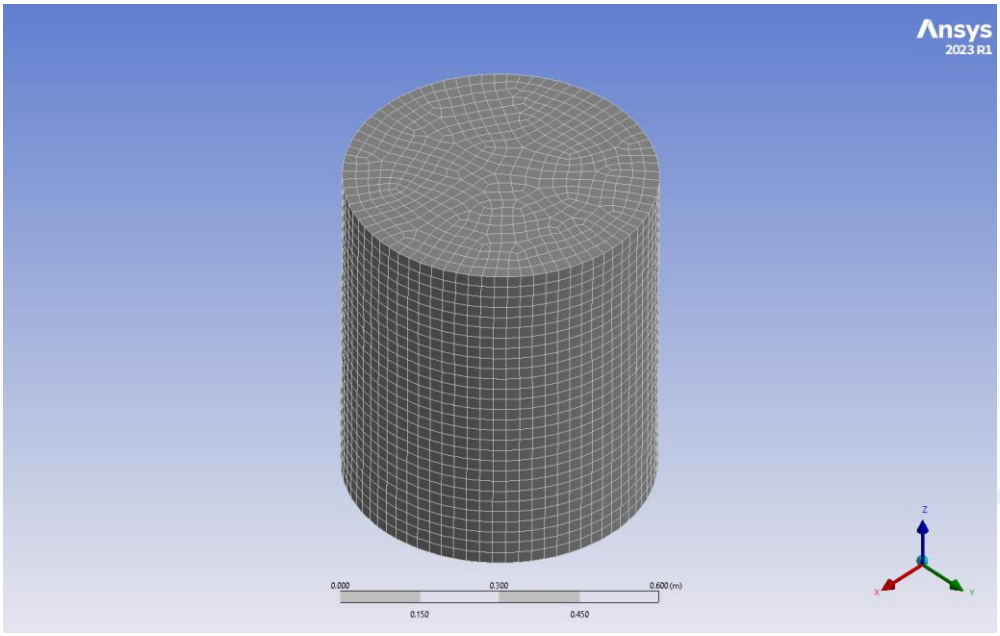

Figure 4.2 : The vertical circular cylinder model in AQWA.

4.2 Analytical Solution of Vertical Circular Cylinder

First, solutions were made for the vertical circular cylinder using analytical methods. The values obtained here are shared in tables and graphics; how these values were obtained is detailed.

4.2.1 Added mass and damping coefficient

To determine the wave excitation forces, the added mass (A_3) and the damping coefficient (B_3) must be known. It is not possible for the vertical cylindrical pontoon studied to use a frequency-independent relation while calculating these parameters. Because the studied frequency range is a broad domain moving from low to high. The study of V. Ferdinande and B. G. Kritis in 1980 was used for the values here [40]. This

study aims to calculate these parameters and the wave excitation forces obtained from these parameters depending on the frequency. The study is on calculating the added mass and damping coefficient for axisymmetric geometries.

The parameters are correlated theoretically and experimentally for the floating bodies. It is then plotted based on frequency for the primary dimension (the radius for the vertical circular cylinder) scenarios from the different axes of draft and symmetry. Among these scenarios, geometry, where the draft is 1.5 times the radius of the vertical circular cylinder, is preferred for study. The added mass and damping coefficient graphs obtained from the mentioned experimental study used for analytical solutions are shared in Figure 4.3 and Figure 4.4 [40].

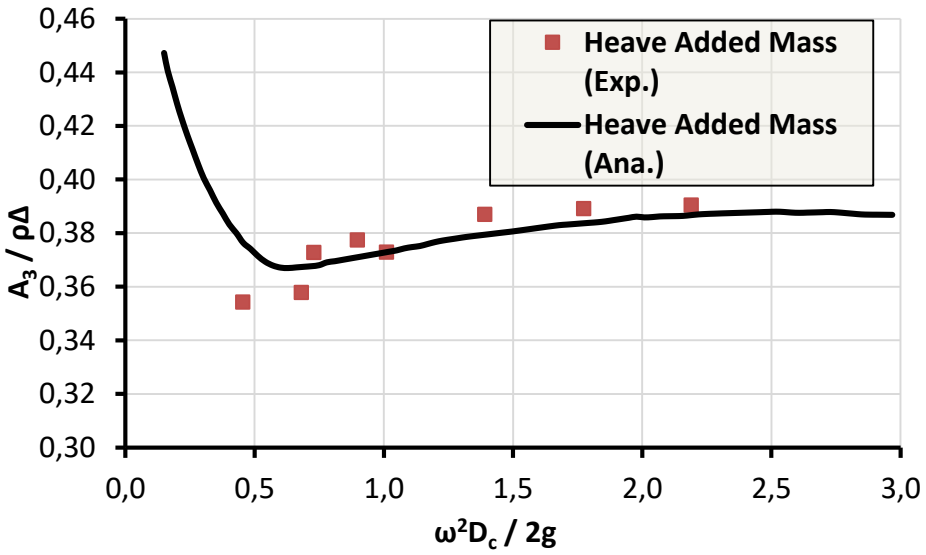

Figure 4.3 : Added Mass (A_3) for analytical solution.

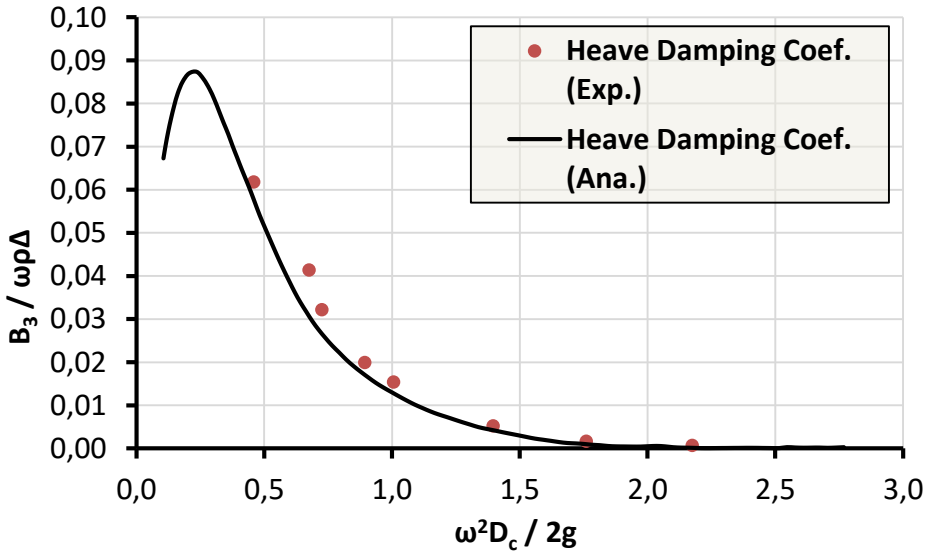

Figure 4.4 : Damping coefficient (B_3) for analytical solution.

4.2.2 Wave exciting force (F_3)

The vertical (Heave) wave exciting force can be expressed as a sum of the Froude-Krylov and diffraction force components as follows:

$$F_3 = F_3^{FK} + F_3^D \tag{4.1}$$

For zero forward speed ($\boldsymbol{\omega_e = \omega}$) the incident wave velocity potential becomes

$$\phi_I = \frac{ig\zeta}{\omega} e^{-ik(xcos\mu + ysin\mu)} e^{kz} e^{i\omega t}$$

In head seas ($\mu = 180^0$) and $sin(180^0) = 0$, $cos(180^0) = -1$

$$\phi_I = \frac{ig\zeta}{\omega} e^{ikx} e^{kz} e^{i\omega t} \tag{4.2}$$

Then, the pressure is equal to

$$p = -\rho \frac{\partial \phi_I}{\partial t} = \rho g \zeta e^{-kT_c} e^{ikx} e^{i\omega t} \tag{4.3}$$

The vertical Froude-Krylov force is

$$F_3^{FK} = \iint_S pnds = \rho g \zeta \frac{\pi \omega^2}{4} e^{-kT_c} e^{ik0} e^{i\omega t}$$

$$F_3^{FK} = \rho g \zeta \frac{\pi D^2}{4} e^{-kT_c} \cos(\omega t) \tag{4.4}$$

The vertical diffraction force is

$$F_3^D = (A_3 \ddot{\eta}_3) + i(B_3 \dot{\eta}_3) \#(4.5)$$

Vertical velocity due to heave motion in head seas

$$\dot{\eta}_3 = \frac{\partial \phi_I}{\partial z} = \frac{igk\zeta}{\omega} \left(\zeta e^{ikx} e^{kz} e^{i\omega t}\right) = i\omega \zeta e^{ikx} e^{-kT_c} \cos(\omega t) \tag{4.6}$$

Vertical acceleration due to heave motion in head seas

$$\ddot{\eta}_3 = \frac{\partial}{\partial t}\left(\frac{\partial \phi_I}{\partial z}\right) = \frac{\partial}{\partial t}\left(i\omega \zeta e^{ikx} e^{kz} e^{i\omega t}\right) = -\omega^2 \zeta e^{ikx} e^{-kT_c} \cos(\omega t) \tag{4.7}$$

Different approaches exist for the diffraction force's added mass (A_3) and damping coefficient (B_3) parameters. Single empirical formulas can be used, especially for incoming fixed-frequency waves. However, a frequency-varying formulation should be used for the vertical circular cylinder pontoon studied here because the motions and

forces observed within the scope of the study were examined between 1 rad/sec and 10 rad/sec. In this regard, the added mass and damping coefficient correlated with the experimental results prepared by Ferdinande and Kritis in the literature was taken as the basis [40]. The values in the study were digitised and then compared with the outputs obtained from the numerical analysis.

Heave added mass and heave damping coefficient for a vertical circular cylinder are given as A_3 and B_3, were digitised from Ferdinande and Kritis' work and obtained in tables and graphics depending on frequency. Relevant data are shared in the comparison section [40].

The Heave Damping coefficient for a vertical circular cylinder is given as

$$F_3^D = -A_3\omega^2\zeta e^{-kT}\cos(\omega t) - B_3\omega\zeta e^{-kT_c}\cos(\omega t) \tag{4.8}$$

The final total vertical (heave) force is

$$F_3 = F_3^{FK} + F_3^D = \rho g\zeta\frac{\pi D_c^2}{4}e^{-kT_c} + (-A_3\omega^2\zeta e^{-kT_c} - B_3\omega\zeta e^{-kT_c})$$

The basic form of total vertical (heave) force is

$$F_3 = F_3^{FK} + F_3^D = e^{-kT_c}\zeta\left[\left(\rho g\frac{\pi D_c^2}{4}\right) - \omega(A_3\omega + B_3)\right] \tag{4.9}$$

Parameters in the Formula

Wave period : $T\ (sec)$

Wave frequency : $\omega = \frac{2\pi}{T}\ (rad/sec)$

Wave number : $k = \frac{\omega^2}{g}\ (m^{-1})$

Wave amplitude : $\zeta = 0.30\ (m)$

Sea water density : $\rho = 1025\ (kg/m^3)$

Gravity acceleration : $g = 9.81\ (m/s^2)$

Draught : $T_c = 0.45\ (m)$

Cylinder diameter : $D_c = 0.60\ (m)$

Added mass : A_3 [40]

Damping coefficient : B_3 [40]

The total vertical (heave) force is

$$F_3 = F_3^{FK} + F_3^D = e^{-kT_c}\zeta\left[(\rho g \frac{\pi D_c^2}{4}) - \omega(A_3\omega + B_3)\right]$$

$$F_3 = e^{-\mathrm{k}*0.45} * 0.30\left[\left(1025 * 9.81 * \frac{\pi * 0.6^2}{4}\right) - \omega(A_3\omega + B_3)\right] \qquad (4.10)$$

The wave amplitude divides the excitation force to make the result more meaningful.

$$\frac{F_3}{\zeta} = \frac{[F_3^{FK} + F_3^D]}{\zeta} = \left[e^{-kT_c}\zeta\left[(\rho g \frac{\pi D_c^2}{4}) - \omega(A_3\omega + B_3)\right]\right]/\zeta$$

$$\frac{F_3}{\zeta} = \left[e^{-\mathrm{k}*0.45} * 0.30\left[\left(1025 * 9.81 * \frac{\pi * 0.6^2}{4}\right) - \omega(A_3\omega + B_3)\right]\right]/\zeta \qquad (4.11)$$

When the previously calculated added mass and damping coefficient values were used for wave excitation forces, the results in the graphics were obtained. Wave Excitation Forces, as calculated by the analytical solution, are shared in Figure 4.5, Figure 4.6 and Figure 4.7.

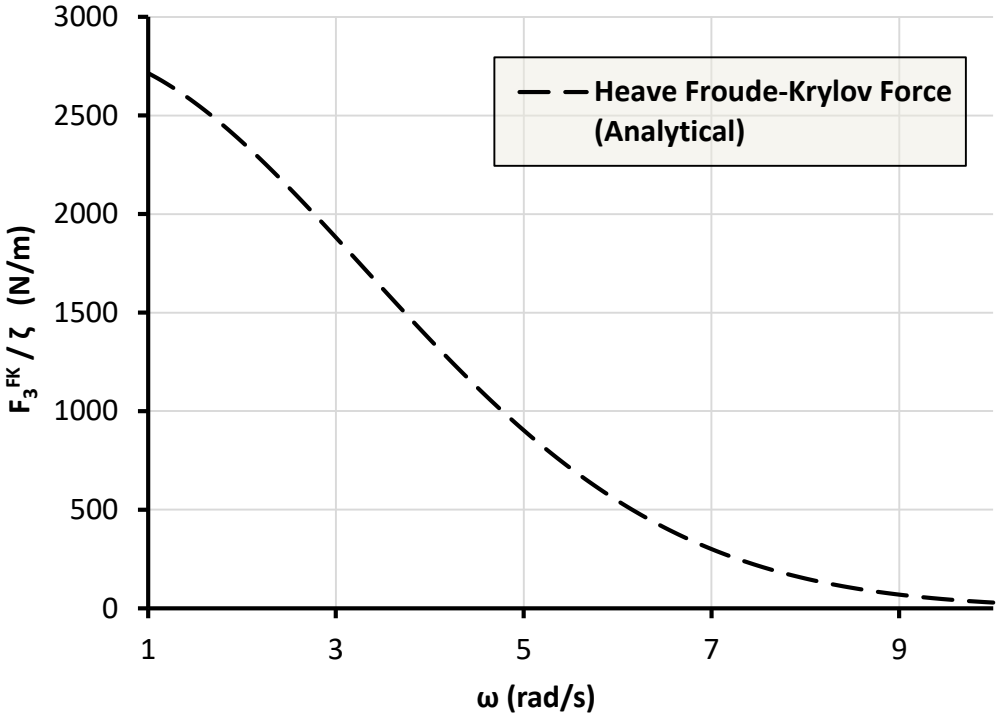

Figure 4.5 : Heave Froude-Krylov force (F_3^{FK}) from analytical solution.

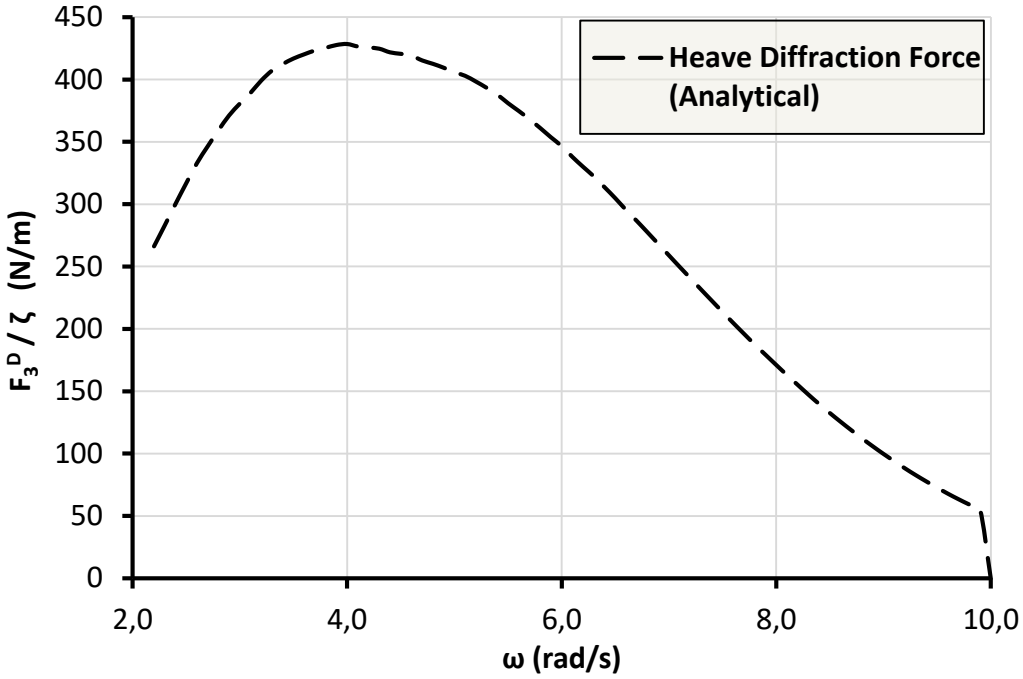

Figure 4.6 : Heave diffraction force (F_3^D) from analytical solution.

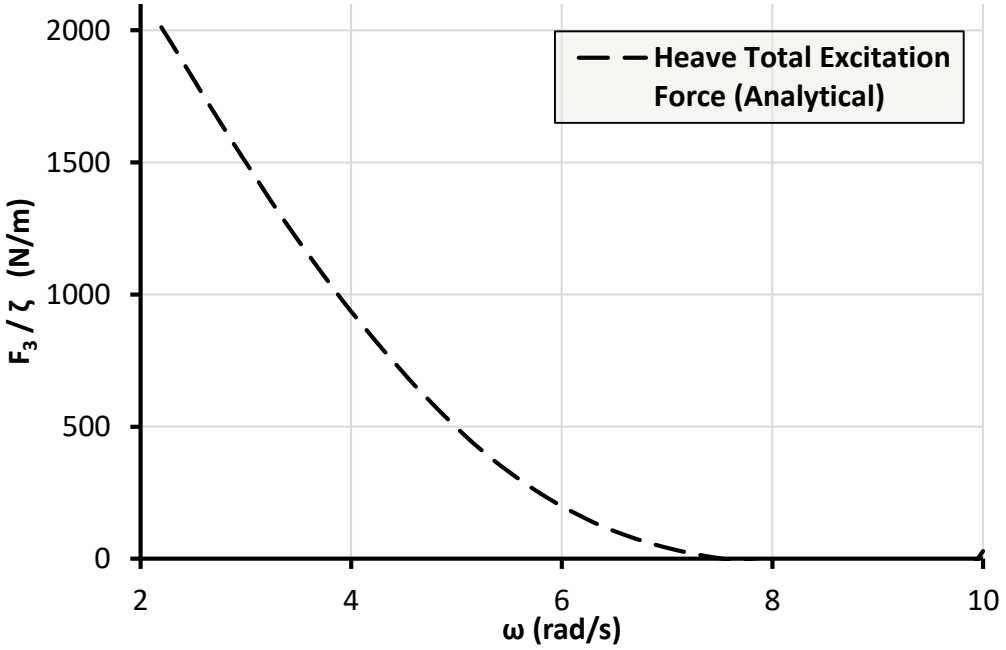

Figure 4.7 : Heave total force (F_3) from analytical solution.

4.2.3 Response amplitude operator (RAO)

When calculating the Response Amplitude Operator (RAO), the total excitation force, added mass and damping coefficient should be known first. These values were found when calculating the excitation forces. In addition, the Restoring force and the object's mass should be known. These values were obtained from the body geometry and the Archimedean principle.

4.2.3.1 Estimate the heaving amplitude

$$\left[\sqrt{[C_3-\omega^2(M+A_3)]^2+[iB_3]^2}\right]*\eta_3=F_3 \tag{4.12}$$

Then, the heave motion amplitude is

$$\eta_3=\frac{F_3}{\sqrt{[C_3-\omega^2(M+A_3)]^2+[iB_3]^2}} \tag{4.13}$$

$$RAO=\frac{\eta_3}{\zeta}=\left[\frac{F_3}{\sqrt{[C_3-\omega^2(M+A_3)]^2+[iB_3]^2}}\right]/\zeta \tag{4.14}$$

From Section 4.2.2

$$F_3=F_3^{FK}+F_3^D=\ e^{-kT_c}\zeta\ [(\rho g\frac{\pi D_c^2}{4})-\omega(A_3\omega+B_3)]$$

$$F_3=e^{-\mathrm{k}*0.45}*0.30\left[\left(1025*9.81*\frac{\pi*0.60^2}{4}\right)-\omega(A_3\omega+B_3)\right] \tag{4.15}$$

The mass is

$$M=\rho\frac{\pi}{4}T_c=1025*\frac{\pi*0.60^2}{4}*0.45$$

$$M=130.415kg \tag{4.16}$$

The restoring coefficient is

$$C_3=\rho g\frac{\pi D_c^2}{4}=1025*9.81*\frac{\pi*0.60^2}{4}$$

$$C_3=2843.055kN/m \tag{4.17}$$

Other parameters required for the Response Amplitude Operator (RAO) were calculated within the scope of wave excitation forces. The following equations are obtained when all the calculated values and parameters are replaced.

$$RAO=\frac{\eta_3}{\zeta}=\left[\frac{F_3}{\sqrt{[C_3-\omega^2(M+A_3)]^2+[iB_3]^2}}\right]/\zeta$$

$$RAO=\frac{\eta_3}{\zeta}=\left[\frac{F_3^{FK}+F_3^D}{\sqrt{[C_3-\omega^2(M+A_3)]^2+[iB_3]^2}}\right]/\zeta$$

$$RAO=\frac{\eta_3}{\zeta}=\left[\frac{e^{-kT}\zeta\left[\left(\rho g\frac{\pi D_c^2}{4}\right)-\omega(A_3\omega+B_3)\right]}{\sqrt{[C_3-\omega^2(M+A_3)]^2+[iB_3]^2}}\right]/\zeta \tag{4.18}$$

$$RAO = \frac{\eta_3}{\zeta} = \left[\frac{e^{-k*0.45} * 0.30 \left[\left(1025 * 9.81 * \frac{\pi * 0.6^2}{4} \right) - \omega(A_3\omega + B_3) \right]}{\sqrt{[2843.06 - \omega^2(130.42 + A_3)]^2 + [iB_3]^2}} \right] / \zeta \quad (4.19)$$

When calculating the Response Amplitude Operator (RAO), the total excitation force, added mass and damping coefficient should be known first. These values were found when calculating the excitation forces. In addition, the restoring coefficient and the object's mass should be known. These values were obtained from the building geometry and the Archimedean principle.

In the RAO relation, wave number (k), added mass (A_3) and damping coefficient (B_3) vary depending on frequency (ω). Figure 4.8 is obtained when these values are substituted according to the frequency.

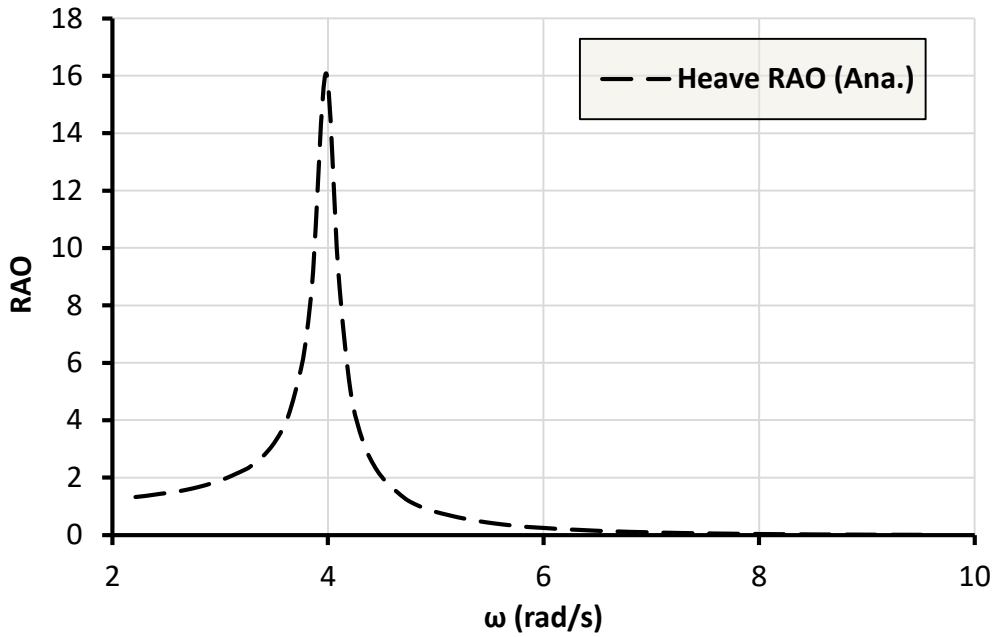

Figure 4.8 : Heave Response Amplitude Operator (RAO) from analytical solution.

4.3 Numerical Solution of Vertical Circular Cylinder

After the analytical solution for the vertical circular cylinder was chosen as the vertical circular cylinder, the same parameters were also calculated with the numerical solution. Choosing one of the ready-made software packages was considered appropriate for the numerical solution. This ready-made package software for complex geometry should give reliable and comparable results. It has been decided to use the ANSYS Workbench-based AQWA module because it gives reliable results as software

and has been preferred for a long time for modelling offshore structures and various situations of ships at sea. The ANSYS Workbench-based AQWA module, typically licensed for a fee, is provided to its students by Istanbul Technical University. The software offers solutions with a 3D panel system. It works with the finite element method and mesh logic and accepts the fluid has ideal behaviour.

Analytical and numerical solutions in this section are compared using the same graph. The results obtained were satisfactory and meaningful. From this, it has been determined that the ANSYS Workbench-based AQWA module gives correct results for numerical solutions and provides a suitable infrastructure for comparison with experimental studies of complex geometry. Below are the comparison charts.

4.3.1 Added mass and damping coefficient

The added mass and damping coefficient values obtained from the ANSYS Workbench-based AQWA module were arranged in the same format as the result graphics in Ferdinand and Kritis' studies. As a result of this arrangement, Figure 4.9 and Figure 4.10 were obtained.

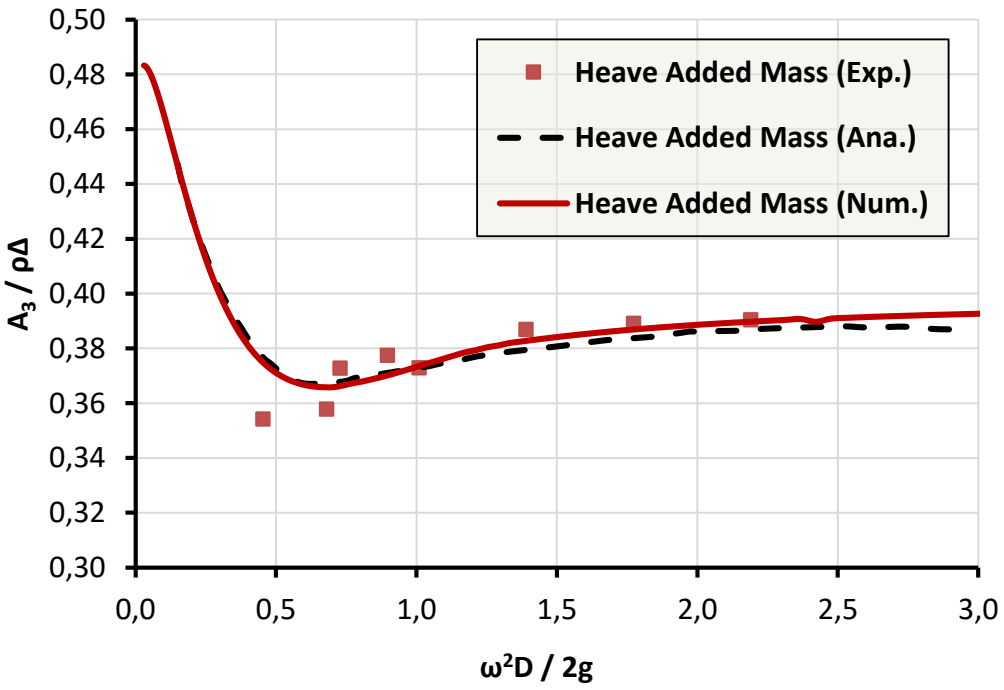

Figure 4.9 : Added mass (A_3) from analytical and numerical solutions.

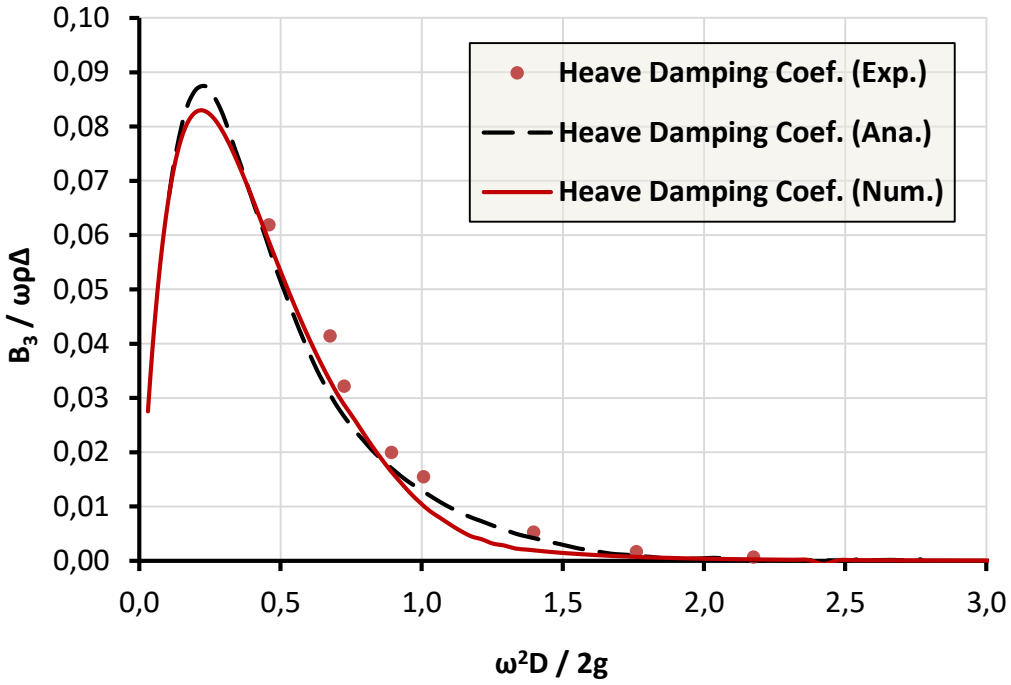

Figure 4.10 : Damping coefficient (B_3) from analytical and numerical solutions.

4.3.2 Wave excitation forces

Outputs for the vertical z-axis (heave motion) from the ANSYS Workbench-based AQWA module are obtained as the force divided by the wave amplitude. The outputs here are shared below in force/wave amplitude format (Figure 4.11, Figure 4.12 and Figure 4.13).

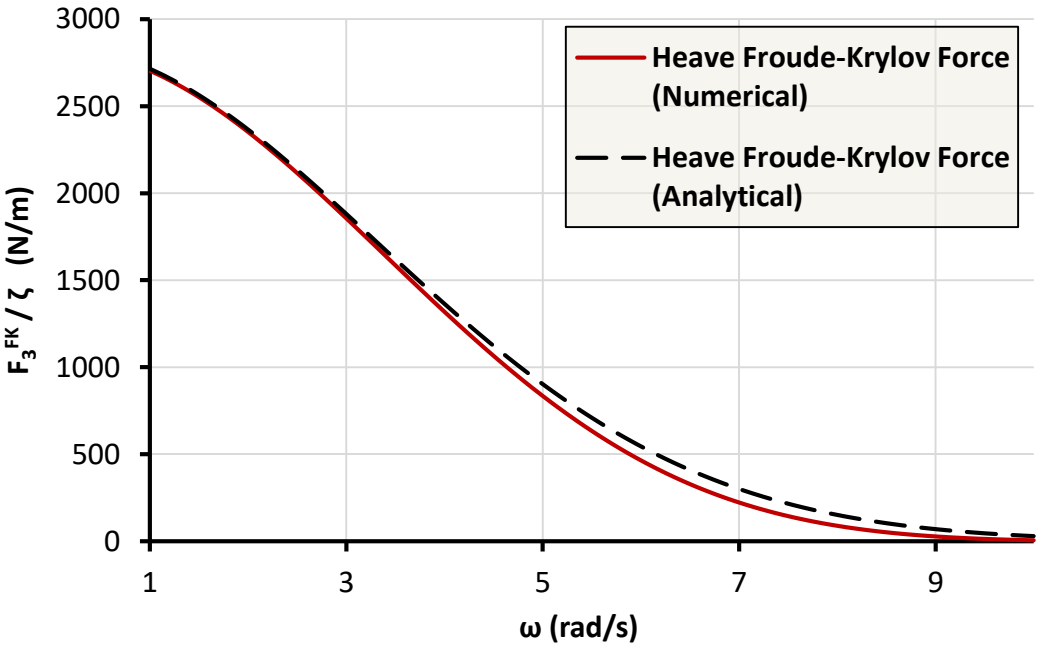

Figure 4.11 : Heave Froude-Krylov force (F_3^{FK}) from analytical and numerical solutions.

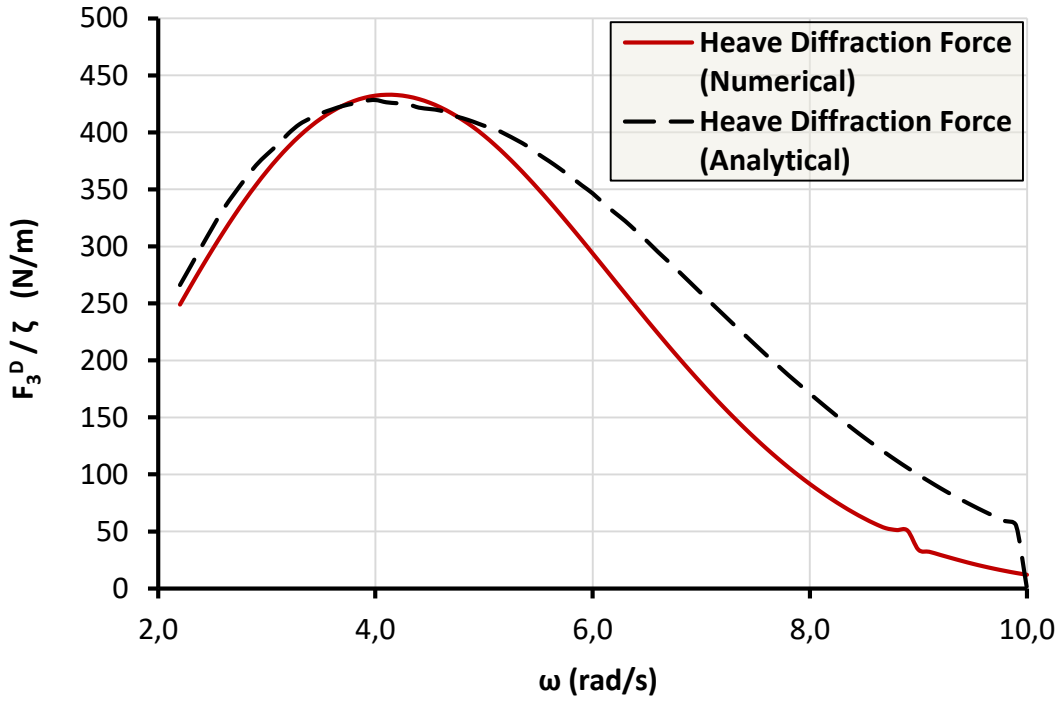

Figure 4.12 : Heave diffraction force (F_3^D) from analytical and numerical solutions.

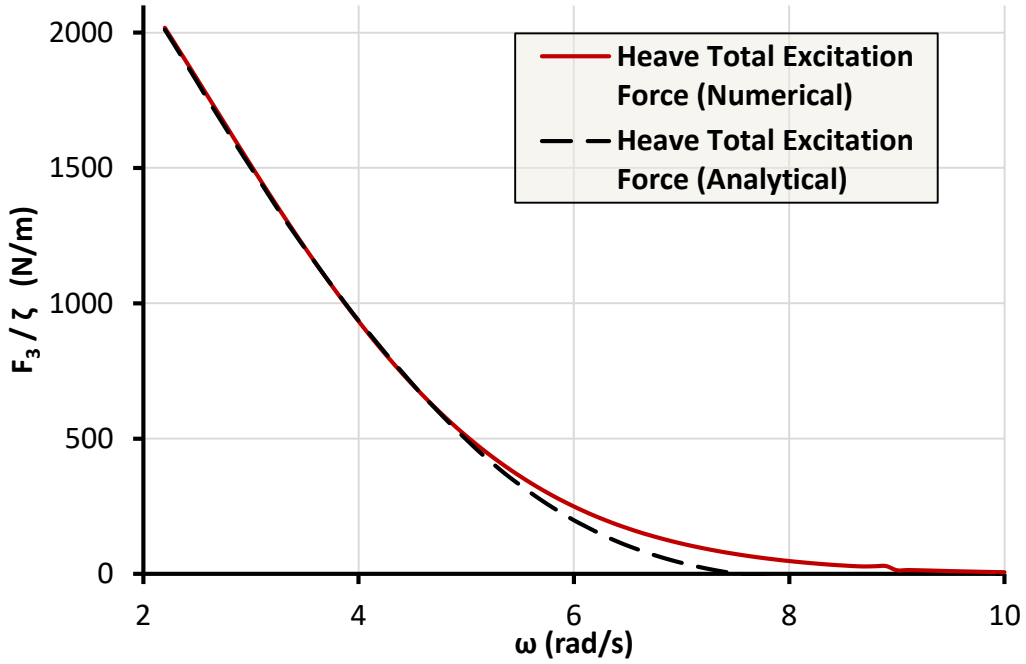

Figure 4.13 : Heave force (F_3) from analytical and numerical solutions.

4.3.3 Response amplitude operator (RAO)

Response Amplitude Operator (RAO) values from the ANSYS Workbench-based AQWA module are in the same format as the RAO format calculated by the analytical method. For this reason, the results were graphed as they were, without format changes in Figure 4.14.

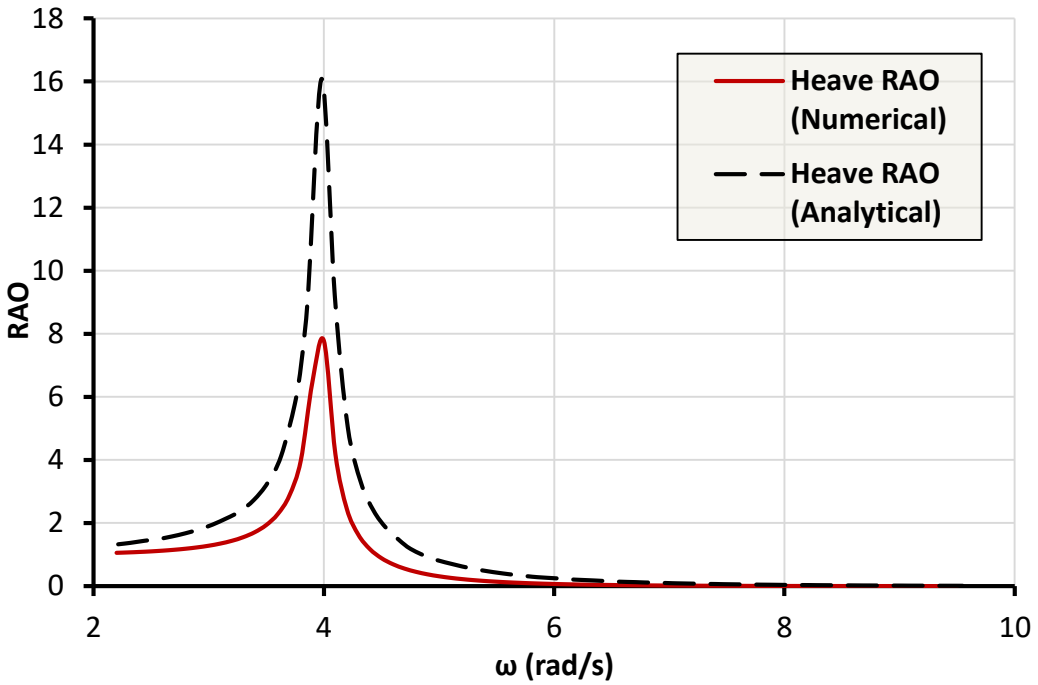

Figure 4.14 : Heave Response Amplitude Operator (RAO) from analytical and numerical solution.

5. EXPERIMENTAL AND NUMERICAL ANALYSIS OF THE FLOATING OFFSHORE PLATFORM

The previous section examined a floating vertical circular cylinder as a simple geometry analytically and numerically. This section compares the analytical, numerical, and experimental results of a tested spar-type (singular floating pile) offshore platform.

5.1 Definition of the Experimental Study

A spar-type offshore platform, OC3-Hywind, was considered the test case for validating numerical response predictions. Early tests with this platform were conducted at the National Renewable Energy Laboratory (NREL) in Colorado, United States [41].

Further experiments with OC3-Hywind were carried out at the Kelvin Hydrodynamics Laboratory (KHL) of the University of Strathclyde with a 1:74 scaled model of OC3-Hywind platform [42]. In these experiments, the focus was the platform's wave-induced hydrodynamic responses and the dynamic behaviour of the mooring lines. The experimental setup did not consider the effects of wind loads on the platform. The main issues that may affect the experimental results and need to be verified were as follows: water depth, scaling factor/methods, mooring design, selected wave frequencies, running time of the tests, sampling frequency and the effect of using a 2D wave channel. The details of this experimental study are summarized in the following sections [42].

5.1.1 Experiment setup

5.1.1.1 Tank design

The water depth of the experimental tank was set as 2.00 meters. In addition, a beach has been prepared where the waves end to eliminate long-term wave traces. It has been stated that the wave produced in KHL has long crests and is like a wave produced in natural offshore conditions. However, compared to the movement of the platform in

the natural sea area, the movement in tank tests is expected to be greater than in the natural sea because wave energy is in one direction instead of spreading to other directions.

When performing tank tests, “the model must be small enough to avoid visible effects of restricted water in the draw tank” [42]. Therefore, tank clogging and wall effects due to propagating and refracting waves must be considered. Clogging refers to the effects of finite width due to tank walls on the flow around a body and the effect of the wall on reflected waves. In this study, the blockage ratio between the model's cross-sectional area and the tank's cross-sectional area is 2.24%, which is stated that this ratio is small [42]. In addition, no movement from the propagating waves' reflections was observed in the free oscillation tests applied to the model. Therefore, this tank test study neglected clogging and wall effects [42]. The tank layout for both scenarios is shared in Figure 5.1.

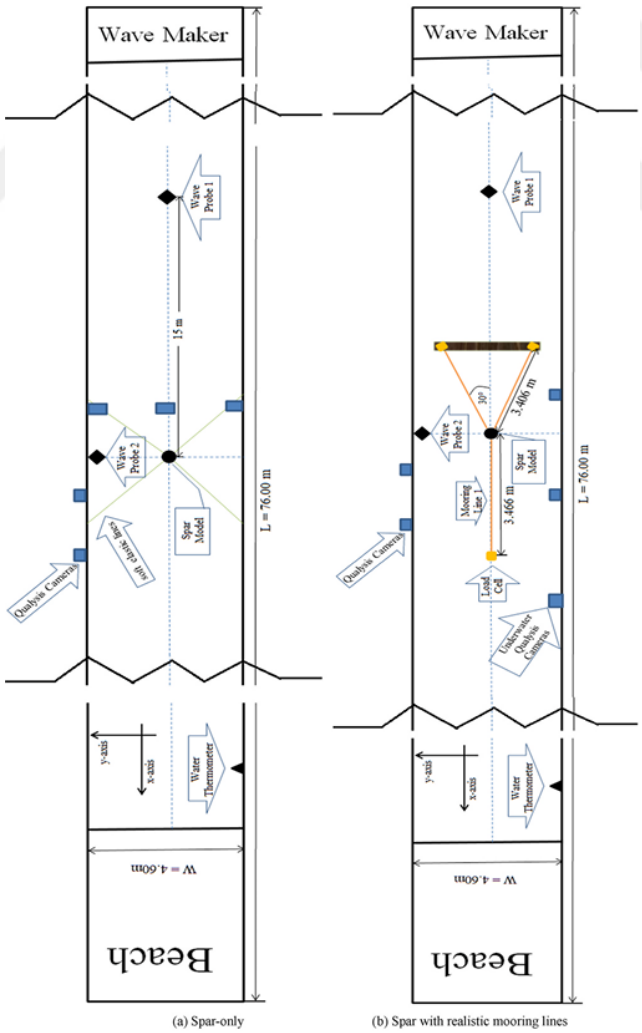

Figure 5.1 : Tank layout (a) Spar-only (b) Spar with realistic mooring lines [42].

5.1.1.2 Mooring design

Within the scope of experimental studies, scenarios were produced for two situations, with and without mooring lines.

Figure 5.1 (a) shows the experimental setup of the case without a mooring line in the Spar-only scenario. In this test model, soft and elastic mooring lines were used. Soft elastic lines were used to prevent the model from sliding down the wave, and the stiffness was chosen to minimize the interaction of the mooring lines with the system dynamics [42].

Figure 5.1 (b) shows the experimental setup of the situation with mooring lines in the Spar with realistic mooring lines scenario. They were scaled down (using a scaling factor) for binding stiffness from the OC3-Hywind binding system [43]. Since viscous effects dominate transverse fluid forces in the mooring lines, the Reynolds scaling method should ideally have been used. However, Xu and Day noted that the tests could not accurately capture all aspects of binding responses, as the experimental work focused on platform dynamic responses dominated by Froude scaling. For this reason, the mooring line's length, diameter, and weight distribution were selected to be close to the target values based on the Froude scale.

Due to the tank's width limitation, the mooring configuration has been slightly redesigned compared to the original layout. For the NREL OC3-Hywind model, the angle between each mooring line is 120^{o}. In this tank test, to make the mooring system as similar as possible to the NREL model, Mooring Line 1 is aligned with the wave direction, i.e., approving of the X axis but at an angle, as shown in Figure 5.1 (b). The angle between the other two mooring lines is reduced to 60^{o}, and the lines are placed symmetrically around the centre line of the tank [42].

5.1.1.3 Scaling methods and factors

In experimental studies, it is essential to scale the entire experimental setup meaningfully for the results to be reliable and meaningful. This issue was also taken into consideration in this experimental study. Reynolds and Froude numbers are important dimensionless scaling parameters for fluids. However, the Reynolds number is commonly used to scale flows around models in unconfined fluids dominated by viscous effects; however, this is not the case in the current experiment. The Froude number describes the relationship between inertial and gravitational forces. It forms

the basis of a scaling method for physical experiments in water waves where viscous forces are less critical, as preserving Froude similarity (i.e., maintaining the correct model scale Froude number) will accurately scale the dynamic behaviour of waves and structures [42, 44]. For this reason, Xu and Day used Froude scaling in their experimental studies.

A table of scaling factors determined for spar-type offshore platform's model testing is presented in Table 5.1 for the scaling factor λ to ensure both geometric similarity and Froude similarity. Considering the 2.0 m water depth in the KHL, the scaling factor was considered 1:74.

For the Hywind Scotland Pilot Park, the water depth on site is 105 m, and the draft of the mast platform is 78 m. This study's ratio between water depth and platform draft is approximately 0.743 and 0.810, indicating that a scaling factor 1:74 is reasonable.

Table 5.1 : Established scaling factors in the experimental study [42, 45].

Parameter	Unit	Scale Factor
Length (e.g., displacement, wave height and length)	L	σ
Area	L^2	σ^2
Volume	L^3	σ^3
Density	M/L^3	1
Mass	M	σ^3
Time (e.g., wave period)	T	$\sigma^{0.5}$
Frequency (e.g., rotor rotational speed)	T^{-1}	$\sigma^{-0.5}$
Velocity (e.g., wind speed)	LT^{-1}	$\sigma^{0.5}$
Acceleration	LT^{-2}	1
Force	MLT^{-2}	σ^3
Moment (e.g., rotor torque)	ML^2T^{-2}	σ^4
Power	ML^2T^{-3}	$\sigma^{3.5}$
Stress	$ML^{-1}T^{-2}$	σ
Mass moment of inertia	MT^2	σ^5
Area moment of inertia	L^4	σ^4

5.1.1.4 Final model definition

The information that may be needed for the experimental setup and model is detailed within the scope of the experimental setup. The features of the spar-type offshore platform in question are shared in Table 5.2. In this study, full-scale values are considered for the model.

Table 5.2 : Model properties and parameters [42].

Final Model Properties	Tank-scale Model	Full-scale Model
Water Depth (m)	2.0	148.0
Depth to Platform Base Below SWL (Total Draft) (m)	1.6	120.0
Depth to Top of Taper Below SWL (m)	0.054	4.0
Depth to Bottom of Taper Below SWL (m)	0.162	12.0
Platform Diameter Above Taper (m)	0.088	6.5
Platform Diameter Below Taper (m)	0.127	9.4
Platform Mass, Including Ballast (kg)	18.5	7.5 E+06
CM Location of the Whole Structure Below SWL Along Platform Centreline (m)	1.1	80.7
Pitch/Roll Inertia of the Whole Structure about CG (kg*m^2)	9.3	2.1E+10
Number of Mooring Lines	3	3
Angle Between Adjacent Lines (deg)	0/150/210	0/150/210
Depth to Fairleads Below SWL (m)	0.9	70.1
Unstretched Mooring Line Length (m)	3.6	263.1
Mooring Line Diameter (m)	0.002	0.1
Equivalent Mooring Line Weight (kg/ m)	0.013	71.2
Equivalent Mooring Line Extensional Stiffness (N/m)	1.6 E+05	8.9 E+08
Radius to Anchors from Platform Centreline (m)	3.5/3.4	256.4/252.1
Anchor Depth (m)	1.9/1.8	139.9/135.3
Radius to Fairleads from Platform Centreline (m)	0.074	5.5
Tower Height (m)	1.2	89.5
Tower Total Mass (kg)	1.3	5.2 E+05

In addition, Figure 5.2 shares the dimensions of the tank-scale model that need to be known when processing the solid model into the numerical simulation. A full-scale model is obtained when the tank-scale model is enlarged 74 times.

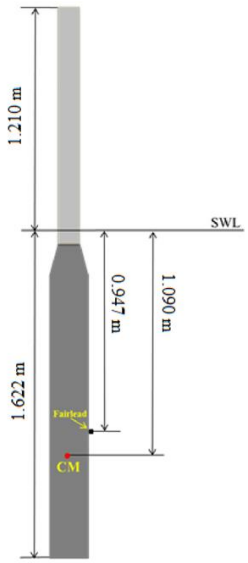

Figure 5.2 : Spar-type offshore platform's tank scale model [42].

5.1.2 Experiment conditions

In their studies, Xu and Day used irregular wave series to represent different sea states. They created these irregular wave series with JONSWAP spectra [42]. Here, the sea state nomenclature in Xu and Day's study differs from the globally accepted nomenclature determined by the World Meteorological Organization (WMO).To avoid confusion, sea state codes compatible with those worldwide were used throughout the study. These codes are mentioned in Table 3.5 and Table 3.6. The codes used for the experiments are also shared in Table 5.3. The study here was carried out on a full scale. Therefore, sea state conditions were studied with full-scale parameters.

Table 5.3 : Wave parameters for the four sea states.

	Target Full Scale		Target Tank Scale	
Sea State	T_p (s)	H_s (m)	T_p (s)	H_s (m)
5	9.700	3.660	1.128	0.050
6	11.300	5.490	1.314	0.074
8	13.600	9.140	1.581	0.124
9	17.000	15.240	1.976	0.206

They studied four sea states and shared results for two (sea states 6 and 8). Experimental studies were conducted on two basic scenarios: the free state without a mooring line and the state with mooring lines.

This study created a numerical model for all experimental conditions, and the results were shared in Xu and Day's studies [42]. The numerical results obtained were compared with the experimental results.

Within the scope of the study, three basic ship motions were studied. These are heave, surge/sway, and pitch/roll. A symmetrical structure will be seen when looking at the platform as a top view from the Z axis (bird's eye view), so the same reaction occurs in the x and y axes, regardless of the wave's direction of arrival. For this reason, surge and sway movements and pitch and roll movements occur similarly. In this way, five of the six basic ship motions were examined.

5.2 Numerical Analysis

For numerical solutions, comparisons were made based on full-scale results. Numerical solutions were performed with the AQWA module in ANSYS Workbench.

The model of the full-scale spar-type offshore platform used for the numerical solution is shared in Figure 5.3.

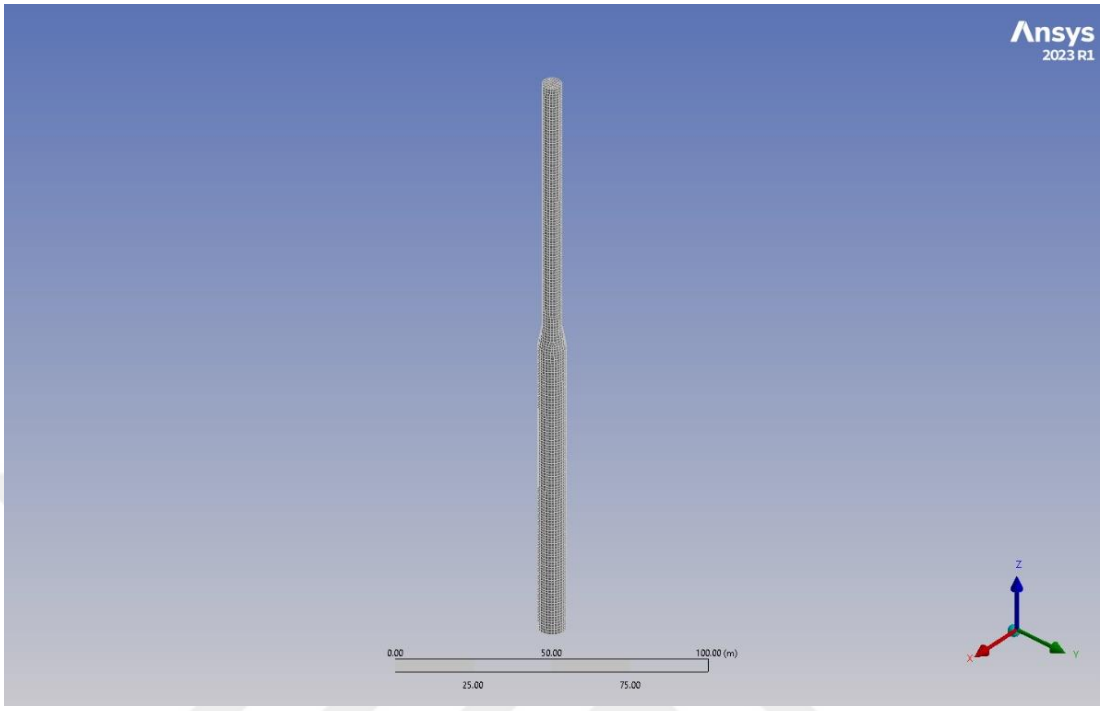

Figure 5.3 : The full-scale spar-type offshore platform model in AQWA.

5.2.1 Comprising of Response Amplitude Operators (RAO)

Response Amplitude Operators were compared for all movements studied in the frequency domain. In the comparison, analytical results, as well as numerical and experimental results, were shared.

When the results were examined, it was observed that the results were satisfactory for all solution methods. Natural frequencies have been captured in similar locations. The increase and decrease values are also compatible. However, there are differences in peak values in the zone that are close to the natural frequency.

Xu and Day also mentioned this situation in their studies. This situation is because the motion of floating objects is extremely sensitive to frequency. RAO graphics for movements are in Figure 5.4, Figure 5.5 and Figure 5.6, and the natural frequency table is shared in Table 5.4.

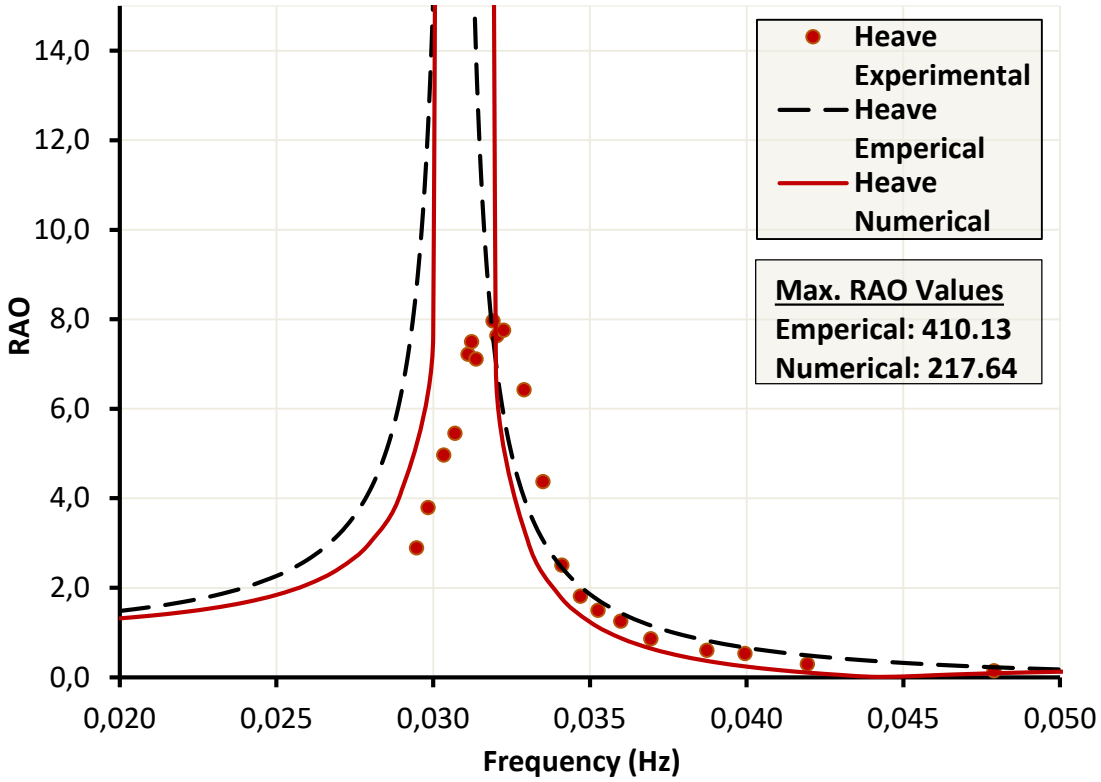

Figure 5.4 : Heave RAO for the spar-type platform.

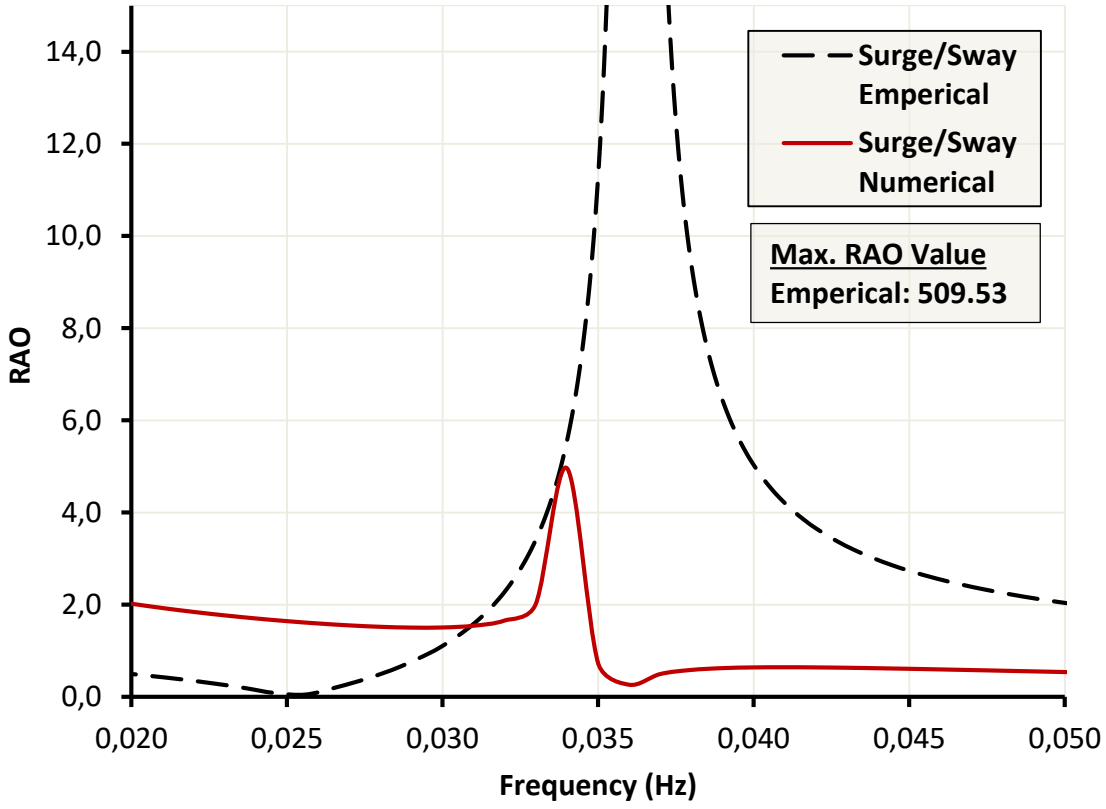

Figure 5.5 : Surge/Sway RAO for spar platform.

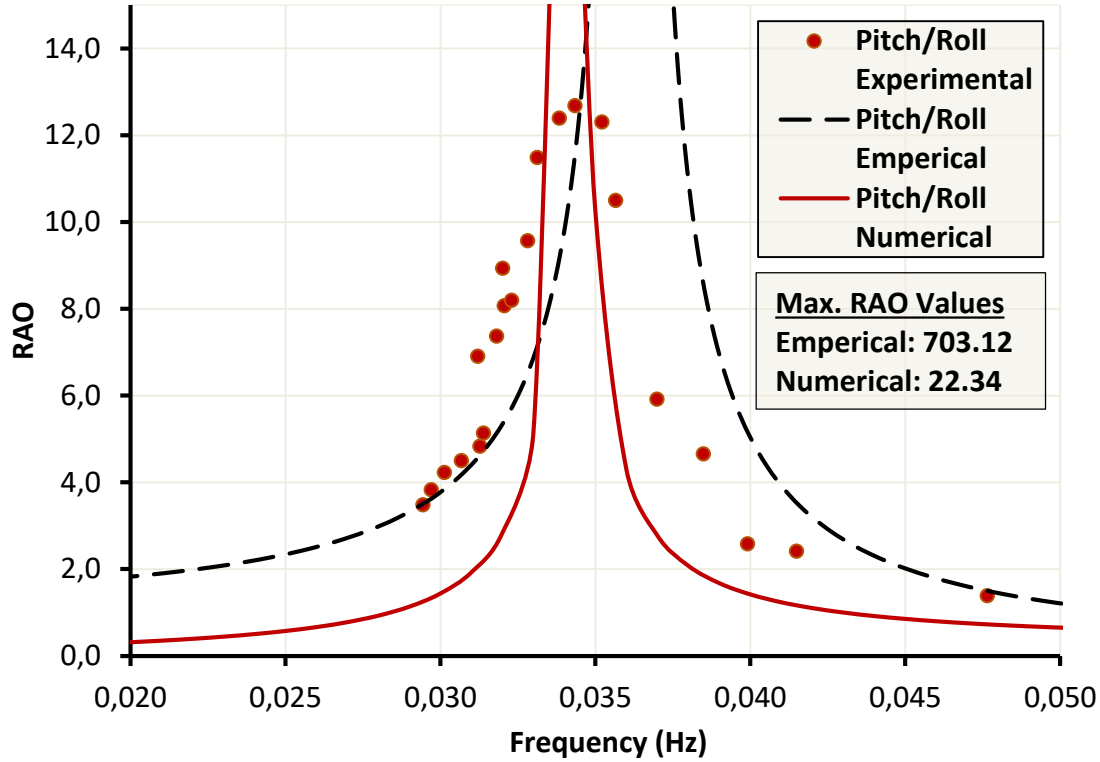

Figure 5.6: Pitch/Roll RAO for spar platform.

Table 5.4 : Natural frequencies.

Motion	Empirical	Numerical	Experimental
Heave	0.031 Hz	0.031 Hz	0.032 Hz
Surge / Sway	0.036 Hz	0.034 Hz	-
Pitch / Roll	0.036 Hz	0.034 Hz	0.034 Hz

As can be seen from the RAO results, natural frequencies for all movements are at minimal values. Wavelengths for natural frequencies in deep sea conditions exceed 1200 meters. These are waves that are impossible to encounter in nature. The frequency relationship with deep sea waves is shared in equation 5.1.

$$\lambda_0 = \frac{g}{2\pi}\left(\frac{1}{f}\right)^2 \tag{5.1}$$

λ_0: $wavelength\ for\ deep\ water$

f: $frequency$

g: $gravity\ acceleration$

5.2.1.1 Extreme deep sea conditions for Turkish seas

The natural frequencies for the spar-type floating offshore platform studied are given in Table 5.4. Since the frequencies found are very low, it is doubtful that deep sea wavelengths will be encountered at this frequency. In order to detect this situation in the Turkish seas, the most significant wavelengths on the country's coastlines were investigated.

For this purpose, Türkiye's sea and wave climate was first examined. While making this analysis, the Turkish Coastal Wind and Deep-Sea Wave Atlas, the most comprehensive coastal marine climate study conducted for the Turkish seas to date, was used [46]. Atlas was published in 2002 by Özhan and Abdalla under the leadership of MEDCOAST (Mediterranean Coastal Foundation), METU (Middle East Technical University), and NATO (North Atlantic Treaty Organization).

The maximum H_s values were determined for each sea separately to find the most significant wavelengths. The determined H_s values and their coordinates are shared in Table 5.5.

Table 5.5 : Maximum H_s values of Turkish seas [46].

Region	$H_{s,max}$	Recurrence period (R_p)	Exceeding probability	Coordinate
Black Sea	10.85 m	100 years	%1.00	42.00º N, 28.40º E
Marmara Sea	6.50 m	30 years	%0.75	40.98º N, 28.57º E
Aegean Sea	10.50 m	100 years	%1.00	36.75º N, 27.70º E
Mediterranean Sea	10.75 m	50 years	%2.00	36.00º N, 32.80º E

$H_{s,max}$ values determined from the atlas are similar except for the Marmara Sea. This situation is possible because the Marmara Sea is a relatively small sea and the fetch distances. As expected, the most enormous H_s value was detected west of the Black Sea.

The period of the waves was estimated from the $H_{s,max}$ values were obtained. For this purpose, the wave steepness relationship for each sea was used. Yüksel et al. studied the wave steepness relationship (H_s - T_m relationship) for the Turkish seas in 2011 [47]. As a result of the study, they determined T_m values for each sea as a variable dependent on H_s (Table 5.6). The R^2 value in the table shows the calibration value of the wave steepness relationship (zero to one).

Table 5.6 : Wave steepness of Turkish seas [47].

Region	Relationship	(R^2)
Black Sea	$T_m = 4.513\ x\ H_s^{0.3235}$	0.9553
Marmara Sea	$T_m = 3.521\ x\ H_s^{0.3327}$	0.9621
Aegean Sea	$T_m = 3.623\ x\ H_s^{0.35}$	0.9426
Mediterranean Sea	$T_m = 4.473\ x\ H_s^{0.3371}$	0.8991

The H_s values obtained in Table 5.5 were substituted in the relationships in Table 5.6, and T_m values were found for $H_{s,max}$ in each sea. Then, these period values were placed into equation 5.1, and the deep-sea wavelength was found. Frequency values corresponding to periods were also calculated. All values found are shared in Table 5.7.

Table 5.7 : T_m and λ_0 values for Turkish seas' $H_{s,max}$

Region	T_m (s)	λ_0 (m)	Frequency (Hz)
Black Sea	9.7595	148.7114	0.1025
Marmara Sea	6.5633	67.2564	0.1524
Aegean Sea	8.2506	106.2821	0.1212
Mediterranean Sea	9.9606	154.9031	0.1004

When the frequency values in Table 5.7 and the natural frequencies in Table 5.4 are compared, the natural frequency cannot be approached for any movement in the Turkish Seas. This result shows that there is no possibility of resonance.

5.2.1.2 Pierson-Moskowitz sea states spectrum

Pierson Moskowitz wave spectra were created for different sea states to compare RAO results with sea states. Spectra were created using the relations in equation 3.50 and equation 3.51. For H_s, which is the primary variable in the relationship; the values in Table 3.6 were used. The created spectra can be seen in Figure 5.7.

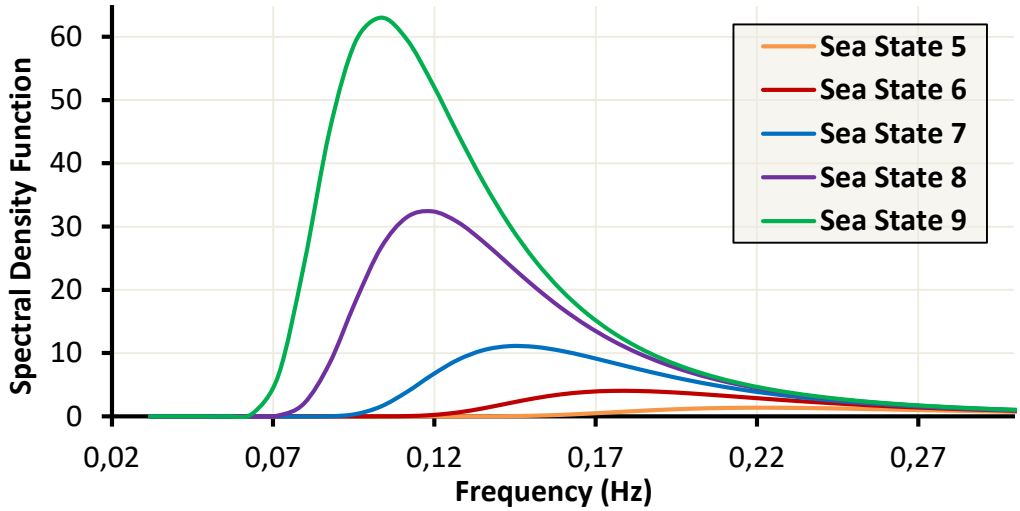

Figure 5.7 : Pierson Moskowitz wave spectrums for sea states.

5.2.1.3 Compearing of RAO and sea states

The obtained wave spectra were moved to the same graph as the RAO graphs, and the results were compared. When the results are evaluated, the natural frequency that the spar-type offshore platform is expected to resonate with is far from the peak region of the spectra for all movements and all sea states. This situation proves the platform will resonate with waves that cannot be encountered in nature, meaning there is no resonance danger. RAO and sea state comparison graphs can be seen in Figure 5.8, Figure 5.9 and Figure 5.10.

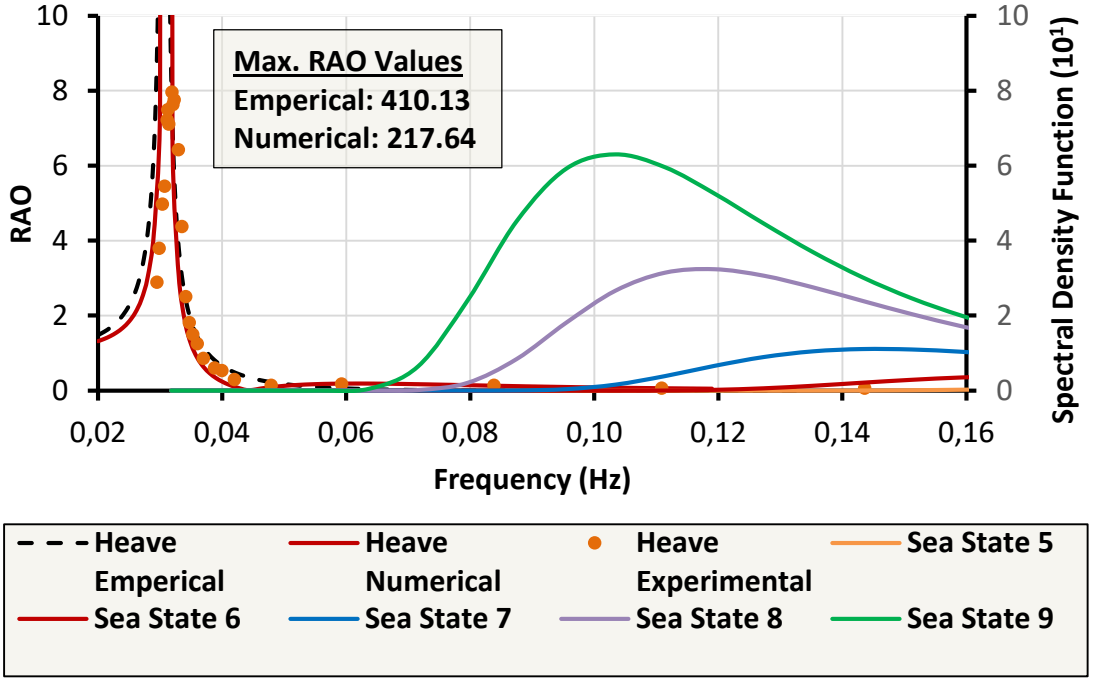

Figure 5.8 : Heave RAO and sea states.

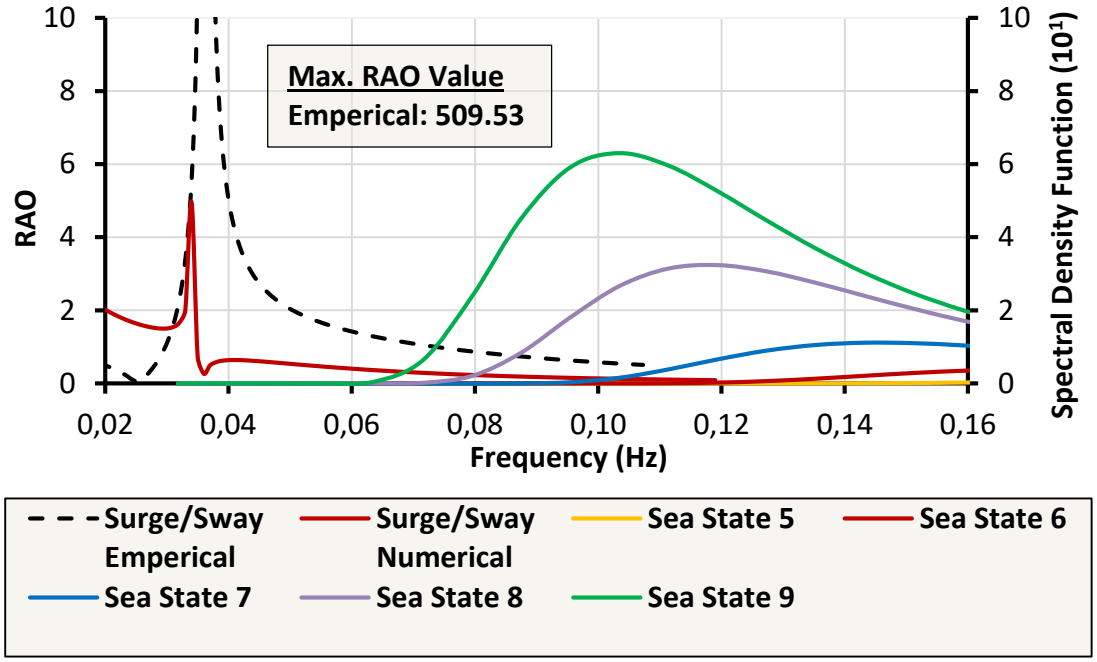

Figure 5.9 : Surge/Sway RAO and sea states.

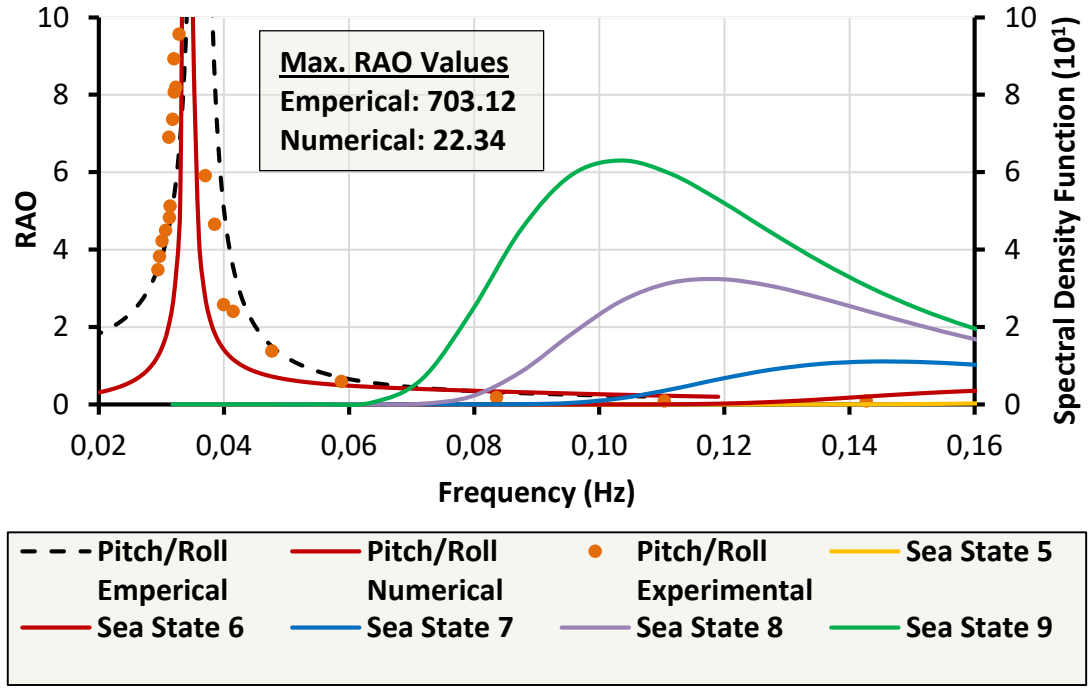

Figure 5.10 : Pitch/Roll RAO and sea states.

5.2.2 Motion Spectrums for no mooring line situation

In this section, comparisons of motion spectra are made for situations with no mooring lines. The results were satisfactory. Increase and decrease, and their trends overlap. There are differences in peak values only in the ranges where the natural frequency exists. This is due to the platforms' sensitivity to the natural frequency at which they

will resonate. This situation was also observed in the RAO graphs. Comparison graphics for the situation with no mooring line are shared in Figure 5.11 and Figure 5.12.

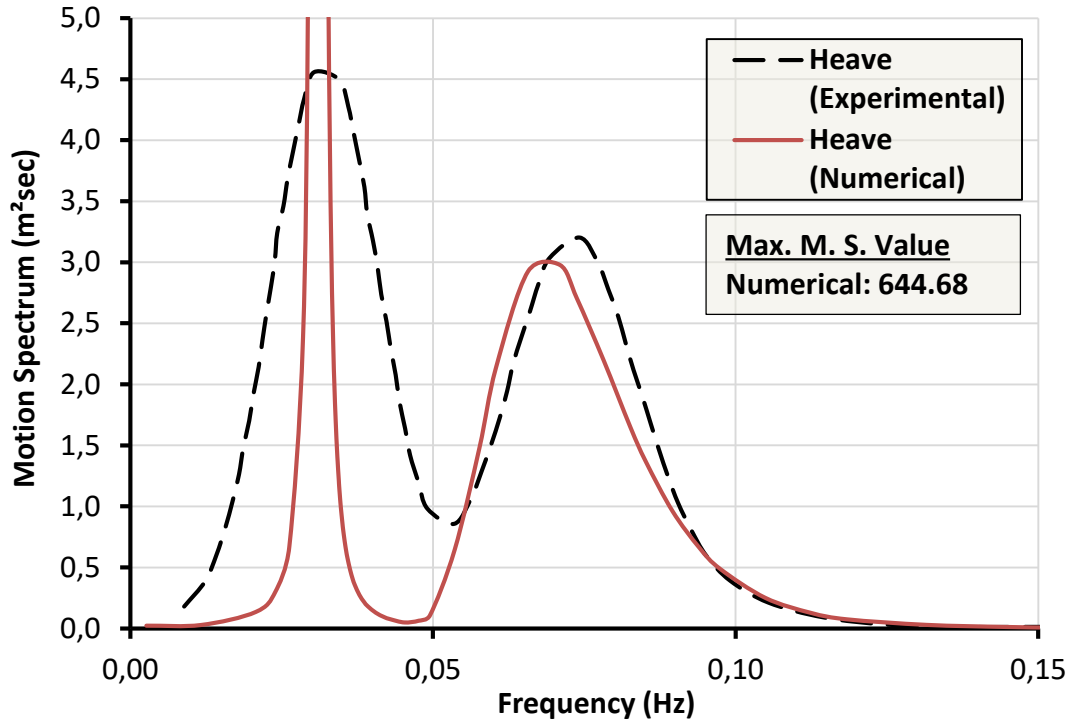

Figure 5.11 : Heave motion spectrum for sea state 8 (no mooring line).

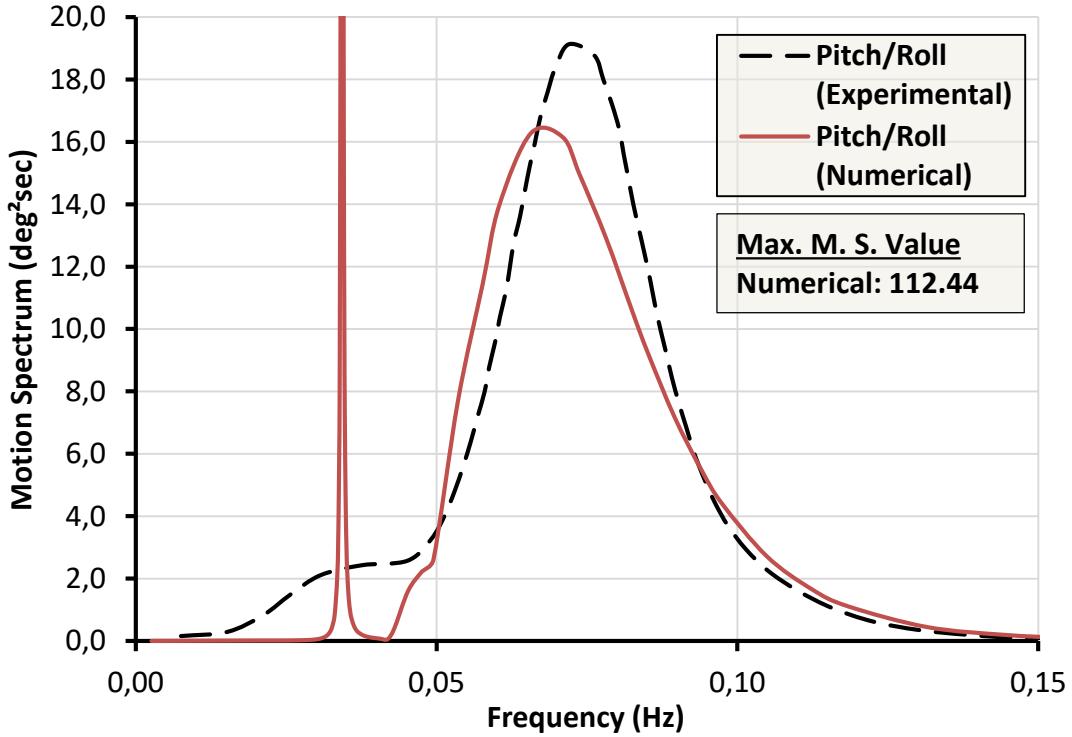

Figure 5.12 : Pitch/Roll motion spectrum for sea state 8 (no mooring line).

5.2.3 Motion Spectrums for with mooring lines situation

In this section, comparisons of motion spectra for cases with mooring lines are made. The results were generally satisfactory. However, for surge/sway movement, there is an order difference between the results in sea state 6 (Figure 5.14). Again, increasing and decreasing trends overlap for all results. There are differences in peak values in ranges where only the natural frequency is present. This is due to the platforms' sensitivity to the natural frequency at which they will resonate. This situation has also been observed in all RAO graphs, and no mooring line situation graphs have been compared. Comparison graphics for the situation with mooring lines are shared in Figure 5.13, Figure 5.14, Figure 5.15 and Figure 5.16.

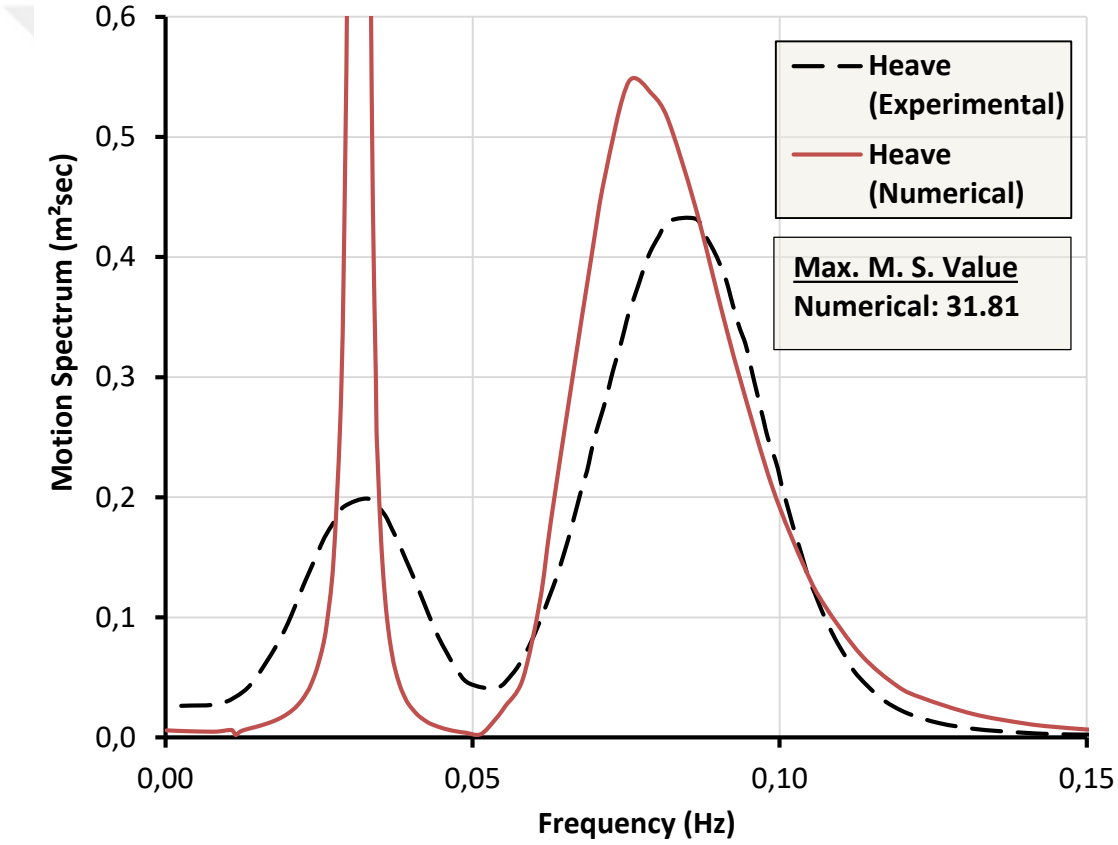

Figure 5.13 : Heave motion spectrum for sea state 6 (with mooring lines).

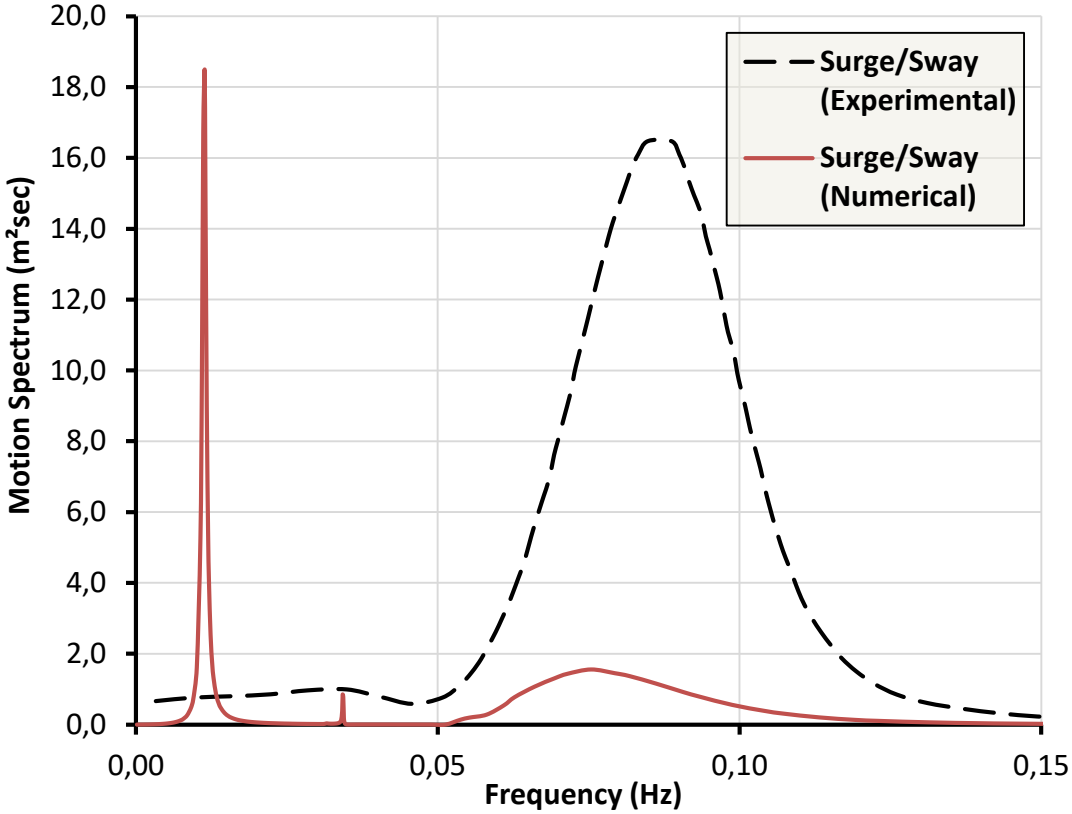

Figure 5.14 : Surge/Sway motion spectrum for sea state 6 (with mooring lines).

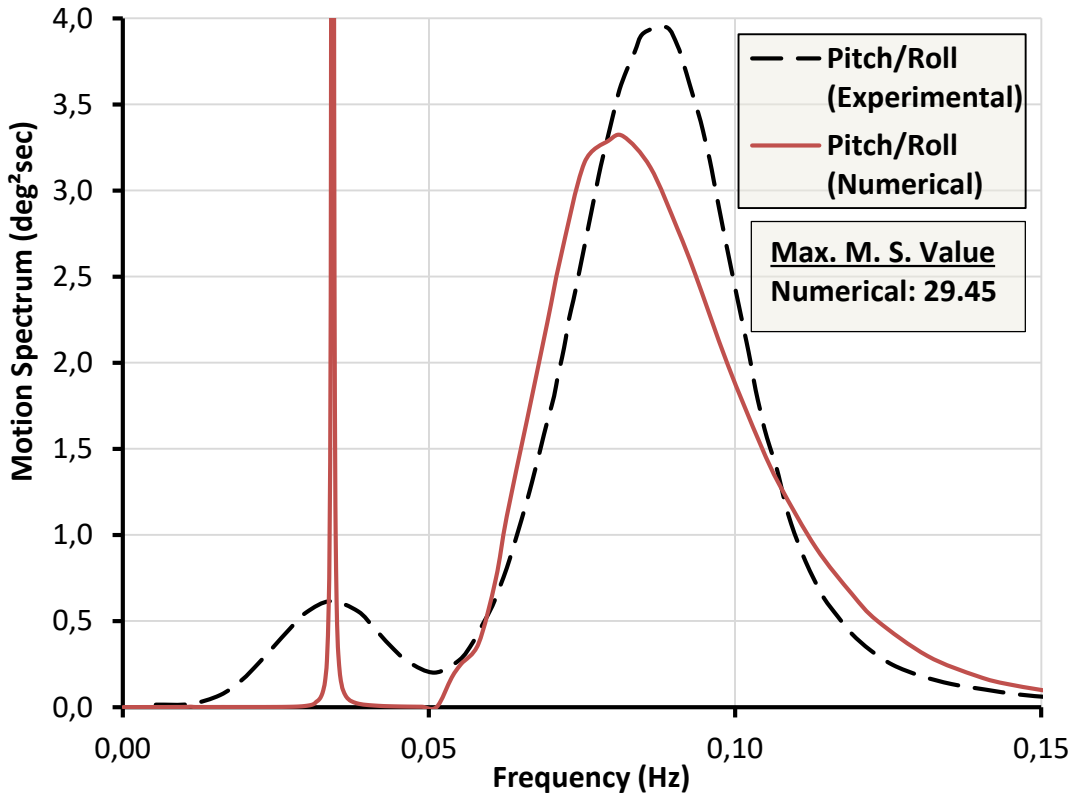

Figure 5.15 : Pitch/Roll motion spectrum for sea state 6 (with mooring lines).

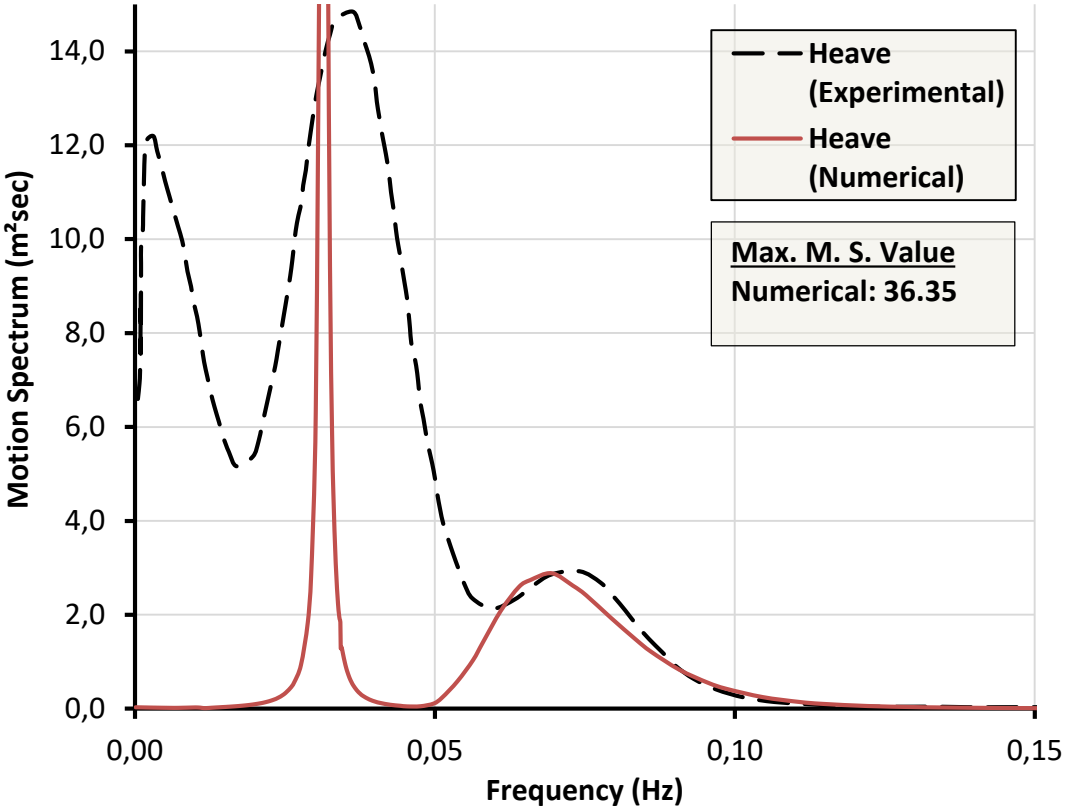

Figure 5.16 : Heave motion spectrum for sea state 8 (with mooring lines).

6. CONCLUSIONS AND RECOMMENDATIONS

This study aims to determine a methodology to examine the movement of a floating offshore platform. Afterwards, it was wanted to determine whether this methodology gives realistic results and whether it is applicable. In this context, the reactions and movements of a floating offshore platform to waves in deep sea conditions were examined.

The floating offshore platform examined in the study is designed to serve with a wind turbine. However, the methodology can also be applied to various floating platforms that serve other purposes. Additionally, it was investigated whether the structure applied to Turkish seas. Again, the research conducted here can also be used for different seas worldwide.

Within the scope of the study, wind turbines, types, working principles, implementation prerequisites, and application areas are mentioned first.

Afterwards, the mathematical background of the movements of floating offshore platforms is explained. The mathematical background explained here explains in general terms how analytical and numerical solutions are created. In addition, wave and wind climates were mentioned for the sea. In this context, methods to determine the effect of climate on the structure are mentioned. With the methods described here, the sea conditions that the platform is likely to encounter in the future have been determined, and the applicability of the structure has been investigated.

A two-stage solution method was applied to examine the movements of the floating offshore platform. First, a primary geometry was determined that could be the precursor of the platform to be examined and that could be analytically solved. This primary geometry is a vertical round cylinder. The cylinder was solved analytically and numerically. AQWA, a submodule of ANSYS Workbench, was used for numerical solutions. The software uses the 3D panel method. It is a software that works with mesh logic and provides solutions using the finite element method. Analytical and numerical solutions based on the primary geometry are satisfactorily compatible.

Based on this, it can be said that the numerical solution method used has been validated.

After the verification phase, the spar-type offshore platform selected as the final geometry was solved numerically. The solution was compared with experimental results. While examining the experimental results, two separate model scenarios with and without mooring lines were studied on different wave conditions. In this context, the results are valuable in questioning the mooring effect. When the entire solution process is evaluated, the results obtained can be listed as follows:

- When the vertical circular cylinder, determined as primary geometry, was solved analytically and numerically, satisfactory compatible results were obtained. This harmony showed that the numerical method used was appropriate and usable.
- The spar-type floating offshore platform is solved by a validated numerical method. The numerical solution was compared with the experimental solution made in the laboratory environment. In this comparison, satisfactory compatible results were achieved.
    - The natural frequency values of the platform were solved analytically, numerically, and experimentally. The values were determined to be very close to each other.
    - It is observed that the increase and decrease trends match for all conditions and movements.
    - It has been determined that the result ranges largely agree.
    - For all parameters examined, the results of the numerical solution at the natural frequency are far above the experimental solution. This situation only occurs at a point in the natural frequency zone. The reason for the difference is the sensitivity to frequency in the responses. The peak value at the natural frequency could not be captured in the experimental solution due to frequency resolution.
    - Compatible results were obtained for both scenarios when the results with and without mooring lines were compared separately. This situation shows that the solutions accurately reflect the mooring effect.

It can be said that the solution methods applied for the floating spar-type offshore platform provide realistic and acceptable results. However, within the scope of this study, only wave-induced loads were investigated. In addition, it would be helpful to investigate the effects of wind and current-induced loads on the platform. However, considering that the significant loads for a floating structure are wave-induced, the results obtained in the study are valuable.

In addition to investigating the validity of the implemented solutions, it was investigated whether there was a danger of resonance throughout the economic life of the platform. For this purpose, natural frequencies were determined for the structure's movements. Natural frequencies were determined using three different methods: analytical, numerical, and experimental. The values detected for all methods were compatible with each other. Based on this, it can be said that natural frequencies are reliable. Afterwards, the most extreme sea conditions that the structure may encounter during its economic life were investigated. For this purpose, the frequencies at which the most prominent wavelengths could occur in the Turkish seas were investigated. In addition, Pierson-Moskowitz wave spectra were created for different sea states, and the frequencies at which the peak values of the spectra occurred were determined. Finally, natural frequencies were compared with the frequency values for extreme sea conditions. It has been observed that the natural frequency values of the platform are much smaller than the frequencies expected in extreme sea conditions. This situation shows that there is no danger of resonance during the economic life of the platform. Being away from resonance is very important for the feasibility of a floating marine structure.

REFERENCES

[1] **Türkiye Rüzgar Enerjisi Birliği (TÜREB)**. (2023). *Türkiye Rüzgar Enerjisi İstatistik Raporu*. Ankara.

[2] **Guedes Soares, Carlos, Joydip Bhattacharjee and Debabrata Karmakar**. (2014). Overview and prospects for development of wave and offshore wind energy,. *hrcak.srce.hr*, **65**,.

[3] **Alawi, M. B.** (2018). *The integration of wind turbines for generating sustainable energy in skyscrapers*.

[4] **Ibrahim Al-Bahadly**. (2011). *Wind Turbines*. Ibrahim Al-Bahadly, ed InTech, Rijeka.

[5] **Tortumoğlu, M. İ. and Doğan, M.** (2021). Açık Deniz Rüzgar Türbinleri için Uygun Yer Seçim Kriterlerinin İrdelenmesi ve Kuzey Ege Kıyılarına Uygulanması,. *Deu Muhendislik Fakultesi Fen ve Muhendislik*, **23**, 25–41.

[6] **Url-1** <*https://www.energy.gov/eere/wind/how-wind-turbine-works-text-version*>, date retrieved 21.04.2024.

[7] **Url-2** <*https://www.donanimhaber.com/cin-dunyanin-en-buyuk-ruzgar-turbinini-devreye-soktu--166023*>, date retrieved 21.04.2024.

[8] **Url-3** <*https://www.nrel.gov/wind/data-tools.html*>, date retrieved 21.04.2024.

[9] **Cheikchouk, N., Benretem, A., Khalfa, D. and Herous, L.** (2017). Comparative study of wind speed extrapolation methods for sites with different roughness,. *International Journal of Power and Energy Conversion*, **1**, 1.

[10] **Anslow, R. and O'sullivan, D.** (2020). *Choosing the Best Vibration Sensor for Wind Turbine Condition Monitoring*. vol 54.

[11] **Url-4** <*https://www.vestas.com/en/products/offshore/V236-15MW*>, date retrieved 21.04.2024.

[12] **Url-5** <*https://www.vestas.com/en/products/offshore*>, date retrieved 21.04.2024.

[13] **Url-6** <*https://www.siemensgamesa.com/en-int/products-and-services/offshore*>, date retrieved 21.04.2024

[14] **Barlas, T. K. and van Kuik, G. A. M.** (2010). Review of state of the art in smart rotor control research for wind turbines,. *Progress in Aerospace Sciences*, **46**, 1–27.

[15] **Henderson, A. R., Morgan, C., Smith, B., Sørensen, H. C., Barthelmie, R. and Boesmans, B.** (2002). Offshore windpower: A major new source of energy for Europe,. *International Journal of Environment and Sustainable Development*, **1**, 356–69.

[16] **Url-7** <*https://globalwindatlas.info/en*>, date retrieved 21.04.2024.

[17] **Url-8** <*https://tethys.pnnl.gov/technology/fixed-offshore-wind*>, date retrieved 21.04.2024.

[18] **Url-9** <*https://webapp.navionics.com/#boating@0&key=mxpyFaehmC*>, date retrieved 21.04.2024.

[19] **Url-10** <*https://www.instra.es/en/new/the-future-of-offshore-wind-farms-in-spain-and-portugal*>, date retrieved 21.04.2024.

[20] **Froude, W.** (1888). *The resistance of ships*. US Government Printing Office.

[21] **Froude, W.** (1873). Apparatus for Automatically Recording the Rolling of a Ship in a Sea-Way, and the Contemporaneous Wave-Slopes,. *Royal United Services Institution. Journal*, **17**, 858–87.

[22] **Kriloff, A.** (1898). A general theory of the oscillation of a ship on waves,. *Naval Academy St. Petersburg, Russia, Publication on the 39th Session of the Royal Institution of Naval Architects, RINA Transactions 1898-21*,.

[23] **Faltinsen, O. M.** (1990). *Sea Loads on Ships and Offshore Structures*. Cambridge University Press.

[24] **Persson, A.** (1885). The Coriolis effect: four centuries of conflict between common sense and mathematics,. *Part I: a history to*, 1–24.

[25] **Sarıöz, K.** (2023). *Ship Design for Seakeeping Lecture Notes*. Istanbul.

[26] **Tran, T., Kim, D. and Song, J.** (2014). Computational fluid dynamic analysis of a floating offshore wind turbine experiencing platform pitching motion,. *Energies (Basel)*, **7**, 5011–26.

[27] **ANSYS.** 2023. *Aqwa Theory Manual Third-Party Software*.

[28] **Froude, R. E.** (1905). Model Experiments on Hollow versus Straight Lines in Still Water and Among Artificial Waves,. *RINA Transactions: London, UK*,.

[29] **St Denis, M. and Pierson, W. J.** (1953). On the motions of ships in confused seas,. *Trans. SnAMe*, **61**, 280–357.

[30] **Journée, J. M. J. and Massie, W. W.** (2001). *Offshore Hydromechanics*. Delft University of Technology, Delft.

[31] **Tureyen, O. E. and Akyıldız, H.** (2019). *Numerical Analysis Of Wave Loads On Offshore Observation Buoys*. Istanbul Technical University.

[32] **Hogben, N. and Lumb, F. E.** (1967). Ocean wave statistics,. *Her Majesty's Stationery Office (HMSO)*,.

[33] **Bales, S. L., Lee, W. T., Voelker, J. M. and Taylor, D. W.** (1981). *Standardized wave and wind environments for NATO operational areas*. David W. Taylor Naval Ship Research and Development Center.

[34] **Pierson Jr, W. J. and Moskowitz, L.** (1964). A proposed spectral form for fully developed wind seas based on the similarity theory of SA Kitaigorodskii,. *J Geophys Res*, **69**, 5181–90.

[35] **Bretschneider, C. L.** (1957). Revisions in wave forecasting: deep and shallow water,. *Coastal Engineering Proceedings*, 3.

[36] **Oosterveld, M. W. C.** (1978). Proceedings of the 15th International Towing Tank Conference,. In *ITTC 1978*. ITTC, Hauge.

[37] **Hasselmann, D. E., Dunckel, M. and Ewing, J. A.** (1980). Directional wave spectra observed during JONSWAP 1973,. *J Phys Oceanogr*, **10**, 1264–80.

[38] **Hasselmann, K., Barnett, T. P., Bouws, E., Carlson, H., Cartwright, D. E., Enke, K., Ewing, J. A., Gienapp, A., Hasselmann, D. E. and Kruseman, P.** (1973). Measurements of wind-wave growth and swell decay during the Joint North Sea Wave Project (JONSWAP).,. *Ergaenzungsheft zur Deutschen Hydrographischen Zeitschrift, Reihe A,*.

[39] **Norrbin, N. H. and Ohlsson, C. S.** (1984). Proceedings of the 17th International Towing Tank Conference,. In *ITTC 1984*. ITTC, Goteborg.

[40] **Ferdinande, V. and Kritis, B. G.** (1980). An Economical Method of Determining Added Mass and Damping Coefficients of Axisymmetric Floating Bodies in Oscillatory Heaving Motion,. *nternational Shipbuilding Progress*, **27**, 231–40.

[41] **Jonkman, J.** (2010). *Definition of the Floating System for Phase IV of OC3*. National Renewable Energy Lab.(NREL), Golden, CO (United States).

[42] **Xu, X. and Day, S.** (2021). Experimental investigation on dynamic responses of a spar-type offshore floating wind turbine and its mooring system behaviour,. *Ocean Engineering*, **236**, 109488.

[43] **Zürcher, K.** (2016). Waterjet testing techniques for powering performance estimation using a single catamaran demihull,.

[44] **Chakrabarti, S. K.** (1994). *Offshore structure modeling*. vol 9 world scientific.

[45] **Rolo, L.** (2014). Design, testing and validation of a scale model semisubmersible offshore wind turbine under regular/irregular waves and wind loads,.

[46] **Özhan, E. and Abdalla, S.** (2002). *Türkiye kıyıları rüzgar ve derin deniz dalga atlası*. MEDCOAST, ODTÜ.

[47] **Yüksel, Y., Çevik, E., Aydoğan, B., Arı, A., Saraçoğlu, K. E., Alpli, R. and Bekar, B.** (2011). Türkiye Denizleri Dalga Iklim Modeli Ve Uzun Dönem Dalga Iklim Analizi. 7,. *Ulusal Kıyı Mühendisliği Sempozyumu*, 411–20.

CURRICULUM VITAE

Name Surname **:** Abdullah Emin ULAŞ

EDUCATION **:**

- **B.Sc.** **:** 2021, Yıldız Technical University, Faculty of Civil Engineering, Department of Civil Engineering

PROFESSIONAL EXPERIENCE AND REWARDS:

- 08.2021 - … DENAR Ocean Engineering S.A. (Civil Engineer - Coastal and Offshore Structures)

PUBLICATIONS, PRESENTATIONS AND PATENTS ON THE THESIS:

- **Ulaş A.E., and Sarıöz K.** 2023. Investigation of Floating Vertical Circular Cylinder's Wave Excitation Forces and RAO for Heave Motion. International Graduate Research Symposium - IGRS'23, May 16-19, 2023 İstanbul, Türkiye.